5-2015

The Structural Mechanism of Allosteric Modulation of the NMDA Receptor: A Balance of Tensions

Rita E. Sirrieh

THE STRUCTURAL MECHANISM OF ALLOSTERIC MODULATION OF THE

NMDA RECEPTOR:

A BALANCE OF TENSIONS

by

Rita Evelyn Sirrieh, B.S.

APPROVED:

_____
Vasanthi Jayaraman, Ph.D.
Advisory Professor

_____
Jianping Jin, Ph.D.

_____
John O'Brien, Ph.D.

_____
John A. Putkey, Ph.D.

_____
John L. Spudich, Ph.D.

APPROVED:

_____
Dean, The University of Texas
Graduate School of Biomedical Sciences at Houston

THE STRUCTURAL MECHANISM OF ALLOSTERIC MODULATION OF THE NMDA RECEPTOR:

A BALANCE OF TENSIONS

A

DISSERTATION

Presented to the Faculty of
The University of Texas
Health Science Center at Houston
and
The University of Texas
MD Anderson Cancer Center
Graduate School of Biomedical Sciences
in Partial Fulfillment

of the Requirements

for the Degree of

DOCTOR OF PHILOSOPHY

by

Rita Evelyn Sirrieh, B.S.
Houston, Texas

May, 2015

Dedication

I dedicate this dissertation to my loving and extremely supportive family. My parents Peter and Flavia Sirrieh have been a constant source of guidance and encouragement. My three siblings Loretta, John, and Kathryn are my best friends and are always there to listen and make me laugh. Even when I did not think I could get an experiment to work or that I could meet a given goal, they always believed in me.

Acknowledgements

I would first like to thank my advisor, Vasanthi Jayaraman, for being an outstanding mentor! She took me into her lab when I knew so little about protein structure and biophysics! Her guidance and encouragement throughout my time in her lab helped me navigate not only my project but also my professional and personal development. Her love of science was contagious and made coming to work enjoyable, and her high expectations continually challenged me to improve. I could not have asked for a better mentor. I have learned much from working with her and have enjoyed my time immensely.

Second, I would like to thank all the past and present lab members. I have had the good fortune to work with many wonderful people who helped shape my scientific training but who were also wonderful friends. Dr. Swarna Ramaswamy and I started graduate school together and she was my partner in crime, so to speak. I enjoyed being roommates at conferences and all the time we spent outside of the lab together, but also her presence in the lab challenged me to work harder and improve as a scientist. Dr. Dave MacLean was a source of answers to my endless questions. He encouraged me to ask questions, and, after patiently answering my questions, he would direct me to the appropriate literature to help me learn more. This direction was instrumental to my success. Our conversations about science were exciting and helpful to my project, but we also had interesting conversations about philosophy, religion, literature, and politics that were always very fun. Drew Dolino motivated me to always learn more because he would ask me so many questions, and when I did not know the answer, I would realize how much more I had to learn. He was also very helpful in troubleshooting experiments in the lab. I always enjoyed our ritual food runs when we were both working late in the lab (Shiva?!). Dr. Garam Lee was a great help in cloning and basic molecular biology. Dr. Anu Rambhadran was a good friend who guided me through my rotation and modestly gave an example of what an ideal graduate student should be like. Dr.

Jennifer Gonzalez helped me learn how to do oocyte experiments and answered many questions. Caitlin Nurik kept me company after Swarna graduated and was a great addition to our lab. Finally, Douglas Litwin, the most recent addition to our lab, was really fun to talk to and asked me many questions to keep on my toes during my last few months in the lab!

The Biochemistry and Molecular Biology department is a unique place to get a Ph.D. because it is full of many wonderful people and very diverse research. I made many friends in the department and would like to thank specifically William (Tre') O'Brien, Nicholas Parchim, Dr. Harry Karmouty-Quintana, and Natoya Peart for their support and friendship throughout the years. I would like to thank especially Dr. Heidi Vitrac for her mentorship and friendship, especially as I was preparing for my candidacy exam and applying for post-doctoral positions. Interactions with my peers in the department made life more bearable when experiments were not working or when I had to work too many hours in a week!

I would like to also thank all of my committee members for their direction throughout the years. Meetings with you motivated me to keep reading and to improve my ability to answer questions about my work. These committee members include: Drs. John Spudich, John Putkey, Jianping Jin, John O'Brien, Andrew Morris, Irina Serysheva, Lei Zheng, and Shane Cunha.

Finally, I would like to thank the Gulf Coast Consortium for funding through the Houston Area Molecular Biophysics Fellowship and for the many opportunities to network and expand my scientific knowledge through seminars and conferences.

THE STRUCTURAL MECHANISM OF ALLOSTERIC MODULATION OF THE NMDA RECEPTOR: A BALANCE OF TENSIONS

Rita Evelyn Sirrieh, B.S.

Advisory Professor: Vasanthi Jayaraman, Ph.D.

N-methyl-D-aspartate (NMDA) receptors are one of the three main types of ionotropic glutamate receptors in the central nervous system. NMDA receptors mediate the rapid excitatory neurotransmission that underlies learning and memory formation. Conversely, NMDA receptors are implicated in a variety of neurological disorders. Studies targeting the mechanism of allosteric modulation, such as this study, hope to contribute to the understanding of how NMDA receptors are modulated to allow for better drug development.

NMDA receptors are obligate heterotetramers, typically composed of glycine-binding GluN1 subunits and glutamate-binding GluN2 subunits. The GluN2 subunits can be one of four subtypes (A-D). Each subunit is organized into distinct domains: extracellular amino-terminal (ATD) and ligand-binding domains, the transmembrane, pore-forming domain, and an intracellular carboxyl-terminal domain. The ATD includes the binding site of a number of allosteric modulators. Endogenous modulators such as the zinc cation or spermine can inhibit and potentiate current through the receptor, respectively. The synthetic compound ifenprodil also binds the ATDs and inhibits the receptor. We used luminescence resonance energy transfer to study the structural changes accompanying modulator binding and then linked those conformational changes to the function of the receptor using electrophysiology. LRET

measurements were made between subunits to determine the architecture of the ATDs in an assembled receptor.

Our studies reveal that the ATDs have a compact overall organization, and that the inherent conformation of a GluN1 or GluN2 ATD varies in a fashion that correlates with the open channel probability of the receptor. Additionally, modulator binding to the ATDs induces conformational changes. Inhibitors, such as zinc and ifenprodil, induce a closure in the GluN2 ATD, whereas the potentiator spermine induces an opening of the GluN2 ATD. The lower lobes of the ATDs undergo a rotational movement when any allosteric modulator was bound, suggesting the rotation of the domain is independent of the open/close mechanism. These studies reveal that the receptor can be modulated by influencing the conformation of the ATD.

Table of Contents

List of Illustrations

List of Tables

Abbreviations

iGluR	ionotropic glutamate receptor
AMPA	α-amino-3-hydroxy-5-methyl-4-isoxazolepropionic acid
NMDA	*N*-methyl-D-aspartate
ATD	Amino-Terminal Domain
LBD	Ligand-Binding Domain
TMD	Transmembrane Domain
CTD	Carboxyl-Terminal Domain
M1-M4	Transmembrane Domain 1-4
S1	Upper Lobe of Ligand Binding Domain
S2	Lower Lobe of Ligand Binding Domain
MOT	Mean Open Time
MCT	Mean Closed Time
Po	Channel Open Probability
LRET	Luminescence Resonance Energy Transfer
FRET	Fluorescence Resonance Energy Transfer
smFRET	single molecule Fluorescence Resonance Energy Transfer
APV	2-Amino-5-phosphonopentanoic acid
DCKA	5,7-dichlorokynurenic acid
MK-801	(5S,10R)-(+)-5-Methyl-10,11-dihydro-5H-dibenzo[a,d]cyclohepten-5,10-imine
ACPC	1-aminocyclopropanecarboxylic acid
t-ACBD	trans-1-aminocyclobutane-1,3-dicarboxylic acid

Chapter 1:
Introduction to Glutamate Receptors

1.1 Introduction to Synaptic Transmission and iGluRs

Glutamate is the primary excitatory neurotransmitter in the central nervous system. Glutamatergic signaling is responsible for processes which underlie learning and memory formation through long-term potentiation and long-term depression. When an action potential reaches the pre-synaptic nerve terminal, membrane depolarization followed by a calcium influx into the presynaptic nerve terminal triggers the release of synaptic vesicles containing glutamate. The released glutamate travels across the synaptic cleft and binds to one of three glutamate receptors on the post-synaptic nerve terminal. The glutamate signal is then cleared away, partly by the diffusion of glutamate out of the synapse, but mostly by the action of glutamate transporters which recycle glutamate to be re-packaged into synaptic vesicles. Glutamatergic signaling results in rearrangements of the synapse resulting in a long-term change in the mechanism of synaptic signaling. The focus of this dissertation is on the glutamate receptors that receive the signal on the post-synaptic nerve terminal.

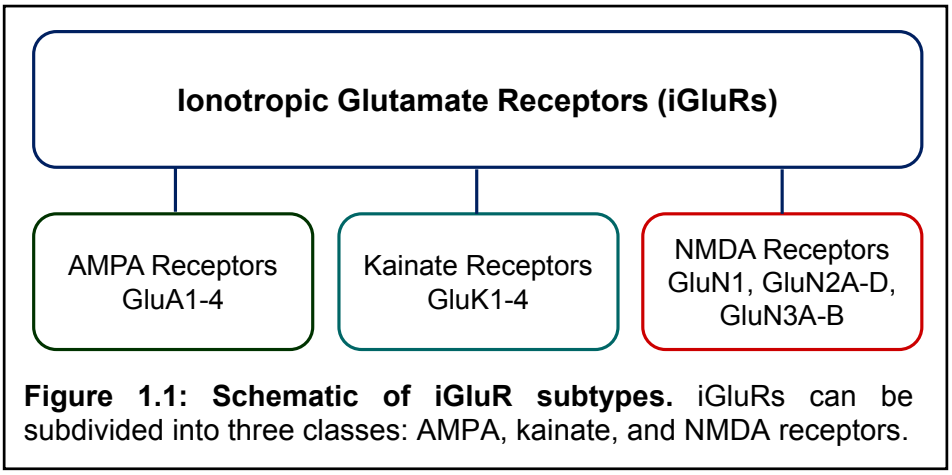

Figure 1.1: Schematic of iGluR subtypes. iGluRs can be subdivided into three classes: AMPA, kainate, and NMDA receptors.

Ionotropic glutamate receptors (iGluRs) can be subdivided into three subtypes, which are named for the synthetic agonist that can activate the channel to the same extent as glutamate, a full agonist: α-amino-3-hydroxy-5-methyl-4-isoxazolepropionic acid (AMPA), *N*-methyl-D-aspartate (NMDA), and kainate receptors (Figure 1.1). iGluRs were first cloned in early 1989, followed by a flurry of additional clones in the early 1990s (Hollmann, O'Shea-

Greenfield et al. 1989, Bettler, Boulter et al. 1990, Boulter, Hollmann et al. 1990, Egebjerg, Bettler et al. 1991, Moriyoshi, Masu et al. 1991, Werner, Voigt et al. 1991, Sugihara, Moriyoshi et al. 1992), and their discovery spurred decades of intense research. The receptors are named for the synthetic agonists which activate the channel to the same extent as the physiological full agonist, glutamate. Kainate receptors play roles on both the pre- and post-synaptic terminals and are more involved on the postsynaptic side early in development. In adults, AMPA and NMDA receptors are the primary post-synaptic receptors. Glutamate released from the pre-synaptic terminal binds to both the AMPA and NMDA receptors. At resting membrane potentials, however, NMDA receptors are pore-blocked by the Mg^{2+} cation (Mayer, Westbrook et al. 1984, Nowak, Bregestovski et al. 1984). AMPA receptor activation results in a sodium influx into the post-synaptic neuron, which induces membrane depolarization, and relieves the magnesium block of the NMDA receptor. For this reason, NMDA receptors are called coincidence detectors; they detect a coincident electrical (membrane depolarization) and chemical (glutamate) signal. NMDA receptors require two ligands to activate the receptor, glycine or D-serine in addition to glutamate. Glycine or D-serine are always present in the synaptic cleft, and a recent study suggests that the type of agonist present depends on the brain region and stage of development (Le Bail, Martineau et al. 2014). These activated NMDA receptors are sodium and calcium permeable and further depolarize the post-synaptic neuron. Moreover, calcium entering the post-synaptic neuron activates many downstream processes, which during learning and memory formation and consolidation result in growth and rearrangement of the synapse.

1.2 Overall Architecture of iGluRs

iGluRs share a common overall assembly in that they are tetrameric in nature and organized into distinct domains (Figure 1.2). AMPA and kainate receptors can form as

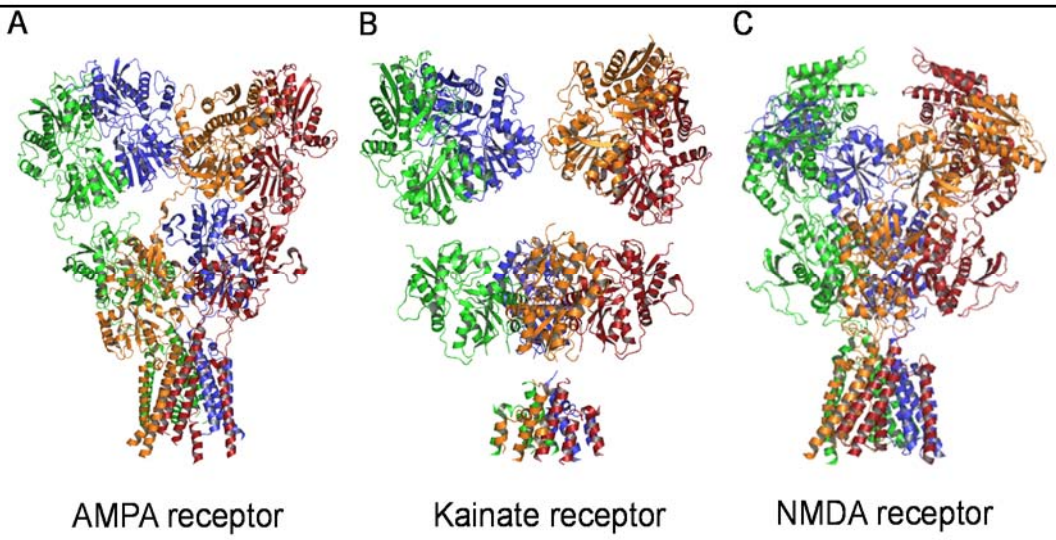

Figure 1.2: Full-length structures of iGluRs. (A) The crystal structure of the GluA2 AMPA receptor bound to the antagonist ZK 200775 (PDB ID 3KG2) was the first full iGluR structure solved (Sobolevsky, Rosconi et al. 2009, Tomitori, Suganami et al. 2012). The four subunits of the AMPA receptor are assigned a letter to make it easier to refer to the subunit: A-red, B-gold, C-green, D-blue. (B) The cryo-EM structure of the GluK2 kainate receptor (PDB ID 4UQQ) was solved bound to 2S,4R-4-methylglutamate (Meyerson, Kumar et al. 2014). (C) The crystal structure of the heteromeric GluN1-GluN2B NMDA receptor (PDB ID 4PE5) bound to glutamate, glycine, and ifenprodil is shown with the GluN1 subunits in green and red and the GluN2B subunits in gold and blue. Each of the structures lacks the intracellular carboxyl-terminal domain.

homomeric or heteromeric species, whereas the NMDA receptor is an obligate heteromer. Each of the four subunits in the AMPA receptor is, by convention, assigned a letter (A-D) to facilitate talking about specific subunits and interactions. In Figure 1.2 the subunits are shown in different colors: A-red, B-gold, C-green, D-blue. The receptor assembles as a pair of dimers that has four-fold symmetry at the pore, but only a two-fold symmetry at the LBDs, so that there is asymmetry among the LBDs despite the structure being of a homomer. At the LBDs, the pairs of domains are of the B/C and A/D subunits. Before the structure of the NMDA receptor was available, fluorescence studies and cross-linking followed by western blots were used to determine the arrangement of subunits (Rambhadran, Gonzalez et al. 2010, Salussolia, Prodromou et al. 2011, Riou, Stroebel et al. 2012, Sirrieh, MacLean et al. 2013). These studies all showed that the NMDA receptor subunits assemble in an alternating fashion,

also called a dimer of heterodimers. The GluN1 subunits were found to correspond to the A/C positions on the AMPA receptor, while GluN2 subunits correspond to B/D positions at the LBDs. Additionally, the cross-over between the ATD and LBD layer was predicted to be maintained in NMDA receptors. At the ATD layer, the dimers are of the A/B and C/D subunits due to the crossover. When the receptor is viewed from the side, it appears in layers due to the association of the distinct domains with each other (Figure 1.2). The assembly of subunits is quite similar between AMPA and kainate receptors; the receptor has an overall 'Y' shape. NMDA receptors have a more compact arrangement between the extracellular domains (Figure 1.2 and 1.2).

Recently, the full-length structure of the NMDA receptor was solved by two labs (Karakas and Furukawa 2014, Lee, Lü et al. 2014). These structures, though lacking the CTDs, are the most complete structures to date of the NMDA receptor. One structure is bound by ifenprodil, glutamate, and glycine (shown in Figure 1.2) (Karakas and Furukawa 2014). The second structure is bound by Ro25-6981, ACPC, t-ACBD, and the open-channel blocker MK-801 (Lee, Lü et al. 2014). These structures reveal that, like the kainate and AMPA receptors (Sobolevsky, Rosconi et al. 2009, Meyerson, Kumar et al. 2014), the LBDs and ATDs are organized as a dimer of heterodimers. Further, there is a crossover between the LBD and ATD layers, where the ATD of a subunit sits atop the LBD of the adjacent subunit (Figure 1.2 and 1.3). This crossover is especially clear if panels B and C of Figure 1.3 are compared; the ATD of a subunit does not sit directly above the LBD contributing to the LBD dimer pair. Likewise, the LBD of a subunit does not sit directly below the ATD contributing to the ATD dimer pair (Figure 1.3).

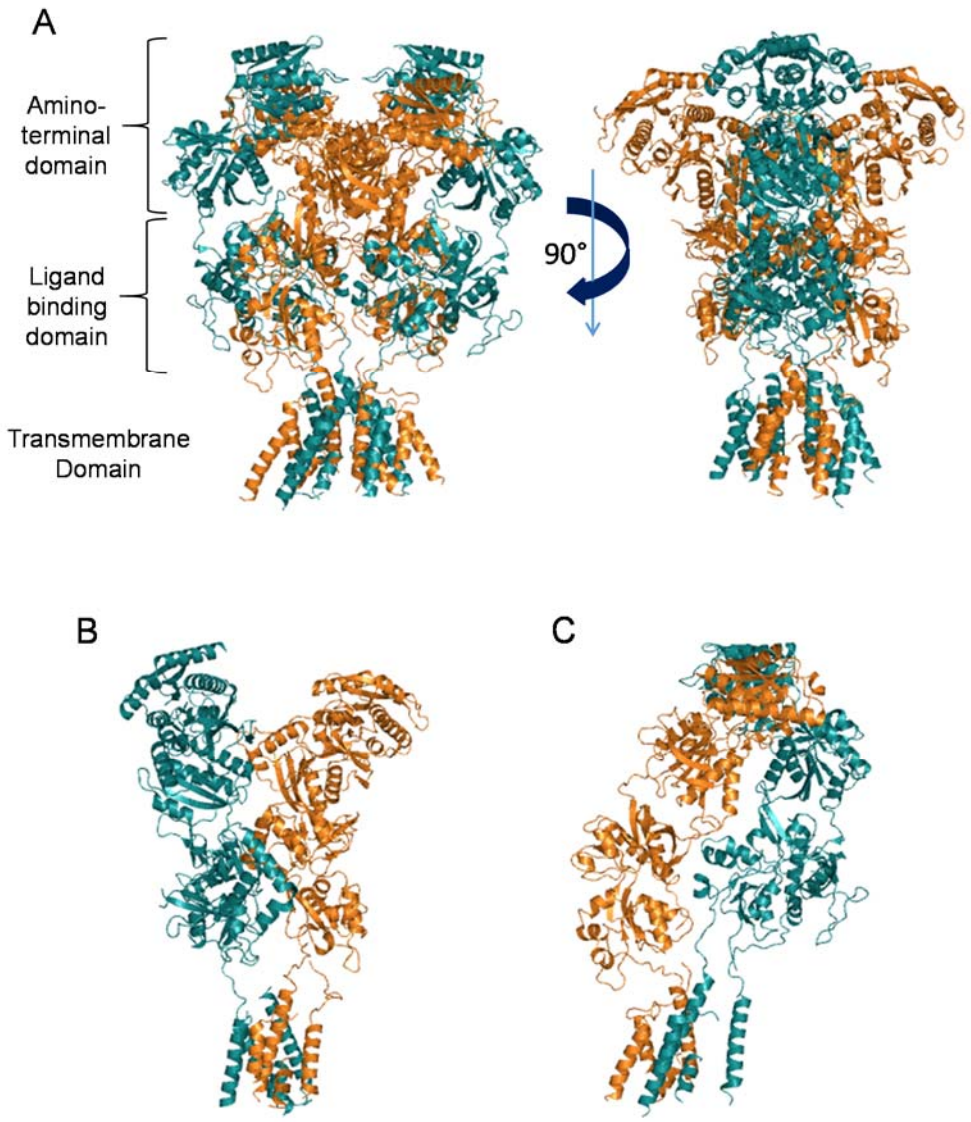

Figure 1.3: Crystal structures of the full-length NMDA receptor. (A) The heterotetrameric crystal structure of the GluN1/GluN2B NMDA receptor in complex with the agonists glutamate and glycine and the allosteric inhibitor ifenprodil (PDB ID 4PE5). The structure in the right half of panel A shows the structure 90°. (B) The full structure of a dimer highlighting the dimer pair at the LBD layer is shown. (C) The full subunit structure of a dimer highlighting the dimer pair at the ATD layer is shown.

Each subunit of the NMDA receptor is structurally organized into distinct domains: an extracellular amino terminal domain (ATD) and ligand-binding domain (LBD), the pore-forming transmembrane domain (TMD), and an intracellular carboxyl-terminal domain (CTD) (Figure

1.3). The upper lobe and lower lobes of the LBD are called S1 and S2, respectively. The topology of the protein is such that the extracellular N-terminus begins with the amino terminal domain, connects to S1 of the LBD, then inserts into the membrane to form the M1, M2, and M3 helices, then forms the S2 of the LBD, which finally connects to M4 and then the intracellular CTD. As such, the LBD is connected to the TMD via three linkers, called the S1-M1 linker, M3-S2 linker, and S2-M4 linker. Each domain of the NMDA receptor has a distinct function. The ATD and LBD are structurally distinct enough that an individual domain can be expressed as soluble protein, and the first crystal structures of iGluRs were of isolated domains (Armstrong and Gouaux 2000, Furukawa and Gouaux 2003, Furukawa, Singh et al. 2005).

1.3 Subtypes and Splice Variants of Glutamate Receptors

The NMDA receptor can be composed of three different types of subunits: GluN1, GluN2, and GluN3. GluN1 subunits bind glycine or D-serine as the agonist and can be one of eight different splice variants (GluN1-1 to GluN1-4 and each can be either a or b). The GluN1 splice variant is designated ‘a’ if it does not include exon 5 or ‘b’ if it does. The ‘a’ splice variant is more common than the ‘b’ splice variant (Paoletti 2011). The other two exons that can be differentially spliced are in the intracellular C-terminus. GluN2 subunits bind glutamate as the agonist and can be one of four subtypes arising from four different genes, designated A-D. GluN3 subunits also bind glycine or D-serine as the agonist and can be one of two subtypes, A or B. Functional NMDA receptors are composed of at least two different subunits, most commonly GluN1 and GluN2. The different splice variants and subtypes are expressed variably throughout the central nervous system, and the subunit composition in various brain regions changes during development. During fetal development GluN2B is the primary GluN2 subtype until a switch takes place a few weeks after birth and GluN2A becomes the most common subtype (Paoletti 2011). GluN2C subunits are expressed late in embryonic

development and in the adult brain are mostly found in the cerebellum (Paoletti 2011). Finally, the GluN2D subunit is always poorly expressed and in adults is found only in the diencephalon and brainstem (Paoletti 2011). The subunit composition dictates the gating kinetics of the receptor and the affinity for agonists, antagonists, and modulators. As a result, the variability in NMDA receptor subunit composition defines the shape of synaptic signaling in a particular brain region.

The different subtypes of the NMDA receptor share varying degrees of sequence homology. Across all four GluN2 subtypes, there is an overall 25% sequence identity. This identity varies depending on the domain of the receptor being compared. The TMDs have the highest sequence identity (73%), with higher sequence identity if comparing certain pairs of subunits. The LBDs have a sequence homology of 63%, while the ATDs have only 19% sequence homology. The CTDs have the least sequence homology, only 2% across all GluN2 subtypes. The GluN1 and GluN3 subunits, despite both being glycine binding subunits, have relatively low sequence homology across all domains, up to 19%, with an overall sequence homology of 5% across all splice variants and subunits. These values were all reviewed in S.F. Traynelis, et al., 2010 (Traynelis, Wollmuth et al. 2010).

1.4 Functions of ATDs and binding sites of modulators

The ATDs of the NMDA receptor are the most extracellular part of the receptor (most distal to the membrane) and are about 350-400 amino acids in length. The domain is organized in two lobes that form a clam-shell like structure, similar to the bacterial leucine-isoleucine-valine binding proteins (LIVBPs) to which they are structurally homologous. The ATDs are involved in receptor assembly (Meddows, Bourdellès et al. 2001) and dictate the open probability (Po) of the channel (Gielen, Retchless et al. 2009, Yuan, Hansen et al. 2009). Additionally, the GluN2 ATD determines agonist potency (Yuan, Hansen et al. 2009). Most importantly, the ATDs contain the binding sites for allosteric modulators of receptor function. Endogenous and exogenous modulators of the receptor have been identified that bind to the ATDs (Figure 1.4 for binding sites). The zinc cation is an endogenous inhibitor of the receptor that binds within the bi-lobed cleft of the GluN2 ATD. Spermine, an endogenous potentiator,

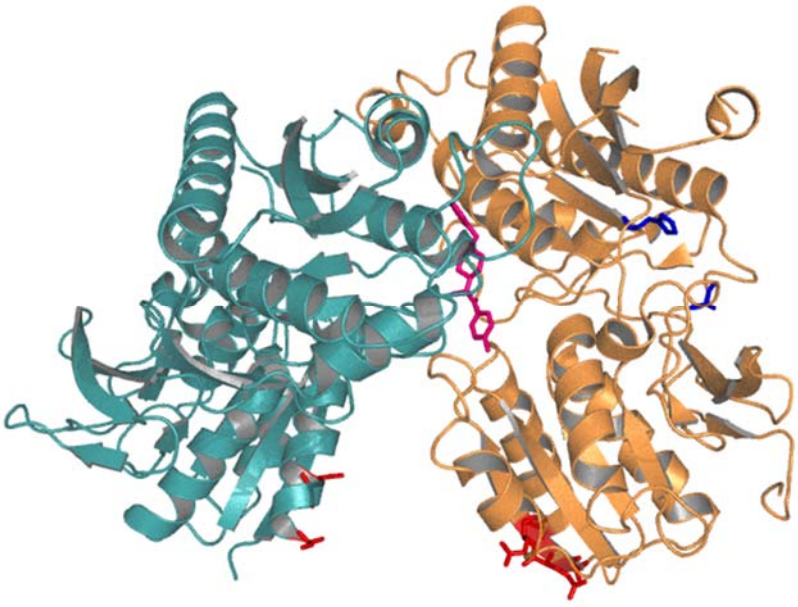

Figure 1.4: Modulator Binding Sites. The GluN1-GluN2B ATD dimer is shown with GluN1 in teal and GluN2B in orange. Highlighted in red are the acidic residues involved in spermine binding. In pink is ifenprodil in its binding site. The blue residues in GluN2B are His128 and Asp284, which coordinate the zinc cation. In GluN2A, His42 and His44 help these residues to coordinate zinc.

is thought to bind between the GluN1 and GluN2 ATDs, but only potentiates GluN2B containing receptors. Synthetic compounds called phenylethanolamines similarly bind between the GluN1 and GluN2B ATDs and inhibit current from the receptor. Two compounds from this class, ifenprodil and Ro25-6981 were found to bind to the same binding site between the two ATDs (Karakas, Simorowski et al. 2011).

A linker connects the ATD to the LBD (called the ATD-LBD linker). This linker is important to the modulation of Po by the ATD. Chimeras that swap just the ATD-LBD linker between GluN2A and GluN2D subunits, can alter the Po of the receptor to match that which

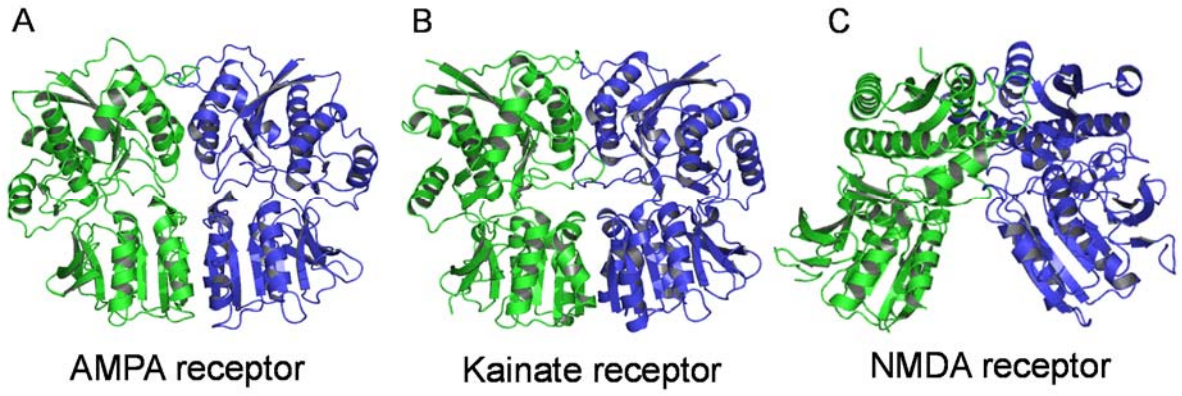

Figure 1.5: iGluR ATDs. The ATD dimers from AMPA (A), kainate (B), and NMDA (C) receptors are shown. The NMDA ATD dimer is of the GluN1-GluN2B ATDs (GluN1-green, GluN2B-blue). It is clear from looking at these structures that the ATDs of NMDA receptors adopt unique conformations. The upper lobes make extensive contacts, but the lower lobes are uninhibited by contacts and free to move.

contributed the linker (Gielen, Retchless et al. 2009, Yuan, Hansen et al. 2009). The linkers are about ~15 residues long, and about 1/3 of the residues are conserved between the GluN2A and GluN2D subtypes.

The structures of AMPA and kainate receptor ATDs are quite similar (Figure 1.5). The structures of individual ATDs align to each other with an RMSD of 2.116 Å, while homomeric ATD dimers align with an RMSD of 2.431 Å. These structures align fairly well to the GluN1 ATD, but the GluN2B ATD in the dimer seems rotated. When the GluN2B ATD structure was initially solved, the authors noted how the lower lobe of the GluN2B ATD was rotated by about

45° and 54° compared to the ATDs of AMPA and kainate receptors, respectively (Karakas, Simorowski et al. 2009). The difference in the structure of the GluN2B ATD was suggested as a critical component to the ability of NMDA receptors to bind allosteric modulators at the ATDs. AMPA and kainate receptor ATDs have extensive contacts along the whole of the ATDs. However, the contacts between GluN1 and GluN2 ATD are contained solely at the upper lobes, such that the lower lobes of the ATDs are free to move or interact with other domains as needed or spurred to by a modulator (Karakas, Simorowski et al. 2009, Stroebel, Carvalho et al. 2011).

1.5 LBDs and gating

The LBDs are about 250-300 amino acids in length and also form a clamshell which contains the binding sites for the agonists. In the AMPA receptor, the agonist first interacts with the upper lobe of the LBD, and subsequent contacts with the lower lobe of the LBD cause the domain to close around the agonist. This domain closure around the agonist has been confirmed by crystal structures, functional studies, and LRET studies of the isolated LBDs (Armstrong and Gouaux 2000, Furukawa and Gouaux 2003, Furukawa, Singh et al. 2005, Gonzalez, Rambhadran et al. 2008, Rambhadran, Gonzalez et al. 2011). Further, single molecule studies reveal the dynamics involved and the spread of states explored by the LBDs; LBDs tend to explore a greater degree of conformations in the apo or antagonist bound states, but lesser conformations (i.e. a more narrow distribution of states) with increasing efficacy of the agonist (Landes, Rambhadran et al. 2011, Ramaswamy, Cooper et al. 2012, Dolino, Cooper et al. 2014). The extent that the domain closes around the ligand can be directly correlated to the extent of activation of the receptor.

Much work has focused on understanding the structural mechanism of iGluR gating. Studies in AMPA receptors showed that when the agonist binds to the LBD and the domain closes around the agonist, the interface between subunits, aptly named the dimer interface,

forms new contacts that stabilize the state (Figure 1.6). The conformational changes at the LBDs pull on the linkers to the TMD to open the channel. Much early work was done on AMPA receptors, and in the AMPA receptor, only two subunits need to be bound to agonist for the channel to activate, corresponding to the lowest subconductance state (Rosenmund, Stern-Bach et al. 1998). Subsequent binding of a third and fourth agonist to their respective subunit results in activation of the receptor to two additional subconductance states (Rosenmund, Stern-Bach et al. 1998). Eventually, the dimer interface contacts rupture, and although the LBDs remain closed around the agonist, the channel is closed, a state called the desensitized state. A mutation in the dimer interface of the AMPA receptor, Leu483Tyr, eliminates desensitization because the tyrosine aromatic rings stack together and stabilize the LBD dimer interface to where it does not break in the continual presence of agonist (Stern-Bach, Russo et al. 1998, Robert, Irizarry et al. 2001). The compound cyclothiazide, which binds at the AMPA receptor dimer interface, similarly prevents the receptor from desensitizing by stabilizing the dimer interface in the continual presence of agonist (CM 1993, Trussell, Zhang et al. 1993, Partin, Patneau et al. 1994). The time course for the entry into desensitization is 18-34 msec, and the receptors desensitize almost completely (Indira and Trussell 1992, Robert, Irizarry et al. 2001). The entry into desensitization depends on the subtype composing the AMPA receptor and also on whether the receptor is recombinantly expressed or being recorded in neurons; the neuronal AMPA receptors interact with regulatory proteins that greatly influence receptor kinetics. AMPA receptors recover from desensitization with a τ_{rec} on the order of milliseconds, but the actual time constant varies with the subtype forming the receptor (Raman and Trussell 1995, Robert and Howe 2003). AMPA receptors desensitize from the closed state, and binding of one glutamate to one subunit is sufficient to desensitize the receptor (Robert and Howe 2003).

NMDA receptors activate in a similar fashion to AMPA receptors, but they require two agonists, glutamate and either glycine or D-serine, because the receptors are obligate heterotetramers. Unlike the AMPA receptor, all four ligands, two glutamates and two glycines, need to bind in order for the channel to open. Also, the NMDA receptor desensitizes to a much lesser degree than the AMPA receptor, and on a much slower time scale (Table 1.1). The role of the dimer interface in NMDA receptor gating remains poorly understood, and experiments targeting the dimer interface yield interesting and sometimes conflicting results. Cross-links that are intended to stabilize the NMDA receptor dimer interface instead result in a reduction in the peak current elicited in a patch and the receptors still desensitize (Borschel, Murthy et al. 2011). Additionally, the cross-links across the LBDs result in a decrease in agonist affinity (Gielen, Le Goff et al. 2008). Further, no mutation or pharmacological agent has been discovered that completely eliminates desensitization exists as has been found for AMPA receptors. The kinetics of desensitization when the receptor include the GluN2A subtype also

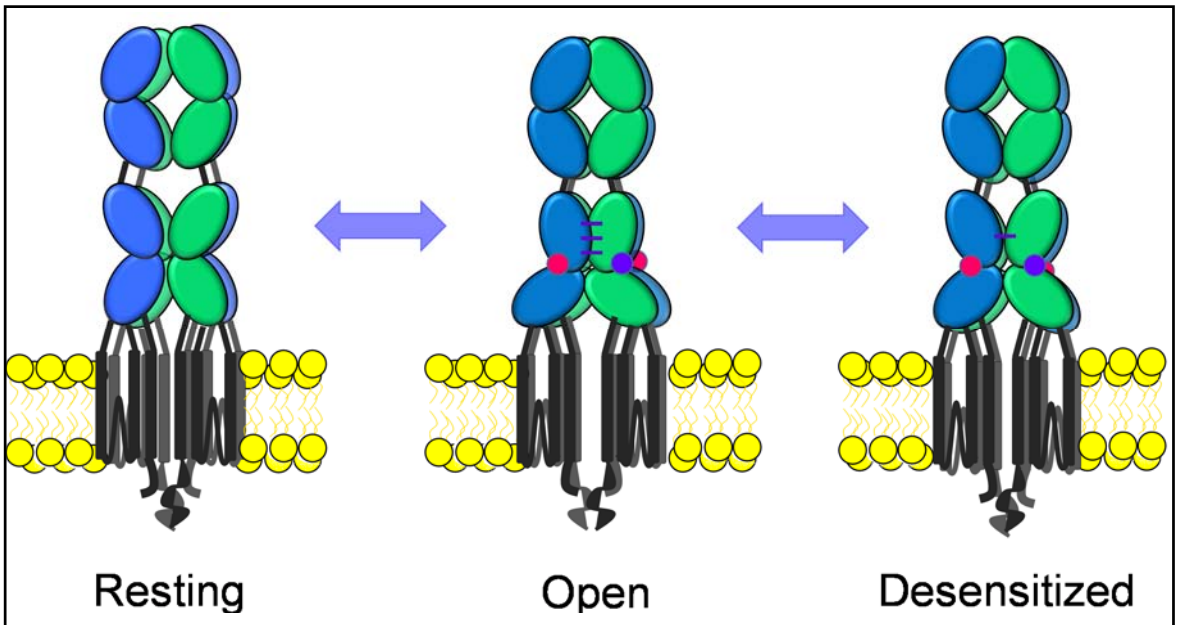

Figure 1.6: Schematic of iGluR gating. Upon binding of the agonists to the LBDs, the domain closes around the agonist, the dimer interface forms new contact, and the pore of the channel is opened. Eventually, the dimer interface ruptures and, although the agonists are bound and the domain is closed around the agonist, the channel is closed.

depend on the extracellular zinc concentrations, as zinc increases the rate of desensitization (Erreger and Traynelis 2008).

The LBD-TMD linkers play a role in gating because they propagate the conformational changes induced by agonist binding at the LBD to open the pore of the receptor. Recent work has demonstrated that inserting a single glycine residue in the M3-S2 linker is enough to decouple conformational changes at the LBD from the TMD, resulting in an inability to efficiently open the pore of the receptor (Kazi, Dai et al. 2014). The TMD is composed of three transmembrane helices (M1, M3, and M4) and a reentrant pore loop (M2). The M3 helices, one from each subunit, come together to form the pore of the channel. M4 connects to the intracellular CTD. A residue at the base of the M3 helix of GluN2 subunits has been identified which confers sensitivity to magnesium pore block and dictates single channel conductance and calcium permeability (Retchless, Gao et al. 2012). In GluN2A and GluN2B subunits, this residue is a serine (residue 632 and 633, respectively). GluN2A and GluN2B subunits have higher affinity for magnesium, higher

	GluN2A	GluN2B	GluN2C	GluN2D
P_{open}	0.61 ± 0.05	0.20 ± 0.03	0.032 ± 0.015	0.012 ± 0.002
Glutamate EC_{50} (μM)	3.3	1.3	0.8	0.35
Glycine EC_{50} (μM)	1.1	0.18	0.14	0.23
Deactivation (ms)	40 ± 4, 560 ± 140 (15)	310 ± 30, 1100 ± 190 (40)	110 ± 30, 310 ± 35 (50)	2100 ± 150, 5700 ± 510 (53)
MOT (ms)	8.3 ± 0.8	5.1 ± 0.4	0.35 ± 0.07	0.42 ± 0.037
MCT (ms)	5.1 ± 0.7	37 ± 6	24.3 ± 10.6	24 ± 5.6
Rise Time (ms)	7.4 ± 0.7	11.6 ± 1.2	3.9 ± 0.4	4.4 ± 0.59
Rate of Entry into Desensitization (ms)	59.9, 257	142, 888	59, 720	N.D.
ΔATD Po	0.006 ± 0.003	N.D.	N.D.	0.065 ± 0.015
Zinc IC_{50}	16 nM	760 nM	18 μM	9.2 μM

Table 1.1: Properties of NMDA receptors. Kinetics of gating and sensitivity to modulators vary based on the GluN2 subtype. Values were taken from the following papers: (Erreger, Dravid et al. 2005, Rachline, Perin-Dureau et al. 2005, Erreger and Traynelis 2008, Gielen, Retchless et al. 2009, Yuan, Hansen et al. 2009, Mullasseril, Hansen et al. 2010, Talukder and Wollmuth 2011, Amico-Ruvio, Paganelli et al. 2012, Vance, Hansen et al. 2013, Khatri, Burger et al. 2014). N.D. Not Determined

single channel conductance, and greater calcium permeability. However, in GluN2C and GluN2D subunits, the residue is a leucine. These receptors have a lower affinity for magnesium, low single channel conductance, and less calcium permeability (Retchless, Gao et al. 2012). The serine residue in GluN2A/B interacts with Trp608 in the GluN1 subunit and effects receptor properties by this interaction rather than by direct interaction with permeating

ions (Retchless, Gao et al. 2012). Additionally, by using the substituted cysteine accessibility method, many exposed residues in the TMD were identified, and changes due to binding of an agonist results in different accessibilities (Talukder, Borker et al. 2010).

1.6 Gating Kinetics

Kinetic studies of iGluR gating reveal that there are several kinetic steps that the receptor goes through after binding the agonists but prior to activation of the channel. Several kinetic models have been proposed to explain NMDA receptor gating. Additionally, the activated NMDA receptor undergoes modal gating: while the channel is open, the channel will vary between three different 'modes' of activation corresponding to different lifetimes of open states (Popescu and Auerbach 2003). The three modes of activation were identified and named high, medium, and low. Only transitions between adjacent states (high-medium, medium-low, and vice versa) were identified. These states have lifetimes on the order of milliseconds and occur within a burst from an individual channel. Recordings from NMDA receptors in neurons show that these receptors also undergo modal gating (Zhang, Howe et al. 2008). The physiological purpose of modal gating is still largely unknown.

Open probability, the chance that the channel is open at any given time, varies based on the type of GluN2 subunit (Chen, Luo et al. 1999, Erreger, Dravid et al. 2005). Receptors containing the GluN2A subtype have the highest Po (0.61 ± 0.05), the GluN2B subtype confers intermediate Po (0.20 ± 0.03), and GluN2C and GluN2D containing receptors have low Po (0.032 ± 0.015 and 0.012 ± 0.002, respectively) (Table 1.1). Also given in Table 1.1 are various kinetic parameters of the NMDA receptor for each of the GluN2 subtypes. The desensitization rate of GluN2D receptors has not been quantified because the GluN2D containing receptors do not desensitize (<10%) [8]. GluN2A and GluN2B containing receptors have a high main conductance state of ~50 pS, with a subconductance state of ~37 pS [63].

GluN2C and GluN2D containing receptors have a lower main conductance state of ~37 pS and a subconductance state of ~18 pS [63].

1.7 Cooperativity between ATD and LBD

As mentioned above, the GluN2 ATD dictates open probability, glutamate EC_{50}, glycine EC_{50}, and deactivation kinetics (Zheng, Erreger et al. 2001, Erreger and Traynelis 2005, Madry, Mesic et al. 2007, Gielen, Retchless et al. 2009, Yuan, Hansen et al. 2009). Studies where chimeric receptors were made so that the ATD of GluN2 subunits were switched to the ATD of other subtypes showed that the kinetics matched those of the subunit which contributed the ATD. Further, deletion of the ATD alters kinetics. In GluN2A subunits, the Po is significantly decreased when the ATD is deleted. GluN2B containing receptors, which have an inherently lower Po, do not have a significantly different Po when the ATD is deleted. The structural link between the ATD and LBD remains unknown. The recent crystal structures reveal a quite compact arrangement of the subunits with more extensive direct contacts between the ATD and LBD layers than previously anticipated based on the structure of the AMPA receptor, although the constructs used to generate these crystal structures had several deletions in the ATD-LBD linker which may have artificially increased the interface between the ATD and LBD layer, as seen recently in the AMPA receptor (Sobolevsky, Rosconi et al. 2009, Meyerson, Kumar et al. 2014).

Several links have been established between the ATD and LBD. The binding of allosteric inhibitors zinc or ifenprodil to the ATD increases the receptor's affinity for the agonists. In the case of allosteric inhibition, this is especially interesting when the inhibitor is thought to push the receptor to the desensitized state, because the AMPA receptor has increased affinity for the agonist in the desensitized state. This similarity suggests that the inhibitors do indeed push the receptor a desensitized state, at least structurally. However, the link extends beyond desensitization, because the potentiator spermine also increases the

affinity for the agonists. Binding of zinc to the ATD of the NMDA receptor results in an increase in the affinity of the agonists glutamate and glycine. The coooperativity also exists in reverse; binding of NMDA to the receptor increases the apparent affinity of ifenprodil to the NMDA receptor (Kew, Trube et al. 1996).

1.8 Functions of the CTD

The CTD of NMDA receptors is rather large, especially as compared to that of other glutamate receptors, and is thought to be intrinsically disordered (Choi, Kazi et al. 2013). The CTD is involved in trafficking, synaptic localization, anchoring to the post-synaptic density, and can modulate receptor function via phosphorylation and protein-protein and protein-lipid interactions (Traynelis, Wollmuth et al. 2010). Proteins including α-actinin, calmodulin, CaMKII, and PSD-95 bind to the CTD (Ehlers, Zhang et al. 1996, Merrill, Malik et al. 2007). The CTDs are phosphorylated by the kinases CaMKII, PKA, PKC, and Src (Maki, Program et al. 2013, Wang, Guo et al. 2014). Recent studies have shown that post-translational modifications at the CTD can influence conductance and decay kinetics (Maki, Aman et al. 2012, Maki, Program et al. 2013). Phosphorylation of the CTD can reduce the extent of zinc inhibition (Zheng, Gingrich et al. 1998). Also, calcium that enters the cell through the activated NMDA receptor, binds to calmodulin, which binds to the CTD of GluN1 subunits and causes calcium dependent inactivation of the receptor (Ehlers, Zhang et al. 1996, Zhang, Ehlers et al. 1998, Ataman, Gakhar et al. 2007, Merrill, Malik et al. 2007). The structural mechanism of calcium dependent inactivation is still unknown.

Chapter 2:

Allosteric Modulators of the NMDA Receptor: Zinc, Ifenprodil, and Spermine

2.1 Zinc at Synapses

In the central nervous system, the zinc cation is a specific inhibitor of several ion channels, including the NMDA receptor (Peters, Koh et al. 1987, Westbrook and Mayer 1987), the $GABA_A$ receptor (Ruiz, Walker et al. 2004), and the glycine receptor (Trombley, Blakemore et al. 2011), and can modulate kainate receptor function (Veran, Kumar et al. 2012). There was growing evidence at the time of synaptically present and released zinc, something that has now been firmly established, and the predicted concentrations range from the low nM to the high μM (Assaf and Chung 1984, Howell, Welch et al. 1984, Aniksztejn, Chraton et al. 1987, Vogt, Mellor et al. 2000, Li, Hough et al. 2001, Molnar and Nadler 2001, Ueno, Tsukamoto et al. 2002, JL 2006, Besser, Chorin et al. 2009). Conversely, there have been a few studies that suggest that zinc is not released in a fashion where it can interact with NMDA receptors on the post-synaptic neuron, but rather that zinc coats the pre-synaptic membrane (AR 2003, Kay and Tóth 2008, Nydegger, Rumschik et al. 2010). The vesicular zinc transporter ZnT3 (Palmiter, Cole et al. 1996)has been found at glutamatergic synapses, suggesting that zinc is loaded into the same synaptic vesicles as glutamate (Sindreu, Varoqui et al. 2003). Knockout of ZnT3 results in mice that are more susceptible to seizures due to an excess of excitatory transmission . Furthermore, mice with a knock-in mutation rendering GluN2 subunits insensitive to zinc are hypersensitive to pain, suggesting that zinc does indeed have a physiological synaptic role (Nozaki, Vergnano et al. 2011) and does travel across the synaptic cleft.

2.2 Zinc Inhibition of NMDA receptors

Zinc is a voltage-dependent and a voltage-independent inhibitor of the NMDA receptor (Paoletti, Ascher et al. 1997). Zinc pore-blocks the receptor at negative membrane potentials. Mutations to the pore, including residues N616 in GluN1, N595 in GluN2A, N615 in GluN2A, and N614 in GluN2A, result in a loss of zinc pore-block (Paoletti, Ascher et al. 1997, Hatton

and Paoletti 2005, Amico-Ruvio, Murthy et al. 2011). Zinc binds to and inhibits all subtypes of the GluN2 subunit in a voltage-independent fashion, with highest affinity for the GluN2A subtype, intermediate affinity for the GluN2B subtype, and low affinity for the GluN2C and GluN2D subtypes (Rachline, Perin-Dureau et al. 2005). The zinc binding site is composed of histidines and aspartates in the cleft between the upper and lower lobes of the GluN2 ATD. In the GluN2A ATD, two histidines in particular were identified as crucial to the zinc binding site, His42 and His44 (Choi and Lipton 1999, Fayyazuddin, Villarroel et al. 2000); these residues are not conserved in the GluN2B subtype. Additionally, His127 and Asp283 are important to zinc binding, and these residues are conserved in GluN2B (His128 and Asp284 in GluN2B) (Rachline, Perin-Dureau et al. 2005, Karakas, Simorowski et al. 2009). Zinc incompletely inhibits receptors composed of the GluN2A subunits, with maximal inhibition ranging from 40-80% (Paoletti, Ascher et al. 1997, Choi and Lipton 1999, Paoletti, Perin-Dureau et al. 2000, Rachline, Perin-Dureau et al. 2005). Diheteromeric receptors containing the GluN2B, GluN2C, or GluN2D subunits are inhibited completely by saturating concentrations of zinc (Rachline, Perin-Dureau et al. 2005). The incomplete inhibition of GluN2A subunits, which are the most common, coupled with the co-release of zinc with glutamate suggests that zinc helps fine tune the final signal transmitted between neurons during normal synaptic transmission.

Mechanistic work studying the nature of zinc inhibition found that the stability and conformation of the ATD influences the Po of the receptor in general. The best supported mechanism of zinc inhibition is that zinc inhibits by modifying the conformation of the ATD, which allosterically destabilizes the gating machinery of the receptor. Cross-linking reagents used to wedge open the cleft of the ATD showed that if the ATD cleft was more open, the receptor was potentiated. The mechanism suggested was that by opening and closing the ATD cleft, zinc affected the stability of the dimer interface of the LBDs (Gielen, Le Goff et al.

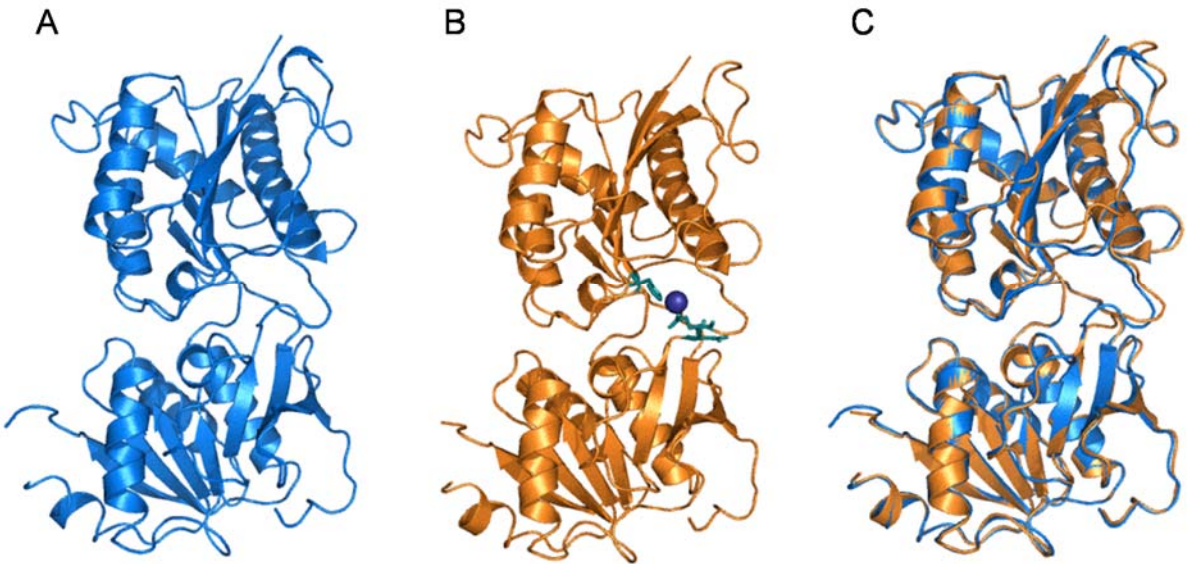

Figure 2.1: Structures of the isolated GluN2B ATD. Shown are crystal structures of the GluN2B ATD without (A) and with (B) zinc bound, PDB IDs 3JPY and 3JPW, respectively. The residues highlighted in (B) are His128, Asp284, and Glu285 which coordinate zinc binding. In panel C, the two crystal structures are aligned to each other. Both structures, although one has zinc bound, captured the same structural state of the ATD. They align with an RMSD of 0.368 Å.

2008). It was hypothesized that an open ATD cleft led to a greater activation of the receptor (higher Po), whereas the receptor was inhibited when the cleft was closed (lower Po). Structural advances have allowed us to visualize zinc in its binding site in the GluN2B ATD. The cleft closure mechanism suggested by functional studies was not present in the crystal structures, as the zinc-free structure of the ATD matched to the zinc-bound structure (Karakas, Simorowski et al. 2009). The zinc-bound and zinc-free ATD structures aligned to each other with an RMSD of 0.368 Å (Karakas, Simorowski et al. 2009); both structures captured the closed-cleft conformation (Figure 2.1). The crystal structure, however, confirmed that in GluN2B subunits, the zinc binding site was composed of His128, Asp283, and Glu284 (Karakas, Simorowski et al. 2009).

Work by the Paoletti lab identified the ligand-binding domain dimer interface, the same interface identified as critical to gating of the AMPA and NMDA receptor, as an important player in the mechanism of zinc inhibition (Gielen, Le Goff et al. 2008). Disrupting the

hydrophobic interface at the ligand-binding domains shifts the zinc dose response curves (reduces IC_{50}) (Gielen, Le Goff et al. 2008). Conversely, stabilizing the LBD dimer interface by the introduction of cysteine crosslinks results in a decreased ability of zinc to inhibit the receptor.

Zinc was shown to have a very slow unbinding rate, on the order of milliseconds (Paoletti, Ascher et al. 1997). Single-channel analysis of GluN1/GluN2A NMDA receptors shows that zinc-bound receptors still proceed through modal gating (Amico-Ruvio, Murthy et al. 2011), but the open state of the receptor is less stable resulting in shorter openings and a lower open probability (Erreger and Traynelis 2008, Amico-Ruvio, Murthy et al. 2011).

2.3 Ifenprodil inhibition

Ifenprodil, a member of the class of phenylethanolamines, was identified as an inhibitor of the NMDA receptor about 25 years ago. Ifenprodil underwent clinical trials as an NMDA receptor antagonist but failed due to significant off-target effects (Chizh, Headley et al. 2001). However, ifenprodil inhibition is still widely studied because it provides insight into subtype specific inhibition of the NMDA receptor. For instance, ifenprodil has been conjugated to fluorescent probes to allow for the specific detection of GluN2B subunits in cells (Williams 1993, Marchand, Becerril-Ortega et al. 2012). Ifenprodil (Figure 2.2) has two ionizable functional groups: a tertiary nitrogen with a pKa of 9.05 and a phenolic hydroxyl with a pKa of 9.66; ifenprodil carries a positive charge on its tertiary nitrogen group at physiological pH (Kobayashi, Washiyama et al. 2006). The binding site remained elusive for some time, with many studies identifying residues within the ATD as important to ifenprodil inhibition (Williams 1993, Gallagher, Huang et al. 1996, Masuko,

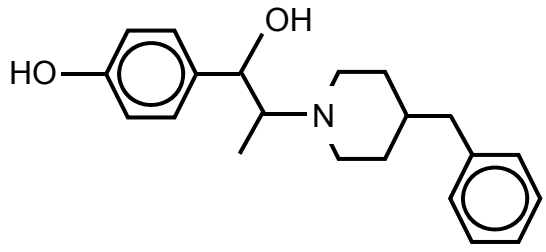

Figure 2.2: Structure of Ifenprodil.

Kashiwagi et al. 1999, Perin-Dureau, Rachline et al. 2002, Mony, Krzaczkowski et al. 2009). Most recently, the crystal structure of the soluble GluN1-GluN2B ATD dimer showed that ifenprodil bound at the interface between the two subunits' ATDs (Karakas, Simorowski et al. 2011). Contacts with both subunits are critical to ifenprodil inhibition (Karakas, Simorowski et al. 2011). Residues identified as crucial to ifenprodil binding in the crystal structure include Ile82, Gln110, Ile111, and Phe114 in GluN2B and Ala75, Phe113, and Leu135 in GluN1 (Karakas, Simorowski et al. 2011, Tomitori, Suganami et al. 2012). An analog of ifenprodil, Ro25-6981, was also found to bind to the same pocket between the ATDs (Karakas, Simorowski et al. 2011). Given that many residues were identified that affect ifenprodil binding, it is possible those mutations affected the electrostatics of the receptor, the proton binding sites, or somehow altered the conformation of particular regions of the ATD resulting in a shift in ifenprodil inhibition (Gallagher, Huang et al. 1996, Karakas, Simorowski et al. 2009, Mony, Krzaczkowski et al. 2009, Tomitori, Suganami et al. 2012). Cross-linking studies suggest that the mobility of the lower lobes of the ATDs is critical to ifenprodil's ability to inhibit the NMDA receptor (Karakas, Simorowski et al. 2011).

Functional analyses of single channels showed that ifenprodil reduces the open probability of the NMDA receptor by increasing the barrier to activation (Amico-Ruvio, Paganelli et al. 2012). Receptors bound by ifenprodil also had longer MCTs and shorter MOTs (Amico-Ruvio, Murthy et al. 2011). Taken together, these data suggests that the binding of ifenprodil to the ATDs and the ensuing conformational movements of the lower lobes of the ATDs destabilize the gating machinery of the receptor, similar to zinc binding. However, direct structural evidence of the conformational changes associated with ifenprodil inhibition are still lacking. The crystal structure of the apo GluN2B ATD (PDB ID 3JPW), aligns to the GluN2B ATD in the dimeric GluN1/GluN2B ATD structure (PDB ID 3QEL) with an RMSD of 0.618,

further demonstrating that the crystal structures are only capturing one of the states that the ATDs can adopt.

2.4 Spermine Potentiation

Another endogenous modulator of the NMDA receptor, the polyamine spermine, has several effects on receptor function depending on its interaction site. Each spermine molecule has four amine groups (Figure 2.3), two primary and two secondary, that are all protonated at physiological pH, (has four amino groups with pKa values of 10.9, 10.1, 8.9, and 8.1) so spermine carries several positive charges (Palmer and Powell 1974, Geall, Taylor et al. 2000, Woster and University 2006). Spermine has many known roles in cellular processes throughout the body (Morgan 1999), and in the central nervous system intracellular spermine in neurons pore blocks ion channels. Spermine can pore block the NMDA receptor in a subtype-independent manner. There is evidence that spermine is also released into the synapse in an activity dependent fashion (Masuko, Kusama-Eguchi et al. 2003), so that spermine can be an extracellular modulator of the NMDA receptor during normal synaptic transmission. Spermine binding to the extracellular side of the NMDA receptor potentiates responses elicited by the agonist, with specificity for GluN2B subtypes of the NMDA receptor.

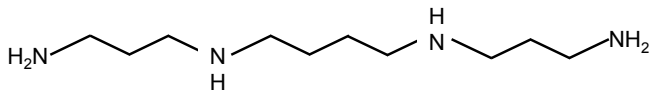

Figure 2.3: Structure of Spermine.

Spermine is thought to bind at the interface between the lower lobes of the GluN1 and GluN2B ATDs. Deletion of either the GluN1 or GluN2B ATD results in a loss of spermine potentiation, supporting the idea that spermine binds at the interface between the two ATDs (Mony, Zhu et al. 2011). Mutating acidic residues in the lower lobes of the GluN1 or GluN2B ATDs to basic residues results in a loss of spermine potentiation (Masuko, Kashiwagi et al. 1999, Mony, Zhu et al. 2011). The basic residues are likely unable to bind to the positively charged spermine. Splice variants of GluN1

that contain exon 5, which sits in the lower lobe of the ATD, are insensitive to spermine potentiation, even when the receptor is composed of GluN2B subunits. Exon 5 adds six basic residues to the lower lobe of the GluN1 ATD, suggesting that the positive charges introduced by exon 5 function similarly to spermine and obviate the spermine binding site (Durand, Bennett et al. 1993, Traynelis, Hartley et al. 1995). Spermine binding to the extracellular portion of the NMDA receptor also results in an increase in apparent glycine affinity (K., Zappia et al. 1994). Independent of the effect on glycine affinity, spermine increases the frequency of channel openings in single channel recordings from neurons (Rock and MacDonald 1992).

When a bulky thiol-reactive group is bound within the GluN2B cleft, Mony, et al., showed that spermine no longer potentiates the receptor, suggesting that spermine stabilizes an open-cleft conformation of the GluN2B ATD (Mony, Zhu et al. 2011). If the cleft is already propped open, spermine cannot do any more to the receptor. Spermine seems to potentiate the receptor by employing the opposite mechanism of zinc, which inhibits the receptor by closing the ATD cleft. Since spermine binds at the GluN1/GluN2B interface at the ATDs and specifically potentiates receptors that contain GluN2B, one possible explanation of the specificity is that there is something unique about the GluN1/GluN2B ATD dimer interface that allows for the specificity. Another possibility is that GluN2B containing receptors have an inherent structural feature, including the opening of the bi-lobed ATD cleft, that is unique and allows spermine to potentiate the receptor. GluN2A containing receptors could have a more open ATD cleft to begin with, potentially explaining why spermine does not potentiate and why GluN2A containing receptors have inherently higher open probabilities. Chimeras that swap the ATDs of GluN2A and GluN2B confirm that the specificity of binding is to the GluN2B ATD. Interestingly, as noted when studying zinc inhibition, swapping the linker that connects the ATD to the ligand binding domain is necessary to fully swap the function of the subunit to that of its counterpart (Gielen, Retchless et al. 2009, Mony, Zhu et al. 2011). Spermine potentiation

proceeds by stabilizing the open state of the receptor, reducing the rate of entry into desensitization, and increasing the rate of recovery from desensitization (Rumbaugh, Prybylowski et al. 2000).

2.5 Proton Inhibition

Synaptic transmission is known to change pH at the synaptic cleft. When neurotransmitters are initially released, there is a slight acidification of the synaptic cleft, followed by a slight alkilination. Proton concentrations are tightly regulated and important at the synapse because proton gradients are necessary to the process of loading neurotransmitters into synaptic vesicles. The pH changes on the order of 0.1-0.2 units, changes that are enough to alter the function of the NMDA receptor. Protons inhibit the NMDA receptor (Giffard, Monyer et al. 1990, Tang, Dichter et al. 1990, Traynelis and Cull-Candy 1990, Traynelis and Cull-Candy 1991), and the proton IC_{50} is at physiological pH (Traynelis, Hartley et al. 1995). Many studies have tried to identify the proton sensor, and tens of residues have been identified throughout the GluN1 and GluN2 subunits, including exon 5 of GluN1 (Traynelis, Hartley et al. 1995, Keiko, Fukuchi et al. 1996, Low, Lyuboslavsky et al. 2003). Some of the residues identified do not have ionizable side chains, suggesting their mutation disrupts coordination of water or other properties of the receptor. Deletion of the ATD does not abolish proton inhibition, although it does shift the IC_{50} (Gielen, Retchless et al. 2009).

Proton inhibition of the NMDA receptor is closely tied to modulation of the receptor by zinc, ifenprodil, and spermine (Mott, Doherty et al. 1998, Traynelis, Burgess et al. 1998, Mony, Zhu et al. 2011). The NMDA receptor is more greatly inhibited by zinc and ifenprodil at lower pHs, suggesting that zinc and ifenprodil sensitize the receptor to protons (Traynelis, Burgess et al. 1998, Low, Zheng et al. 2000). Ifenprodil inhibits less at more alkaline pHs, although it is still able to bind (Mott, Doherty et al. 1998). Conversely, spermine potentiates the receptor more at lower than at higher pHs, suggesting that spermine potentiates the receptor by

relieving proton inhibition. It remains unclear what the structural mechanism is that links these processes. It is possible that the binding of protons modifies the overall surface electrostatic charges on the surface of the receptor, thereby altering the environments of the binding sites of the other modulators. Binding of the other modulators could reverse this shift, in addition to the conformational changes they are known to induce. The residue H128 in GluN2A has been shown to affect both zinc inhibition and proton inhibition of the receptor (Low, Zheng et al. 2000). This residue is potentially a link between the zinc and proton binding sites.

2.6 The Role of the GluN1 ATD

The GluN1 ATD is important to allosteric modulation of the NMDA receptor, although there are no known ligands that bind only to the GluN1 ATD. Deletion or cleavage of the GluN1 ATD results in decreased zinc inhibition of NMDA receptors composed of GluN2A or GluN2B subunits (Madry, Mesic et al. 2007). Further, deletion of the GluN1 ATD abolishes spermine potentiation of the receptor. The GluN1 subunit, as mentioned above, can be one of eight splice variants. Exon 5 is in the lower lobe of the GluN1 ATD, is 21 amino acids long, and has six basic residues. The sequence of exon 5 is 'SKKRNYENLDQLSYDNKRGPK'. The inclusion of exon 5 greatly alters the affinity to allosteric modulators. The zinc and proton dose-response curves for GluN1-GluN2B receptors are right-shifted when exon 5 is included, meaning that zinc and protons have a lower affinity for the GluN2B subunit (Traynelis, Hartley et al. 1995, Traynelis, Burgess et al. 1998). As mentioned above, spermine no longer potentiates the receptor when exon 5 is included in GluN1. Mutations in GluN1 have been identified that shift ifenprodil and pH IC50s, solidifying both a role for GluN1 in allosteric modulation and a link between proton and ifenprodil modulation (Mott, Doherty et al. 1998).

The fact that GluN1 ATD deletion results in abolished zinc inhibition is particularly interesting given that the zinc binding site is entirely contained in the GluN2 ATD and that zinc binding has been found to influence glutamate affinity but not glycine affinity in GluN2A

containing receptors (Zheng, Erreger et al. 2001, Erreger and Traynelis 2005). However, deleting either the GluN1 or GluN2B ATD in a GluN1/GluN2B diheteromeric receptor reduces glycine potency (Madry, Mesic et al. 2007). Propping open the GluN1 ATD results in a potentiation of the GluN1/GluN2B receptor (Zhu, Stroebel et al. 2013), suggesting that the GluN1 ATD is flexible and its conformational state can influence that of the receptor as a whole. Despite the lack of ligands binding solely to the GluN1 ATD, it is plausible that the GluN1 ATD is critical to the mechanism of modulation, if only to serve as a wedge that holds the GluN2 ATD in a particular state. Modulators such as ifenprodil and spermine, which bind at the interface of the GluN1/GluN2B ATDs, may directly alter the conformation of the GluN1 ATD, a question that remains unanswered. The contacts that could form between the GluN1 and GluN2 ATDs during modulation could be critical to stabilizing a particular state and effecting modulation.

2.7 Allosteric Modulation and Its appeal for subtype specific pharmacology and drug design – Rationale behind project

NMDA receptors, as mentioned above, play an integral role in learning and memory formation. Aberrant activation of NMDA receptors is implicated in a variety of neurological disorders. NMDA receptor overactivation during ischemic stroke leads to neurotoxicity and neuronal cell death. NMDA receptor hypoactivation is implicated in schizophrenia. NMDA receptor dependent neurotoxicity is also implicated in Huntington's disease, Alzheimer's disease, Parkinson's disease, depression, and neuropathic pain (reviewed in (Traynelis, Wollmuth et al. 2010)), although the exact mechanism of involvement in these conditions remains largely unknown. Given the variable expression of different subtypes of the GluN2 subunits, many in the field have focused on subtype specific modulators as a promising avenue for drug design. The hope is that subtype specific modulation will inhibit or potentiate specific receptors in a disease state without impacting normal synaptic transmission.

Ifenprodil, a synthetic compound, was discovered to be a GluN2B specific NMDA receptor inhibitor in the late 1980s (C., Benavies et al. 1988). Ifenprodil failed clinical trials due to significant binding and inhibition of cardiac calcium channels (Chizh, Headley et al. 2001). However, ifenprodil has remained a popular subject of study in attempts to understand the structural and functional mechanism of inhibition. Further, modulators that bind to any part of the receptor in a subtype specific fashion remain the subject of intense study for this exact reason. Given that NMDA receptors exist predominantly as triheteromeric species (Tovar, McGinley et al. 2013), combining two GluN2 subtypes, subtype specific modulators may indeed provide a fine-tuning of NMDA receptor signaling without modulating signaling as a whole. This rationale motivates our experiments to understand the structural mechanism of allosteric modulation of the receptor, in hopes that if we understand the structural mechanism, we could identify hot-spots of the receptor that could be targeted by future drug design attempts.

Within the hippocampus, the region of the brain responsible for memory formation and consolidation, GluN2A is the most prevalent subtype, as mentioned above, and it was at hippocampal neurons that it was discovered that zinc was released in an activity dependent fashion. As such, it is very physiologically relevant to study zinc inhibition as these receptors are likely inhibited at the same time that the receptor is being activated. After studying zinc inhibition, we wanted to determine if the structural mechanism of zinc inhibition was generalizable to other allosteric inhibitors that bind to other sites on the ATD or if it was dependent on zinc binding within the cleft of the ATD. To answer this question, we looked at ifenprodil inhibition of receptors composed of the GluN2B subunit. By switching to the GluN2B subunit, we could compare allosteric inhibition of different subtypes (GluN2A vs. GluN2B) and for inhibitors with different binding sites (zinc vs. ifenprodil). Moreover, as explained above, the mechanism of spermine potentiation is poorly understood, except that it is thought to

proceed in the opposite structural mechanism of zinc inhibition. We are aptly situated to address these questions using a combination of fluorescence spectroscopy to characterize structural changes and functional studies to correlate structure to function.

Chapter 3:
Theory Underlying Luminescence Resonance Energy Transfer (LRET)

The text and figures of this chapter are modified and reprinted with permission from a book chapter which is in press: Sirrieh, R. E. and V. Jayaraman (2015). LRET Methods for Investigating Conformational Changes in Functional Glutamate Receptors. *Ionotropic Glutamate Receptor Technologies.* G. K. Popescu, Springer Business + Science Media.

Luminescence resonance energy transfer (LRET) was used extensively to monitor conformational changes induced by ligand binding and to characterize inherent structural conformations. LRET is an invaluable tool to study the conformational changes of proteins induced by ligands or protein-protein interactions at Ångstrom level resolution. LRET experiments require a pair of fluorophores with overlapping spectra, where the emission of the 'donor' overlaps with the excitation of the 'acceptor' fluorophore. The efficiency of non-radiative energy transfer can be determined by measuring the sensitized emission of the acceptor fluorophore, upon exciting the donor fluorophore. The efficiency of transfer, in turn,

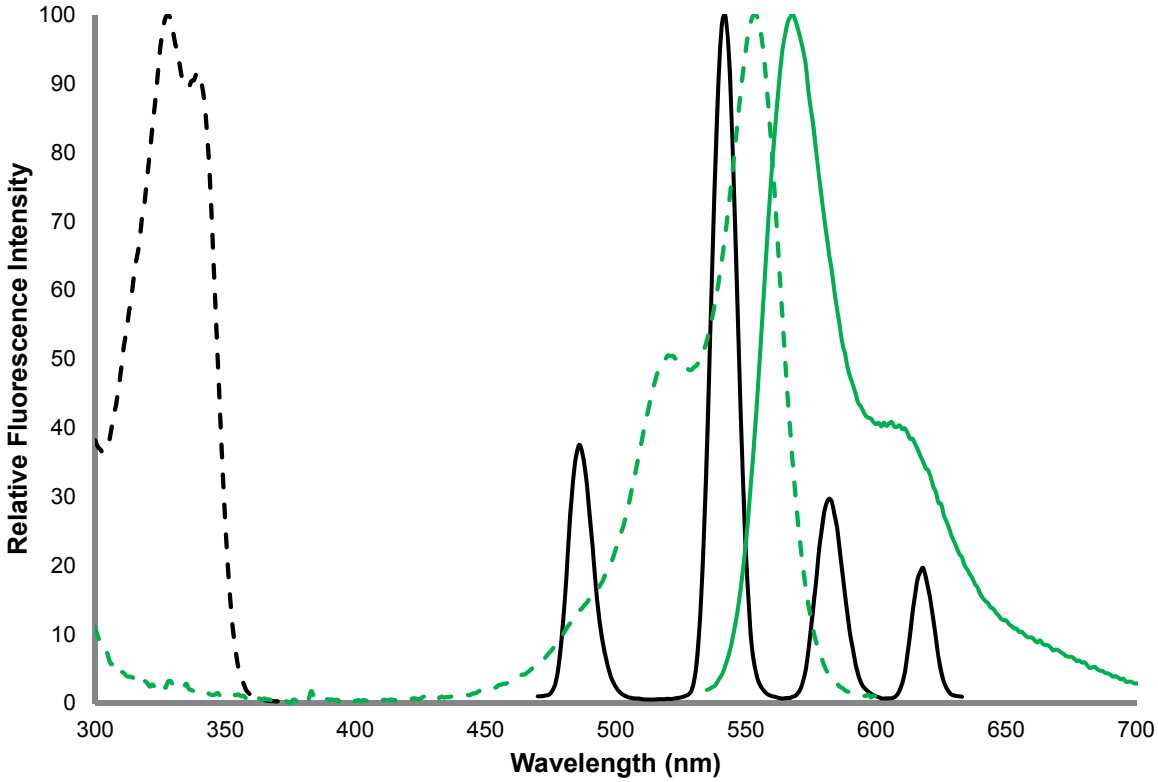

Figure 3.1: LRET requires fluorophores with overlapping spectra. Shown are the excitation and emission curves of terbium chelate in dashed and solid black lines, respectively. The excitation and emission peaks of Alexa555 are shown in dashed and solid green lines, respectively. In order for LRET to occur, the emission of the donor, terbium chelate, and the excitation of the acceptor, Alexa555, must overlap. The integral of the overlap between the two curves is called the overlap integral and is required to calculate the R_0 for the pair of fluorophores.

can be correlated to the distance between the two fluorophores. A modification of the LRET technique, whereby the LRET lifetime is measured before and after protease cleavage of the receptor, allows for the quantification of background fluorescence and for measurements to be made in functional receptors expressed in mammalian cells (Prithwish Pal, Brian E. Holmberg et al. 2005, Gonzalez, Rambhadran et al. 2008, Rambhadran, Gonzalez et al. 2011, Sirrieh, MacLean et al. 2013). The specific LRET lifetime that can be measured in this system can be used to describe conformational changes associated with gating, allosteric modulation, inhibition, partial agonism, protein-protein interactions, and inter-subunit interactions associated with motions of the receptor. By subsequently coupling this technique with functional characterization of the receptor, a direct connection can be drawn between structural changes and the functional consequences.

LRET is a modification of fluorescence resonance energy transfer (FRET) which relies on the same underlying principle of non-radiative energy transfer between a pair of fluorophores dependent on the distance between the two fluorophores (Forster 1946, Stryer and Haugland 1967). Essentially, two fluorescent molecules with overlapping spectra, where the emission spectrum of the 'donor' overlaps with the excitation spectrum of the 'acceptor,' are introduced at particular sites on a macromolecule (Figure 3.1). The efficiency of energy transfer between these two fluorescent molecules can be directly correlated to the distance between the fluorophores using the Förster equation (Forster 1946) (Eq. 3.1), where R_0 is the distance at which there is 50% energy transfer between the two fluorophores, τ_D is the lifetime of the donor in the absence of the acceptor, and τ_{DA} is the sensitized acceptor lifetime. The temporal resolution afforded by luminescence allows for the separation of the LRET lifetime (on the order of microseconds) from receptors labeled only with acceptors (on the order of nanoseconds) and receptors labeled only with donors (on the order of milliseconds).

Equation 3.1 $$R = R_0 \left[\frac{\tau_{DA}}{\tau_D - \tau_{DA}}\right]^{1/6}$$

Distances that can be measured with a particular pair of fluorophores technically range from $0.5R_0$ to $1.5R_0$ (dos Remedios and Moens 1995); therefore, the fluorophore pair should be chosen so that the distance range being measured is within this range of the R_0 (Table 4.2). Additionally, it is best to choose a pair of fluorophores so that the expected sensitized acceptor emission lifetimes are 100-500 μs. Lifetimes within this range allow you to easily subtract out background with a long lifetime due to donor bleed through (800-1500 μs) and the lifetime is not too short so that it aligns with the laser line. The laser line is an intense peak due to light scatter off the cells or bleed-through of the excitation pulse.

Fluorophore (company purchased from)	**Excitation Maximum (nm)**	**Emission Maxium (nm)**	**R_0 with Terbium chelate (Å)**
ATTO465 (Invitrogen)	453	508	35
Fluorescein (Fluka)	492	515	45
Alexa555 (Sigma Aldrich)	555	565	65
$Ni(NTA)_2$Cy3 (bis-reactive Cy3 from GE Healthcare)	550	572	65

Table 3.1: Fluorophores used in LRET experiments. Given are the names of the fluorophores used, the company from which each was purchased, the excitation and emission wavelengths, and the R_0 of the fluorophore with terbium chelate.

Equation 3.2 $$R_0^6 = \frac{8.785*10^{-5}*\kappa^2*\phi_D*J}{n^4}$$

R_0 depends on the orientation of the fluorophores (κ), the quantum yield of the donor (ϕ_D), the overlap integral (J), and the refractive index (n) (Eq. 3.2). The quantum yield of the donor is the ratio of the number of photons emitted to the number of photons absorbed. The overlap integral depends on the pair of fluorophores selected, and an example is shown in

Figure 3.1 where the overlap integral is the integral of the area beneath the overlapping curves between the solid black line and the dotted green line. The refractive index used for biological solutions is 1.4 (dos Remedios and Moens 1995). The orientation factor (κ^2) can be approximated to a value of 2/3 assuming isotropic fluorophores. The error due to this assumption is minimized as the donor terbium is isotropic. Furthermore, the error in the absolute distance can be determined by measuring anisotropy for the acceptor fluorophore. It should be noted that these errors are errors in the absolute distances. The error is further reduced when measuring changes in distances, assuming a similar distribution in the two states being measured.

LRET offers several advantages over FRET that arise from the use of lanthanides as the donor fluorophores. These lanthanides undergo forbidden f-orbital electron transitions upon excitation, and their emission is neither fluorescent nor phosphorescent (Selvin 2002). Since the excited state is still inducing an electric dipole, they can transfer energy to organic fluorophores (Selvin 2002), which we use as the acceptor fluorophores to form LRET pairs. Of the lanthanides, terbium is the most commonly used donor fluorophore. Lanthanides have a long, easily quantified donor only lifetime (Chen and Selvin 1999), four main emission peaks that can be combined with various acceptor fluorophores (Figure 3.1), and narrower emission peaks relative to broad fluorescence peaks, which allows for the investigation of changes at the acceptor wavelength with little or no bleed-through from the donor emission in the acceptor channel. Most importantly, though, as mentioned above terbium is isotropic, so the error associated with the orientation factor κ^2 (Eq. 3.2). The wide availability of maleimide-conjugated fluorophores and chelates of lanthanides has greatly facilitated specific labeling of receptors. Non-disulfide bonded cysteines in the receptor are conservatively mutated to serines so that they will not be labeled, and subsequent introduction of cysteines means that fluorophores will be bound at the sites of choice. While this labeling technique provides a

convenient and relatively straightforward method for introducing the fluorescent tags, one of the early limitations of this methodology is that proteins could not be studied in non-purified systems as other proteins on the cell surface also contain cysteines which will be labeled with the fluorophores. In order to overcome this problem we have adapted a modification to the LRET technique, wherein a protease recognition sequence is introduced in the receptor between the donor and acceptor label sites (Gonzalez, Rambhadran et al. 2008, Gonzalez, Du et al. 2010, Rambhadran, Gonzalez et al. 2010, Rambhadran, Gonzalez et al. 2011, Sirrieh, MacLean et al. 2013). Either the recognition sequence for thrombin (LVPRGS) or Factor Xa (IDGR or IEGR) is used. Measuring the LRET lifetime before and after protease cleavage thus allows for the quantitative characterization of the signal specific to the protein being investigated. The introduction of two cysteines in the receptor to be labeled means that the two cysteines will be labeled through the same binding chemistry, and there is no way to know to which site is bound to the ‘donor’ fluorophore or the ‘acceptor’ fluorophore. However, this ambiguity does not impact the experiment, because, on average, the experiment is measuring a change in the LRET signal under different ligated conditions. Once the receptors are labeled, any change in the observed lifetime has been induced by the ligand, rather than any differences in the orientation or location of the fluorophore, which remains covalently

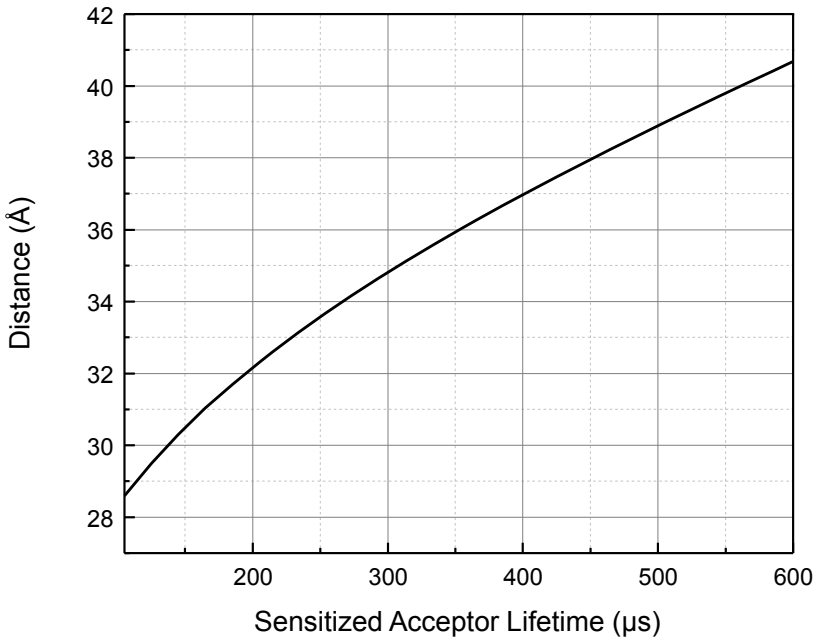

Figure 3.2: Lifetime versus distance in LRET. A representative curve of distance vs. lifetime for a pair of fluorophores with an R_0 of 45 Å highlights the direct relationship between energy transfer and distance.

bound to the same site throughout the experiment. Given the known acceptor fluorophores, when paired with terbium chelate as the donor, the distance range that can be measured with LRET is 20-90 Å. A sample curve of sensitized acceptor lifetime versus distance for an R_0 of 45 Å is shown in Figure 3.2 and was calculated by assuming a donor only lifetime (τ_D) of 1700 μs.

Chapter 4: Methods

4.1 Soluble Protein Expression and LRET Analysis

Spodoptera frugiperda (*Sf9*) cells were maintained in media supplemented with 10% FBS and penicillin/streptomycin and passaged every two days. *Sf9* cells were used to produce a baculovirus that could be used to express the soluble ATD of the NMDA receptor. Bacmid DNA containing the GluN2A or GluN2B ATD was cotransfected with BaculoGold viral DNA (BD Biosciences) into the *Sf9* cells using the Cellfectin Transfection reagent (Life Technologies). The ATD construct had retained Cys231 in GluN2A or Cys232 in GluN2B. Additionally, at the N-terminus of each construct, there had been inserted a cysteine, an octa-histidine tag, and the thrombin recognition sequence (LVPRGS). The GluN2B construct was provided by Dr. Hiro Furukawa, and the GluN2A construct was prepared using traditional PCR methods. Further, both constructs contained the human placental alkaline phosphatase secretion signal at the very N-terminus of the construct so that the synthesized protein would be secreted into the media. The initial virus (P_0 generation) was successively amplified in *Sf9* cells. *Hi5* cells were maintained in serum-free media and passaged every two days. Baculovirus generated in *Sf9* cells was used to infect *Hi5* cells. Cells were cultured to a volume of 200-300 mL and were allowed to express protein for 2 days before the media, which contained the protein, was harvested. The media was concentrated using an Ambion spin column, and the remaining solution was used for protein purification. Either a nickel column attached to an FPLC system or nickel beads were used to purify the protein via the his-tag attached at the N-terminus. Protein was maintained in 200 mM NaCl, 20 mM Tris, pH 8.0 as previously described (Karakas, Simorowski et al. 2009). SDS-PAGE was used to ensure that the protein was present and to check purity. Protein was labeled overnight at 4°C, dialyzed for 3-4 hours the following morning, and then used for the LRET experiments. The buffer used was always 200 mM NaCl, 20 mM Tris, pH 8.0.

4.2 Isothermal Titration Calorimetry

To verify that the soluble ATD protein was functional, isothermal titration calorimetry (ITC) was performed with a VP-ITC instrument (MicroCal). Two milliliters of protein at a 20 μM concentration was inserted into the chamber and titrated by 40 injections of 5 μL of 0.8 mM zinc chloride at 27 °C, as described previously (Karakas, Simorowski et al. 2009). The enthalpy change due to binding would be detected by the instrument, by measuring how much energy was required to maintain the chamber temperature.

4.3 Cloning and Mutagenesis

All full-length receptor constructs were in pcDNA3.1 vectors. To specifically label receptors with maleimide-derived fluorophores, all non-disulfide-bonded cysteines, as identified from existing crystal structures and previous work in our laboratory (18, 19), were mutated to serines: C22S and C459S for GluN1 (called GluN1*), C231S, C395S, and C461S for GluN2A (called GluN2A*), and C232S, C399S, and C495S for GluN2B (GluN2B*). Further mutations were made on these base constructs, unless an inherent cysteine was retained to be labeled. A list of all constructs and the mutations they contain is found in Table 4.1. Mutations were made using traditional PCR methods, and the integrity of the plasmid and insert were verified by sequencing. To measure distance changes in full-length receptors in intact membranes without protein purification, the thrombin (LVPRGS) or Factor Xa (IDGR or IEGR) recognition sequence was introduced between donor and acceptor fluorophores, as discussed in Chapter 3.

Construct Name	Mutations	Construct Co-expressed With	Acceptor Fluorophore
GluN1*	C22S, C459S	GluN2A^{cleft} GluN2B^{cleft}	Ni(NTA)$_2$Cy3
GluN1*^{C22}	C459S	GluN2B*^{H30} GluN2B*^{232} GluN2B*^{210} GluN2A*^{H30} GluN2A*^{231} GluN2A*^{211}	Ni(NTA)$_2$Cy3 Alexa555 Fluorescein Ni(NTA)$_2$Cy3 Alexa555 Fluorescein
GluN1^{cleft}	insertion of the amino acids LVPRGS after residue Cys22, C459S, S224C	GluN2B*, GluN2A*	Alexa555
GluN2A*	C232S, C395S, C461S	GluN1^{cleft}	Alexa555
GluN2A*^{C30}	C232S, C395S, C461S, insertion of a Cys followed by amino acids LVPRGS after residue 30	GluN1*^{C22}	Alexa555
GluN2A*^{H30}	C232S, C395S, C461S, insertion of hexa-his tag followed by amino acids LVPRGS after residue 30	GluN1*^{C22}	Ni(NTA)$_2$Cy3
GluN2A^{cleft}	C395S, C461S, insertion of hexa-his tag followed by amino acids LVPRGS after residue 30	GluN1*	Ni(NTA)$_2$Cy3
GluN2A^{DHM}	H44A, H128S, C395S, C461S, insertion of hexa-his tag followed by amino acids LVPRGS after residue 30	GluN1*	Ni(NTA)$_2$Cy3
GluN2A*^{231}	C395S, C461S	GluN1*^{C22}	Alexa555
GluN2A*^{210}	C232S, C395S, C461S, D210C	GluN1*^{C22}	Fluorescein
GluN2B*	C232S, C399S, C495S	GluN1^{cleft}	Alexa555

GluN2B*^{H30}	C232S, C399S, C495S, insertion of hexa-his tag followed by amino acids LVPRGS after residue 30	GluN1*^{C22}	Ni(NTA)$_2$Cy3
GluN2B^{cleft}	C399S, C495S, insertion of hexa-his tag followed by amino acids LVPRGS after residue 30	GluN1*	Ni(NTA)$_2$Cy3
GluN2B*^{231}	C399S, C495S	GluN1*^{C22}	Alexa555
GluN2B*^{210}	C232S, C399S, C495S, D210C	GluN1*^{C22}	Fluorescein

Table 4.1: Constructs used for experiments. Given in this table are the names of the constructs used for LRET experiments, the mutations each construct includes, the construct it was co-expressed with, and the acceptor fluorophore used for that pair of constructs.

4.4 Fluorophores

The donor fluorophore used was always terbium chelate (Invitrogen), and the acceptor fluorophores were ATTO465 (Invitrogen), Fluorescein (Fluka), Alexa Fluor 555 (Sigma-Aldrich) or Ni(NTA)$_2$Cy3. See Table 3.1 for the corresponding R_0 values with terbium chelate and the excitation and emission wavelengths. Ni(NTA)$_2$Cy3 was prepared as described previously (22) using bis-reactive Cy3 purchased from GE Healthcare. Free NTA (Dojindo Laboratories) was conjugated to the bis-reactive Cy3 dye in 0.1 M sodium carbonate. The doubly conjugated product was purified using preparative thin layer chromatography (TLC) and then conjugated to nickel. Excess nickel was removed and the final product was dried, resuspended in water, and the concentration was quantified.

4.5 Protein expression in Xenopus laevis oocytes

Full-length receptors were expressed in *Xenopus laevis* oocytes as described previously (23). *X. laevis* frogs who had been acclimated to their habitat for at least six weeks, were anesthetized with 0.15% Tricaine solution (Sigma-Aldrich). At the site where the incision

was to be made, the skin was injected with Bupivicaine to minimize post-operative pain. Oocytes were then surgically removed, manually sheared into small clusters of oocytes, and defolliculated in type II collagenase (Worthington) for 2-4 hours at room temperature. Stage V and VI oocytes, which could be identified because of their relatively large size and distinct black and white hemispheres, were selected and stored in Barth's solution containing 88 mM NaCl, 2.5 mM $NaHCO_3$, 1.1 mM KCl, 0.4 mM $CaCl_2$, 0.3 mM $Ca(NO_3)_2$, 0.8 mM $MgCl_2$, 2.5 mM sodium pyruvate, 10 mM HEPES, pH 7.3, and 5 μg/mL gentamicin at 12 °C. Plasmid DNA of the mutant receptor in pcDNA 3.1 was linearized using a restriction enzyme that cut the 3' end of the NMDA gene insert. GluN1 constructs were linearized with HindIII and GluN2A constructs were linearized with XbaI (restriction enzymes from New England Biolabs). This linearized DNA was gel purified and then used as the template with the Ambion T7 mMessage mMachine Kit to produce the RNA. RNA was freshly prepared each time oocytes were to be injected. Each oocyte was injected with 20 ng of RNA at a GluN1:GluN2 ng ratio of 1:2 (23). Oocytes were allowed to recover at 12 °C for 12–24 hours. Oocytes were then induced at 18 °C and preblocked with 1 mM β-maleimidopropionic acid for 1 hour, which limited the number of free cysteines on the surface of the oocytes and subsequently helped reduce nonspecific labeling with the thiol-reactive fluorophores. Additionally, upon induction, oocytes were maintained in saturating concentrations of 5,7-dichlorokynurenic acid (DCKA) to prevent cytotoxicity due to overactivation of expressed NMDA receptors. One day after induction, oocytes were labeled with 2 μM each of donor and acceptor fluorophores for 1 hour at 18 °C and then washed three-five times with Barth's solution. Membrane fractions were prepared using a lysis buffer composed of 20 mM Tris-Cl, pH 8.0, 200 mM NaCl, 1% Triton X-100, and EDTA-free Complete Protease Inhibitor Mixture (Roche Diagnostics) in Barth's solution. Oocytes were homogenized using a Douncer, and the cell lysate was centrifuged for 15 minutes at 13,000 rpm and 4 °C to isolate the soluble membrane fraction. The final volume of

the membrane fraction was then brought up to 2–3 mL with Barth's solution and used for LRET analysis.

4.6 Protein Expression in CHO cells

Chinese hamster ovary (CHO-K1) cells (ATCC) were maintained in Ham's F12 Nutrient Mix (Invitrogen) supplemented with 10% FBS (Sigma-Aldrich) and penicillin/streptomycin (Invitrogen). Cells were passaged once they reached a confluence of 80–90%, approximately every 2 days. CHO cells were transfected using Lipofectamine 2000 (Invitrogen) with 5–12 μg of DNA per 10-cm dish, at a GluN1:GluN2 μg ratio of 1:3 (20), a DNA:Lipofectamine ratio of 1:2, and when cells were 50–80% confluent. To induce expression of the NMDA receptor, cells were maintained in glutamine-free DMEM (Invitrogen) (21) for 1–2 hours prior to transfection through their harvest for use in spectroscopic studies. Cells were allowed to express for at least 40 hours in the presence of saturating concentrations of the inhibitor DL-2-Amino-5-phosphonopentanoic acid (DL-APV) before being harvested, labeled, and used for LRET studies. Cells were collected in extracellular buffer containing 1 mM $CaCl_2$, 150 mM NaCl, 2.8 mM KCl, 10 mM HEPES, and EDTA-free Complete Protease Inhibitor Mixture (Roche Diagnostics), pH 7.3–7.4 (HCl). CHO cells were labeled for 1 hour at room temperature on a rotator in the dark using 200 nM each of the donor and acceptor fluorophores in a 2–3-mL volume. Cells were washed twice after labeling to remove excess fluorophores and then resuspended in extracellular buffer for LRET analysis.

4.7 LRET

Labeled cells or oocyte membrane fractions were probed in a cuvette-based LRET analysis using a QuantaMaster model QM3-SS with Fluorescan software (Photon Technology International). Data were analyzed with Origin 8.6 software (OriginLab Corp.). The lifetime of the sensitized acceptor emission was measured upon directly exciting the donor. Donor-only samples were excited at 337 nm, and emission was collected at 545 nm. Donor-acceptor-

labeled samples were excited at 337 nm, and the emission was collected at the indicated wavelength for the given acceptor fluorophore (Table 4.2). A Peltier TE temperature controller maintained the temperature at 15-20 °C for all recordings.

Because these receptors were expressed in nonpurified systems of CHO cells and *X. laevis* oocytes, we employed a well-established technique to subtract background fluorescence from our lifetime measurements, as discussed in Chapter 3. Specifically, after obtaining acceptor lifetime measurements, five units of high activity bovine thrombin (Calbiochem) or 3 µL of Factor Xa (New England Biolabs) were added to the cuvette and allowed to cleave the receptor; cleavage was complete 2–3 hours following addition of the protease. Any fluorescence detected following protease cleavage was considered background fluorescence due to labeling of other surface proteins and was subtracted from measurements obtained before cleavage.

Paoletti et al. demonstrated that zinc contaminates buffers in the nanomolar range, and considering the high affinity of GluN2A subunits for zinc, it is probable that contaminating zinc would bind to expressed receptors (Paoletti, Ascher et al. 1997). As such, all measurements in CHO cells were also measured in the presence of 10 mM Tricine to ensure any contaminating zinc did not affect our measurements. Tricine was used as opposed to other chelators because, despite its relatively low affinity for zinc ($K_d \leq 10^{-9.7}$ M), it has an even lower affinity for calcium and barium, therefore minimizing the effect of the chelator on the buffer while still removing contaminating zinc. Zinc-bound measurements were made in the absence of Tricine and in the presence of 5–10 µM zinc chloride (Sigma). This concentration of zinc ensures that zinc-bound conformations of the ATD are maximally populated. Glutamate-glycine measurements were collected by adding glutamate and glycine to a final concentration of 1 mM and 100 µM, respectively, to zinc-bound receptors. Spermine solutions were carefully buffered to ensure that the final pH was the same as that of the

extracellular buffer used to re-suspend the cells and was added to a final concentration of 5 mM. Ifenprodil was added to cells at a final concentration of 10 μM.

Distances were calculated using the Förster equation (Equation 3.1), as described in Chapter 3. N values represent the number of biological repeats. Each sample (n) was scanned a minimum of three times, and each scan was an average of 99 sweeps. The lifetime was detected for at least three times the expected LRET lifetime, with adjustments made as needed after the first experiment, so that any longer components in the lifetime would not be missed. The error in the LRET lifetime is the SEM, and the error in the distances was calculated by propagating the errors in the lifetimes using the Error Propagation Calculator developed by Thomas Huber in the Physics Department of Gustavus Adolphus College.

4.8 Electrostatics

For the full-length electrostatics, the recent crystal structure of the rat form of the NMDA receptor (PDB ID 4TLL) was used as the template (Lee, Lü et al. 2014), and the Swiss Protein Modeler was used with the primary sequence of the NMDA receptor to build .pdb files that contain all side chains for residues in the structure. This modeling was necessary because the electrostatics of the protein could not be calculated without the side chains of the amino acids. For the isolated ATDs, the GluN2B ATD (PDB ID 3JPW) was the template for modeling the GluN2A primary sequence, again using the Swiss Protein Modeler. The pdb2pqr converter was used to generate a .pqr file (Dolinsky, Nielsen et al. 2004, Dolinsky, Czodrowski et al. 2007). This file was opened in VMD and the APBS plugin was used to calculate the surface electrostatics of the NMDA receptor tetramer. The APBS plugin works by solving the Poisson-Boltzmann equation for the surface charges of the protein (Baker, Sept et al. 2001).

4.9 Electrophysiology

All electrophysiology experiments were performed by Dr. David M. MacLean. CHO cells were transfected using Lipofectamine 2000 (Invitrogen) with wild-type or mutant GluN1,

GluN2A and enhanced GFP at a µg ratio of 1.25:3.75:1, respectively, with 6 µg of total DNA per 10 mL of media, or with wild-type or mutant GluN1, GluN2B, and enhanced GFP at a µg ratio of 1.5:4.5:1, respectively, with 7 µg of total DNA per 10 mL of medium. Following a 10-12 hour incubation with transfection reagents, cells were plated at low density onto petri dishes coated with poly-D-lysine. 300-400 µM DL-APV and 30 µM DCKA were present in the media during and after transfection. Whole cell patch clamp recordings were performed 24-48 hours post-transfection using borosilicate glass pipettes with 3-5 MΩ resistance, coated with dental wax, fire polished and filled with the following solution (in mM): 135 CsF, 33 CsOH, 2 $MgCl_2$, 1 $CaCl_2$, 11 EGTA and 10 HEPES, pH 7.4. The external solution was (in mM): 140 NaCl, 2.8 KCl, 1 $CaCl_2$, 10 HEPES, and 10 Tricine, pH 7.4 for measurements of zinc inhibition. The external solution was (in mM): 140 NaCl, 2.8 KCl, 1 $CaCl_2$, 10 HEPES, pH 7.4 for measurements of spermine potentiation or ifenprodil inhibition. Free Zn^{2+} solutions up to 1 µM were made as described by Paoletti et al., 1997, with 10 µM zinc added to an external solution lacking tricine (Paoletti, Ascher et al. 1997).

Control, agonist, and agonist plus modulator solutions were locally applied to isolated cells using a solenoid valve system (VC-6, Warner Instruments) and modified theta or quad barrel tubing as previously described (Tang 2001). Glycine (100 µM) was present continuously and glutamate (100 µM) was applied for 12 seconds every 20 seconds. To isolate the voltage-independent component of Zn^{2+} block, glutamate applications were performed at +50 mV with series resistance compensated by 60-80%. For measurements of spermine potentiation, glycine (100 µM) was present continuously, glutamate (100 µM) was applied for 12 s every 30 s, and saturating spermine (5 mM) was applied for 3 seconds during the glutamate pulse. Cells were held at -60 mV prior to ligand application, ramped up to +50 mV several seconds before glutamate application, maintained at this voltage during the application and then ramped down to -60 mV and held between sweeps. All recordings were performed using an

Axopatch 200B amplifier (Molecular Devices, Sunnyvale, CA, USA), acquired at 10 kHz using pCLAMP10 software (Molecular Devices), and filtered online at 3 kHz (8-pole Bessel, Frequency Devices). All experiments were performed at room temperature.

For Zn^{2+} dose-response curves, Zn^{2+} inhibition was calculated as the steady-state current at the end of the glutamate-Zn^{2+} application (I) divided by the current at the end of the glutamate-only application (I_{max}). Data from each cell were fit with the following equation:

$$\frac{I}{I_{max}} = \frac{(1-a)}{\left(1+\frac{[Zn^{2+}]}{IC_{50}}\right)^{n}} + a \qquad \text{Equation 4.1}$$

where a, IC_{50} and n are the residual, the half-maximal inhibition concentration, and the Hill co-efficient, respectively.

Chapter 5:
LRET on Isolated GluN2A and GluN2B ATDs

The ATDs contain the binding sites of small molecule allosteric inhibitors such as zinc. While zinc inhibits NMDA receptors through a voltage-dependent pore-blocking action (Paoletti, Ascher et al. 1997), its allosteric inhibition through binding to the ATD is of particular interest. Allosteric inhibition by zinc is subtype selective, exhibiting micromolar affinity for GluN2B subunits but nanomolar affinity for GluN2A subunits, where zinc binding reduces open channel probability (Paoletti, Ascher et al. 1997, Rachline, Perin-Dureau et al. 2005, Amico-Ruvio, Murthy et al. 2011). Moreover, this inhibition occurs at physiologically relevant zinc levels and/or during co-release of zinc with glutamate (Assaf and Chung 1984, Howell, Welch et al. 1984). Modeling of the GluN2A ATD followed by functional studies of a GluN2A-containing NMDA receptor showed that key negatively charged residues at the 'entrance' of the ATD cleft are involved in screening zinc binding to the ATD (Paoletti, Perin-Dureau et al. 2000). Additionally, use of the substituted cysteine accessibility method (SCAM) within the ATD cleft first suggested that the ATD cleft may be closing around a ligand, similar to the LBDs or leucine/isoleucine/valine-binding proteins (LIVBPs) (Paoletti, Perin-Dureau et al. 2000). Mutagenesis of the GluN2A ATD and the structure of the zinc-bound GluN2B ATD confirmed that zinc binds within the cleft of the bi-lobed structure of the ATD (Choi and Lipton 1999, Fayyazuddin, Villarroel et al. 2000, Karakas, Simorowski et al. 2009). Propping the ATD cleft open using thiol-reactive crosslinking agents increases open channel probability, suggesting that zinc binding to the ATD, proceeds through a cleft-closure mechanism (Gielen, Retchless et al. 2009). Furthermore, molecular dynamics simulations support the premise that the ATD of GluN2A can undergo a cleft closure type conformational change (Dutta, Shrivastava et al. 2012). Taken together, these data provide indirect evidence that zinc inhibits the NMDA receptor by closing the bi-lobed ATD and allosterically influencing the conformational equilibrium between closed and open states. However, this change is not observed in the structure of the zinc-bound ATD of GluN2B (Karakas, Simorowski et al. 2009),

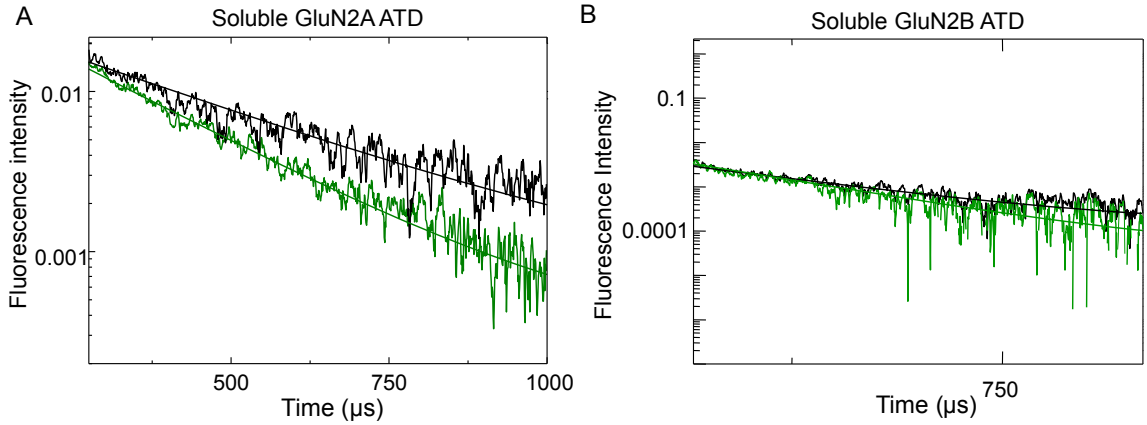

Figure 5.1: LRET on Soluble GluN2 ATDs. (A) LRET from the soluble GluN2A ATD is shown and zinc causes a decrease in the lifetime (green curve) as compared to the apo receptor (black curve). (B) LRET from the soluble GluN2B ATD, the black curve is the apo and the green curve is with zinc.

and no structural data demonstrating this cleft-closure or measuring its extent have been reported (Furukawa 2012). We employed LRET to detect these hypothesized zinc-induced conformational changes in the isolated GluN2A or GluN2B ATD.

To characterize the conformational changes associated with zinc binding, we used the soluble ATD protein, which had recently been crystallized and shown to have a functional zinc binding site (Karakas, Simorowski et al. 2009). The soluble ATD of the GluN2B subunit was monomeric up to a concentration of 5 mg/mL (~120 μM) (Karakas, Simorowski et al. 2009). Soluble GluN2A and GluN2B ATDs were expressed in *Hi5* cells using a baculovirus system. These proteins had the secretion signal from the human placental alkaline phosphatase, so that the media surrounding the cells contained the protein. Protein was concentrated and purified using either a nickel column attached to an FPLC system or nickel beads. However, complete purification was never achieved, due to a contaminating protein that seemed to co-purify with the ATD and was in excess concentration of the ATD. For this reason, it was necessary to include the thrombin recognition sequence and to quantify background due to labeling of cysteines in contaminating proteins. The LRET lifetime was measured between the

cysteine in the upper lobe of the ATD and the inherent cysteine in the lower lobe of the ATD (Cys231 in GluN2A and Cys232 in GluN2B). Protein samples were labeled with terbium chelate and Alexa555. Samples were excited at 337 nm and emission was detected at 565 nm. All measurements yielded a single exponential lifetime. In GluN2A, the apo lifetime was 275 μs (Figure 5.1), corresponding to a distance of 46 ± 0.6 Å (Table 5.1). The lifetime decreased to 199 μs when the ATD was bound by zinc (Figure 5.1), corresponding to a distance of 43 ± 0.3 Å (Table 5.1). The GluN2B lifetime for the apo ATD was 254 μs (Figure 5.1), a distance of 47 ± 0.6 Å. The lifetime similarly decreased when zinc was bound to the ATD, giving a lifetime of 206 μs and a distance of 45 ± 0.6 Å. These data agree with the

	Donor Lifetime (μs)	**Donor:Acceptor Lifetime (μs)**	**Distance (Å)**
GluN2A ATD	1649	275	46 ± 0.6
GluN2A ATD + Zinc	1649	199	43 ± 0.3
GluN2B ATD	1417	254	47 ± 0.6
GluN2B ATD + Zinc	1417	206	45 ± 0.6

Table 5.1: LRET lifetimes and Distances from Soluble ATDs. The error in the distance was calculated by propagating the error in the fit of the LRET decay.

literature, which suggest that if propping open the ATD potentiates the receptor, then an inhibitor must close the ATD conformation. Indeed, the binding of zinc results in a decrease in the lifetime, corresponding to a decrease in the distance between the upper and lower lobes of the ATD.

To ensure we were working with functional protein, we used Isothermal Titration Calorimetry (ITC), as a functional assay. ITC measures the amount of energy it takes to maintain the temperature of the chamber containing the protein, as a ligand is titrated in and

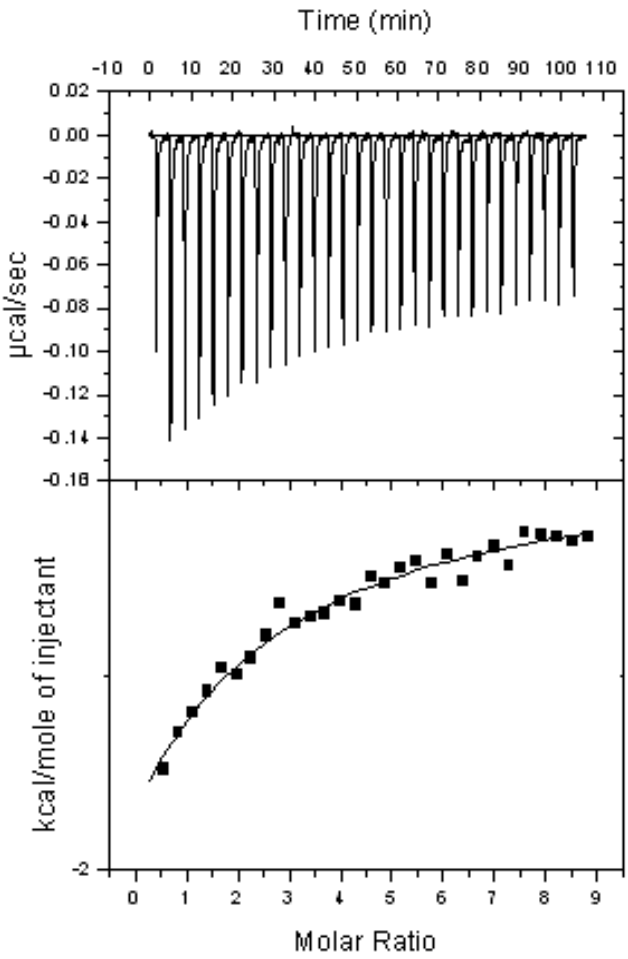

Figure 5.2: Isothermal titration calorimetry characterizing the binding of zinc to the isolated GluN2B ATD. The fit of the binding curve yields a Kd of ~5 µM, similar to the published value for the isolated GluN2B ATD (Karakas, Simorowski et al. 2009, Tomitori, Suganami et al. 2012).

binds to the protein. A successful binding curve could not be established for the GluN2A ATD, but a binding curve was established for GluN2B, and the K_d closely matched what was presented in the literature (Figure 5.2). The fact that the protein was not pure resulted in a much higher initial baseline (background) than expected or hoped for.

Because protein purification could not be achieved completely and functional studies could not confirm we were working in a relevant system, other systems were sought. Full-length receptors, though they come with their own challenges, are a better system because

they reflect conformational changes in the context of a whole receptor, as would be found physiologically. As such, these efforts at working with the soluble ATDs were abandoned, and future studies focused on the full-length receptor.

Chapter 6:
Tetrameric Arrangement of ATDs

This research was originally published in the Journal of Biological Chemistry. The text and figures have been modified and reprinted with permission from Sirrieh, R.E., MacLean, D.M., Jayaraman, V. Amino-terminal Domain Tetramer Organization and Structural Effects of Zinc Binding in the N-Methyl-d-aspartate (NMDA) Receptor. *Journal of Biological Chemistry*. 2013; 288: 22555-64.

6.1 Introduction

Before the crystal structure of the full NMDA receptor was solved, Karakas and colleagues reported the structure of the isolated ATDs of a GluN1-GluN2B NMDA receptor in a dimeric configuration (Karakas, Simorowski et al. 2011). This heterodimer structure was unique among the structures of glutamate receptor ATDs because it showed a very close interaction between the subunits and a novel possible arrangement because the ATDs seemed to be almost perpendicular to each other. This novel arrangement prompted us to study the conformational arrangement of the ATDs of the NMDA receptor in a full receptor. Furthermore, in the AMPA receptor, the ATD layer is said to undergo a crossover, to where the ATD of a subunit sits above the LBD of the adjacent subunits LBD. Due to a lack of a structure, it was unknown whether a similar domain swap takes place in the NMDA receptor. To address these questions, we used luminescence resonance energy transfer (LRET) to map the tetramer organization in full-length, functional GluN1/GluN2A receptors.

6.2 Strategy for LRET measurements in CHO cells and X. laevis *oocytes*

To probe the orientation and distances between ATDs we measured three inter-subunit distances, between the two GluN2A subunits, between GluN2A and GluN1 subunits, and between the two GluN1 subunits. Receptors composed of GluN1 and GluN2A subunits were co-expressed in CHO cells and *X. laevis* oocytes. All constructs used in the LRET measurements were functional with zinc inhibition intact as determined using whole cell current recordings in CHO cells (Figure 8.1).

6.3 Tetramer organization of GluN1/GluN2A ATDs

We measured the inter-subunit distance between GluN2A ATDs by co-expressing GluN2A^{*C30} with GluN1*, and labeling with a donor: acceptor ratio of 1:1 (maleimide derivatives of terbium chelate and Alexa555, respectively). Based on the LRET acceptor and donor only lifetimes (Figures 6.1 and 6.2), the distances were calculated to be 44.2 ± 0.1 Å and 44.9 ±

0.1 Å in CHO cells and oocytes, respectively (Table 6.1). The distances measured in standard solutions which may contain trace amounts of zinc and in tricine buffered solutions which contain no free zinc are identical, suggesting that any contaminating zinc is not significant enough to influence the LRET measurements. These distances are substantially shorter than any distances across analogous sites on the ATDs in the full length AMPA receptor (Figure 6.3).

To measure between the GluN1-GluN2A ATDs, GluN1^{*C30} was co-expressed with GluN2A^{*H30}. The LRET lifetimes for the distance between terbium chelate-labeled GluN1 and Ni(NTA)$_2$Cy3-labeled GluN2A subunits in CHO cells and oocyte membrane fractions are shown in Figures 4 and 5. The lifetimes can be well represented by a single exponential decay, suggesting we are measuring only a single distance. The distance is 50.6 ± 0.1 Å and 50.4 ± 0.1 Å in CHO cells and oocytes, respectively (Table 6.1). This distance is in good agreement with the intra-dimer distance of 59 Å between ATD dimers in the full-length GluA2 AMPA receptor structure.

Similar LRET measurements of GluN1-GluN1 inter-subunit distances in NMDA receptors in CHO cells were made by expressing GluN1^{*C22} with GluN2A^{*H30}. No LRET was detectable when the construct was labeled with maleimide derivatives of terbium chelate and Alexa 555 in both CHO cells and *X. laevis* oocytes (Figures 6.1 and 6.2). The lack of LRET suggests that the inter-subunit distance between Cys22 on GluN1 subunits is >95 Å (corresponding to energy transfer efficiencies of <0.1), consistent with the 97 Å distance in the tetrameric crystal structure of isolated ATDs of the NMDA receptor (Figure 6.3). This measurement does not rule out the configuration in the crystal structure of the full-length AMPA receptor, which shows a distance of 127 Å for analogous sites. However, all three distances taken together suggest that the ATDs in the NMDA receptor are indeed more

compactly arranged (Karakas, Simorowski et al. 2011). The NMDA receptor ATDs do not seem to be as splayed apart as the ATDs in the full length AMPA receptor structure.

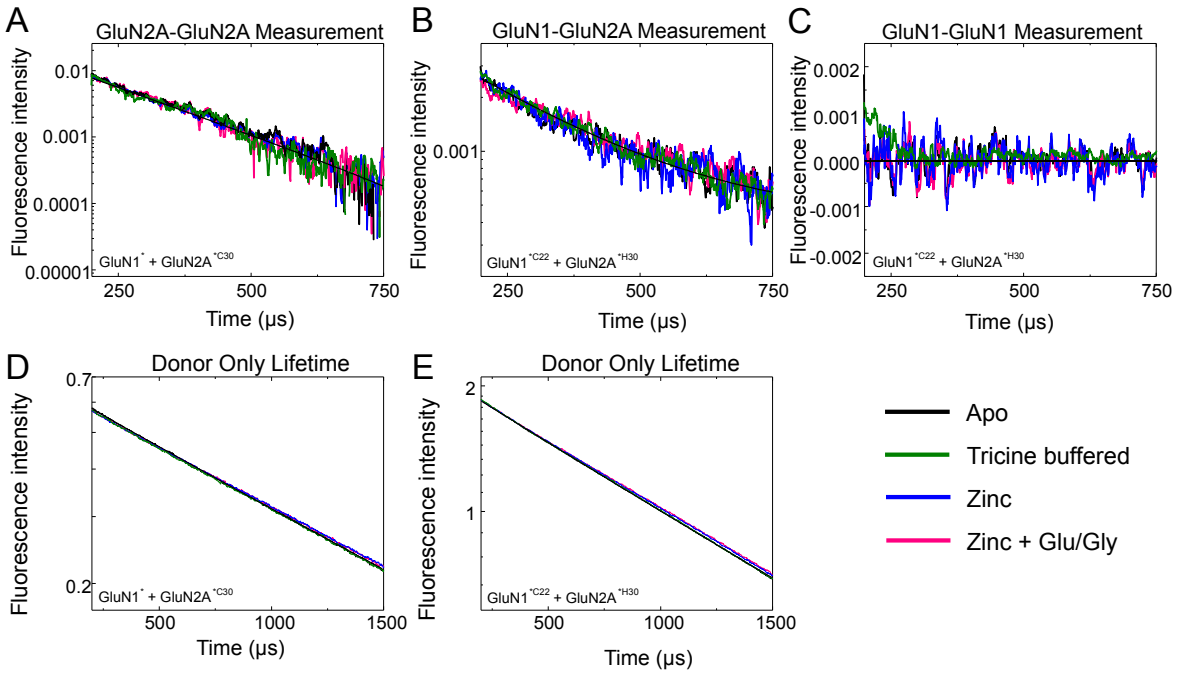

Figure 6.1: Lifetime measurements of NMDA receptor inter-subunit distances in CHO cells. A) The GluN2A-GluN2A LRET lifetimes obtained by co-expressing GluN1* and GluN2A^{*C30} and labeling with terbium and Alexa 555 as donor and acceptor fluorophores, respectively. B) The GluN1-GluN2A LRET lifetimes labeled with terbium and Ni(NTA)$_2$Cy3 as donor and acceptor fluorophores, respectively. C) The GluN1-GluN1 LRET measurements labeled with Terbium and Alexa 555 as donor and acceptor fluorophores, respectively. D) Donor only lifetimes for the GluN2A-GluN2A measurements. E) The donor only lifetimes for measurements between GluN1-GluN2A and GluN1-GluN1 are shown. In all panels, the black line represents lifetimes from receptors in extracellular buffer, green shows tricine-buffered solutions, blue illustrates solutions with saturating zinc, and pink represents solutions with both saturating zinc and glutamate/glycine. All measurements can be fit with a single exponential lifetime decay curve.

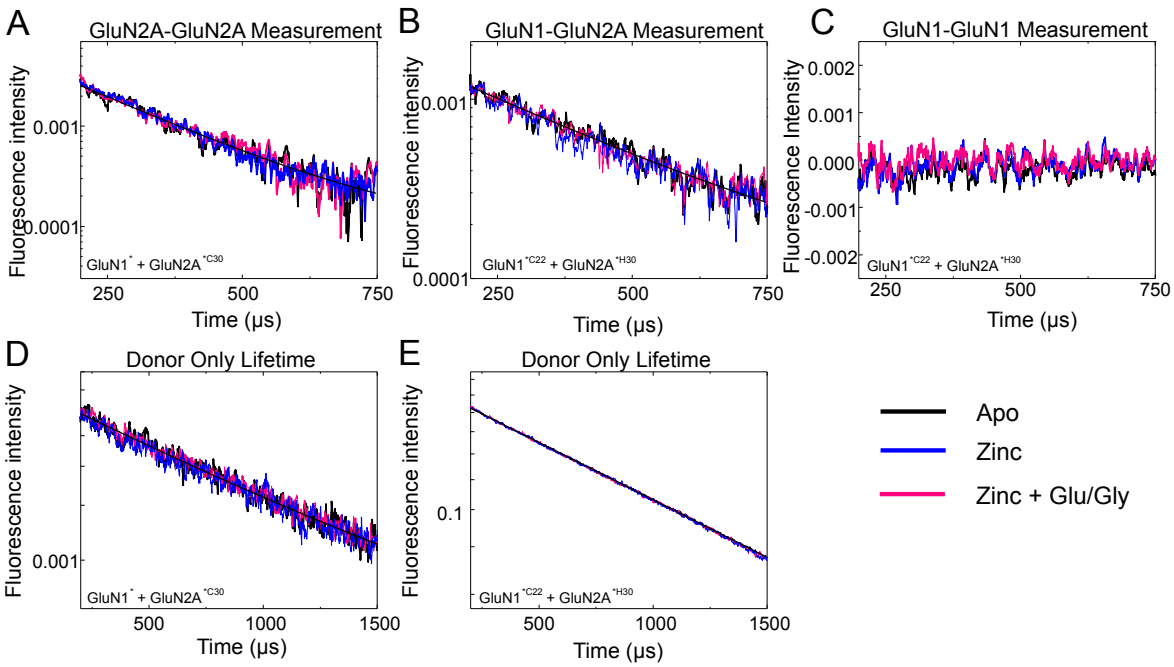

Figure 6.2: Lifetime measurements of inter-subunit distances in NMDA receptors expressed in *X. laevis* oocytes. A) GluN2A-GluN2A LRET lifetimes from co-expressed GluN1* and GluN2A^{*C30} labeled with terbium chelate and Alexa 555. B) The GluN1-GluN2A LRET lifetimes measured from GluN1^{*C22} and GluN2A^{*H30} when labeled with terbium chelate and Ni(NTA)$_2$Cy3. C) The GluN1-GluN1 LRET lifetimes obtained from GluN1^{*C22} co-expressed with GluN2A^{*H30} and labeled with terbium chelate and Alexa 555. D) Lifetimes for donor-labeled GluN2A^{*C30} used to calculate GluN2-GluN2 distances. E) Donor only lifetimes for GluN1^{*C22} labeled receptors to calculate GluN1-GluN2A and GluN1-GluN1 distances. In all panels, the black line represents lifetimes from receptors in extracellular buffer, green shows tricine-buffered solutions, blue illustrates solutions with saturating zinc, and pink represents solutions with both saturating zinc and glutamate/glycine. All measurements can be fit with a single exponential lifetime decay curve.

Similar measurements to those used to probe the tetramer organization were used to characterize inter-subunit distances upon zinc binding and subsequent binding of the agonists glutamate and glycine. The LRET lifetimes that probe the inter-subunit distances show no change in the presence of zinc either alone or with saturating glutamate and glycine in both CHO cells (Figure 6.1) and in oocytes (Figure 6.2). As such, the distances between subunits in these ligated states are indistinguishable from the apo state (Table 6.1). Importantly, these constructs all retain high affinity voltage independent zinc inhibition with IC_{50}'s of 17 ± 2 and

45 ± 2 nM for GluN1^{*C22}/GluN2A^{*H30} and GluN1*/GluN2A^{*C30}, respectively (Figure 8.2), in good agreement with previously reported values for wild-type NMDA receptors composed of GluN1/GluN2A subunits (Fayyazuddin, Villarroel et al. 2000, Zheng, Erreger et al. 2001, Erreger and Traynelis 2005).

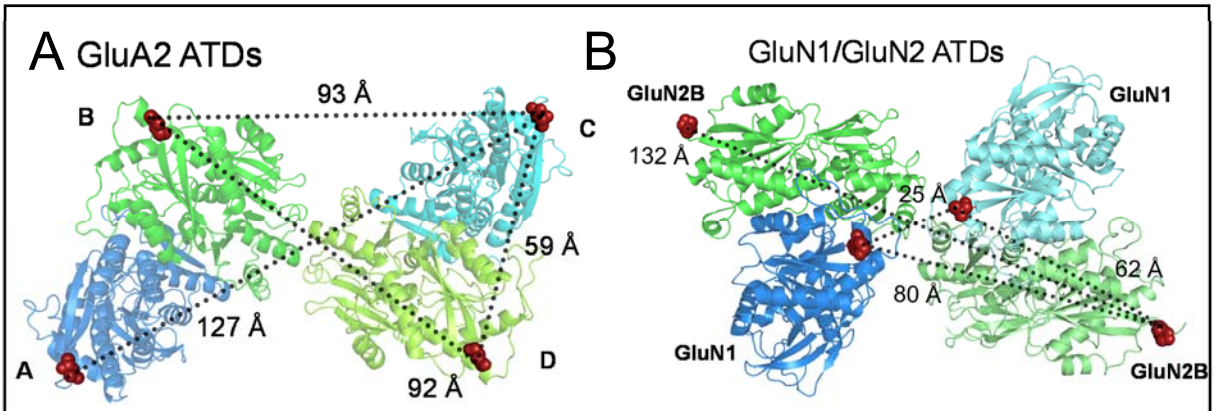

Figure 6.3 Top view of iGluR ATDs with measurements. Shown are the measurements between the N-terminus of the ATDs of the GluA2 AMPA receptor (A). The measurements are made at analogous sites to those measured between in the LRET experiments on the NMDA receptor. Additionally, the subunits are labeled A-D according to the conformation they adopt in the structure (See Chapter 1). (B) The tetramer measurements across the ATDs of the GluN1-GluN2B NMDA receptor at analogous sites to those measured in the LRET experiments.

6.4 Discussion

Our results corroborate that the tetramer organization of the NMDA receptor at the ATD is quite distinct from that of the AMPA receptor. In the full length crystal structure, the AMPA receptor subunits are organized as a dimer of dimers with the dimer pairs relatively far apart from each other. This separation is evident in the distances measured between the α-carbons of the N-terminal residues of the ATD (Figure 6.3 A). The LRET yielded distances that ranged from 45 Å to distances too great to be measured with LRET. The existence of these shorter distances confirms that the ATDs are more compact in the NMDA receptor. The recently solved structure of the GluN1-GluN2B NMDA receptor allows for comparison of our measurements to the distances in the crystal structure. The GluN1-GluN2A distance measured matches quite well to the distance within an ATD dimer (62 Å between α-carbons)

in the GluN1-GluN2B structure (Figure 7.3 B). However, the other two distances, between GluN2A ATDs and between GluN1 ATDs do not match. Several explanations could be offered for this difference. First, the structure is of GluN1-GluN2B subunits, and our LRET measurements were made in GluN1-GluN2A subunits, so the differences could reflect differences in receptor assembly based on GluN2 subtype. Second, the crystal structure was optimized by introducing crosslinks between the lower lobes of the GluN2B subunit (S214C mutation) (Karakas and Furukawa 2014), so the angling of the upper lobes of the GluN2B ATDs away from each other could be an artifact introduced by the construct used for crystallization. The crosslink forms as confirmed by western blots (Karakas and Furukawa 2014), but the ATDs are thought to be very flexible, so although they could form that conformation naturally, they may not occupy it as frequently as when they are held in place by a crosslink. Finally, LRET measures the distance between the fluorophores, which have a linker between the fluorescent moiety and the binding group. As such, the distances could reflect the orientation of the probes in our system. Our data show definitively, however, that the NMDA receptor ATDs are arranged more compactly than those of the AMPA receptor, as later confirmed by the crystal structure. Additionally, the binding of zinc, an allosteric inhibitor, does not cause any large-scale conformational changes at the upper lobes of the ATDs. The addition of the agonists glutamate and glycine, which in these steady state measurements means the desensitized state is being probed, similarly do not induce any large scale movements in the upper lobes of the ATDs. These data suggest that the NMDA receptor desensitizes differently from AMPA receptors, where the ATDs splay apart during desensitization (Meyerson, Kumar et al. 2014).

Using atomic force microscopy, Suzuki and colleagues found that the height of the NMDA receptor decreases approximately 1 nm when both agonists glutamate and glycine are bound to the receptor (Suzuki, Goetze et al. 2013). The LRET data, on the other hand, shows

no change in inter-subunit distances in the presence of glutamate and glycine, suggesting that the upper lobes of the ATDs do not move apart during gating or desensitization. To integrate these two observations, we speculate that LBD closure around the ligand results in rearrangement of the LBD dimer interface (Borschel, Murthy et al. 2011) and a general downward pulling on the ATDs, without altering the orientation of the ATD subunits at the top. Essentially, the ‘shortening’ of the receptor upon agonist binding stems predominantly or exclusively from closure motions of the LBD. Further experiments will be required to examine the motions of the ATD-LBD linker during agonist and modulator binding.

GluN2A-GluN2A LRET Lifetimes and Distances				
	Ligated State (n)	Donor Only Lifetime (μs)	Donor-Acceptor Lifetime (μs)	Distance (Å)
CHO Cells	Apo (3)	1554 ± 1.2	142 ±1.3	44.2 ± 0.1
	Tricine buffered (3)	1529 ± 1.4	149 ± 1.7	44.7 ± 0.1
	Zinc (3)	1599 ± 1.2	147 ± 1.0	44.4 ± 0.1
	Zinc, Glu/Gly (3)	1594 ± 1.3	145 ± 1.7	44.1 ± 0.1
X. laevis oocytes	Apo (3)	1528 ± 7.8	149 ± 2.2	44.9 ± 0.1
	Zinc (3)	1631 ± 9.1	152 ± 1.6	44.5 ± 0.1
	Zinc, Glu/Gly (3)	1578 ± 6.7	158 ± 2.4	45.1 ± 0.1
GluN1-GluN2A LRET Lifetimes and Distances				
CHO Cells	Apo (5)	1502 ± 1.2	273 ± 3.3	50.6 ± 0.1
	Tricine buffered (2)	1497 ± 1.2	272 ± 2.8	50.6 ± 0.1
	Zinc (2)	1549 ± 1.2	295 ± 5.7	51.1 ± 0.2
	Zinc, Glu/Gly (3)	1563 ± 1.3	302 ± 4.4	51.0 ± 0.1
X. laevis oocytes	Apo (6)	1725 ± 1.4	308 ± 3.3	50.4 ± 0.1
	Zinc (3)	1700 ± 1.3	298 ± 4.0	50.2 ± 0.1
	Zinc, Glu/Gly (3)	1710 ± 1.4	299 ± 3.6	50.2 ± 0.1
GluN1-GluN1 LRET Lifetimes and Distances				
CHO Cells	Apo (3)	1502 ± 1.2	no LRET	> 95
	Tricine buffered (1)	1497 ± 1.2	no LRET	> 95
	Zinc (3)	1549 ± 1.2	no LRET	> 95
	Zinc, Glu/Gly (3)	1563 ± 1.3	no LRET	> 95
X. laevis oocytes	Apo (3)	1725 ± 1.4	no LRET	> 95
	Zinc (3)	1700 ± 1.3	no LRET	> 95
	Zinc, Glu/Gly (3)	1710 ± 1.4	no LRET	> 95

Table 6.1: Inter-subunit LRET lifetimes and distances. Shown are the lifetimes and corresponding distances for the measurements between the upper lobes of the ATDs in a GluN1-GluN2A receptor. There were no changes in the distances when the receptor was bound by zinc or zinc and the agonists glutamate and glycine.

Chapter 7: Electrostatics and Subtype-dependent ATD Conformations

Some of the research presented here was originally published in the Journal of Biological Chemistry. The text and figures have been modified and reprinted with permission from Sirrieh, R.E., MacLean, D.M., Jayaraman, V. Amino-terminal Domain Tetramer Organization and Structural Effects of Zinc Binding in the N-Methyl-d-aspartate (NMDA) Receptor. *Journal of Biological Chemistry*. 2013; 288: 22555-64. © The American Society for Biochemistry and Molecular Biology.

7.1 Electrostatics of Isolated GluN2A and GluN2B ATDs

Electrostatics likely influence modulator activity, especially when dealing with charged modulators such as zinc, ifenprodil, and spermine. Surface electrostatics of the isolated GluN2A and GluN2B were calculated (described in 4.8) using the APBS plugin on VMD. The GluN2A ATD primary sequence was modeled on the crystal structure of the GluN2B ATD, because the structure of the GluN2A ATD has not yet been solved. When comparing the electrostatics of the apo ATDs, one can clearly see that at the zinc binding site (white arrows in Figure 7.1), there is a red (negative) patch around the binding site. It is also evident that the size of the electronegative patch is larger in GluN2A than in GluN2B. This difference could help account for the difference in zinc affinity for the GluN2 ATDs. The zinc is more easily attracted to the GluN2A ATD, and the greater number of residues available to coordinate the zinc create a high-affinity binding site. In GluN2B, there is less of an electronegative patch, and less residues available to coordinate the zinc, creating an intermediate affinity zinc binding site.

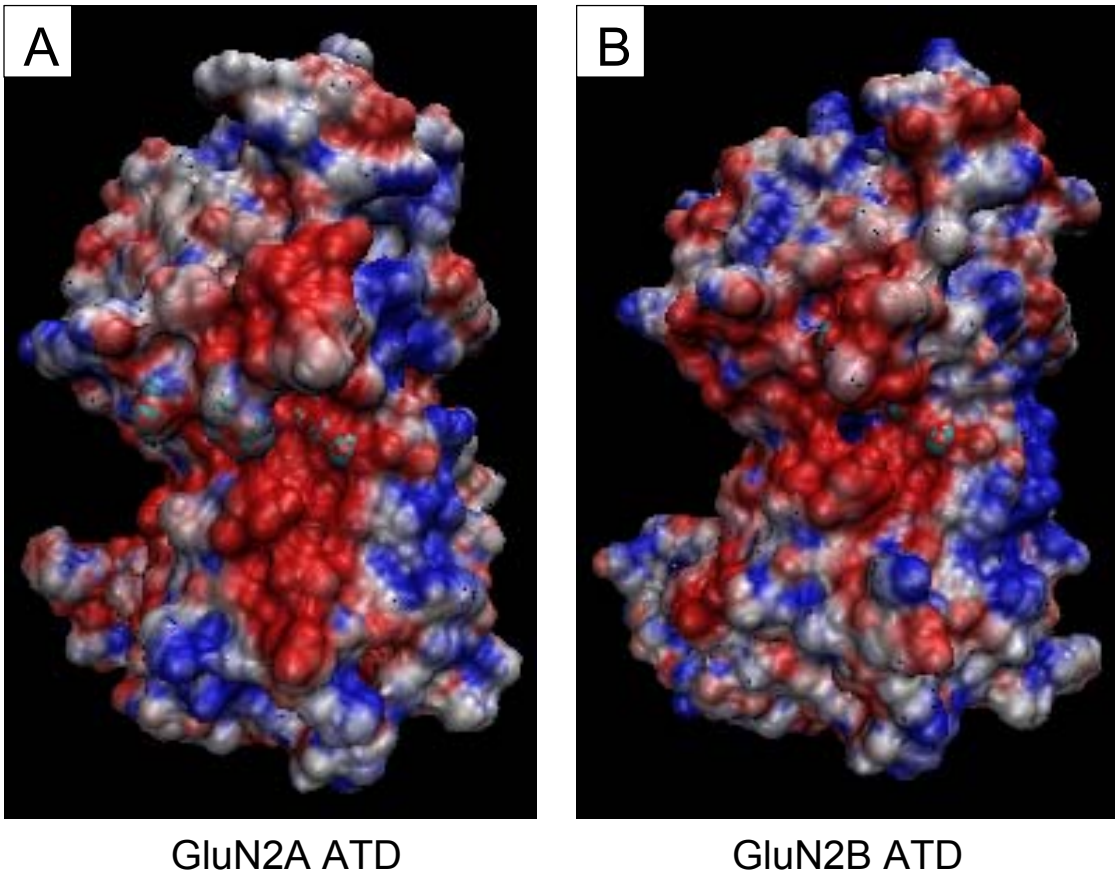

Figure 7.1: Electrostatics of GluN2 ATDs. (A) Electrostatics of the GluN2A ATD, generated by modeling the primary sequence of the GluN2A ATD on the GluN2B ATD crystal structure. There is clearly a red, electronegative patch around the zinc binding site, which is larger than the negative area around the GluN2B zinc binding site (B). Cyan colored residues in the red patches are the zinc binding residues.

In fact, when comparing the electrostatics in the zinc-bound and apo GluN2B ATDs, it is clear that the binding of the zinc cation induces a greater negative charge in the surface of the protein (Figure 7.2). These figures only show the surface of the protein. If the positively charged modulator were included, we would expect, rather, to see a neutral patch at that position.

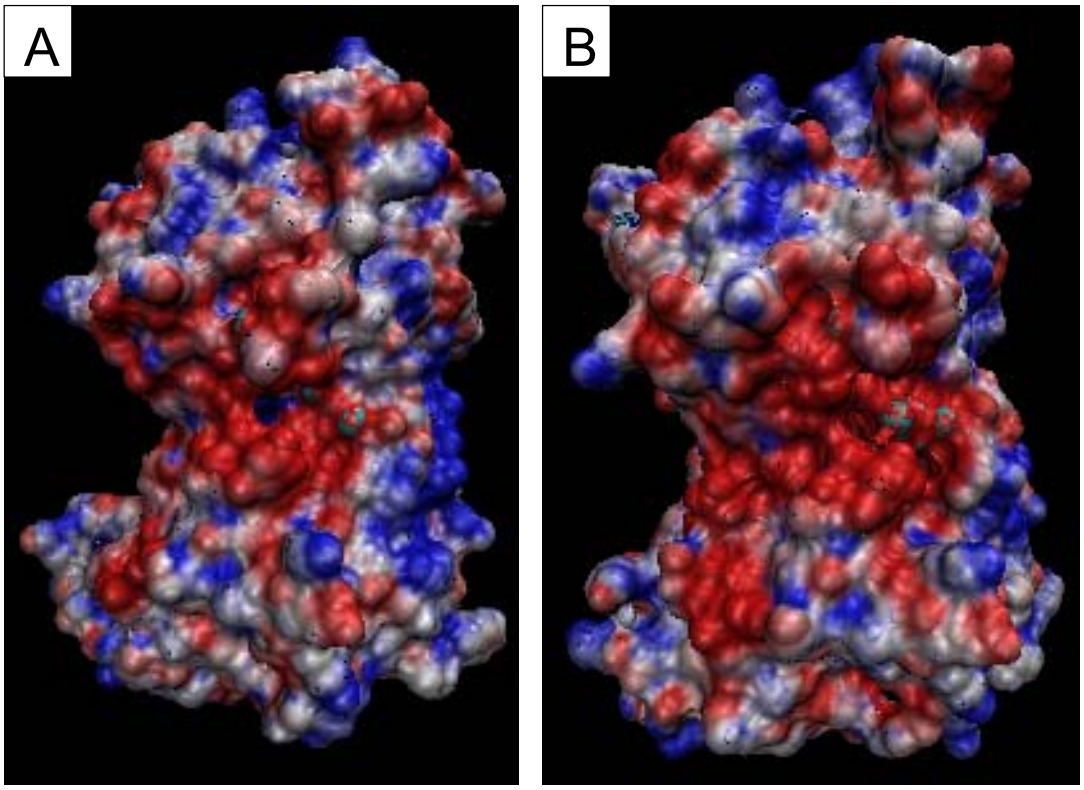

Figure 7.2: Electrostatics of GluN2B ATD with and without zinc. Shown in (A) is the apo GluN2B ATD, and in panel (B) one can clearly see the greater negative (red) patch surrounding the zinc binding site. Highlighted in cyan are the zinc binding residues.

Additionally, as mentioned above, ifenprodil is positively charged, and the binding of ifenprodil at the interface similarly induces an increase in the negative charges upon binding (Figure 7.3). The differences in electrostatics, again, could be influencing the affinity to the modulator.

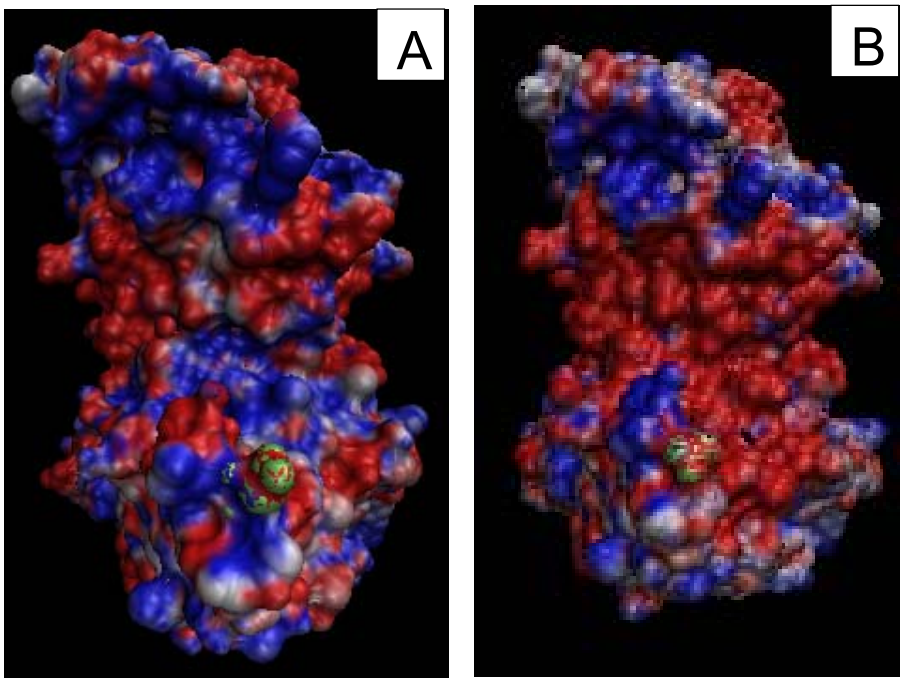

Figure 7.3: Ifenprodil-induced changes in Electrostatics. The interface of the apo GluN2B ATD (A) acquires a more negative surface upon binding of ifenprodil at the surface (B). The green residue highlighted in the lower lobe of the ATDs is Glu211 and serves as a reference point for comparison between the two structures.

7.2 Subtype dependent conformations of the ATD

In addition to differences in the electrostatics, studies have shown that the ATDs dictate Po, and suggested that the conformation of the ATD is what influences Po. In order to directly characterize the differences in the ATDs, we performed LRET and labeled at identical sites in the GluN2A and GluN2B ATDs, with identical fluorophores, and the same buffer system to allow for an easier comparison of the distances measured.

First, the conformational state of the GluN2B ATD was probed by co-expressing the GluN2B^{cleft} construct with a cys-free GluN1 (the GluN1* construct). The GluN2B^{cleft} allows for the inherent cysteine in the lower lobe of the GluN2B at site 232, to be labeled with the donor fluorophore and the N-terminus of the ATD, in the upper lobe, to be labeled with the acceptor fluorophore via a hexa-His tag. The specific introduction of donor and acceptor fluorophores

on the ATD and the introduction of the thrombin cleavage site between the two allowed for isolation of an LRET signal specifically within the labeled ATD of the NMDA receptor expressed in the cells, without a confounding signal across the subunits. The LRET lifetime was determined by measuring the lifetime of sensitized acceptor emission upon donor excitation. The LRET lifetime after background fluorescence subtraction (achieved by thrombin cleavage of the NMDA receptor) is shown in Figure 7.4. The lifetime from the receptor in the apo state could be well represented by a single exponential with a lifetime of 252 ± 12 μs, which corresponds to a distance of 48.8 ± 0.4 Å between the two fluorophores (Table 7.1). The single lifetime suggests that the measurements correspond to distances within the subunit, as expected based on the crystal structures, where there is no cross talk across the subunits for these sites. The same sites had been used to measure across the GluN2A ATD cleft, a hexa-his tag after residue 30 and the inherent cysteine (residue 231 in GluN2A), and the same fluorophores were used to label at these sites (Sirrieh, MacLean et al. 2013). The LRET lifetime measured between these sites in GluN2A was 312 ± 5.4 μs (Figure 7.4), corresponding to a distance of 51.2 ± 0.1 Å (Table 7.1) (Sirrieh, MacLean et al. 2013). These measurements show that the GluN2B cleft is inherently in a more closed conformation than the GluN2A cleft.

Additionally, manipulation of the GluN1 ATD modulates Po of the receptor (Zhu, Stroebel et al. 2013). To determine what the GluN1 ATD conformation was, we co-expressed the GluN1cleft construct with either a cys-free GluN2A (GluN2A*) or GluN2B (GluN2B*). The results surprisingly showed that the GluN1 ATD assumes different conformations when co-assembled with different GluN2 subunits. When co-assembled with GluN2A, the LRET lifetime was 324 ± 13 μs, corresponding to a distance of 51.2 ± 0.3 Å. When co-assembled with GluN2B, the LRET lifetime was 275 ± 3.5 μs, a distance of 49.2 ± 0.1 Å. These data suggest three things. First, the GluN1 ATD adopts a more open conformation when co-assembled with

GluN2A. Second, the GluN1 ATD may be involved in dictating the Po of the receptor in combination with the GluN2 ATD. These receptors have a higher Po than GluN1/GluN2B receptors, and GluN1 is in an inherently more closed conformation when co-assembled with GluN2B. Third, the difference in the conformation suggests that the GluN1-GluN2 ATD interface differs when the receptor is composed of GluN2A or GluN2B. Differences in the interface were thought to arise from differences in the primary sequence and conformation of the GluN2 ATD. Since the GluN1 ATD is in a different conformation with different partners, there are likely different residues contributed to the ATD interface.

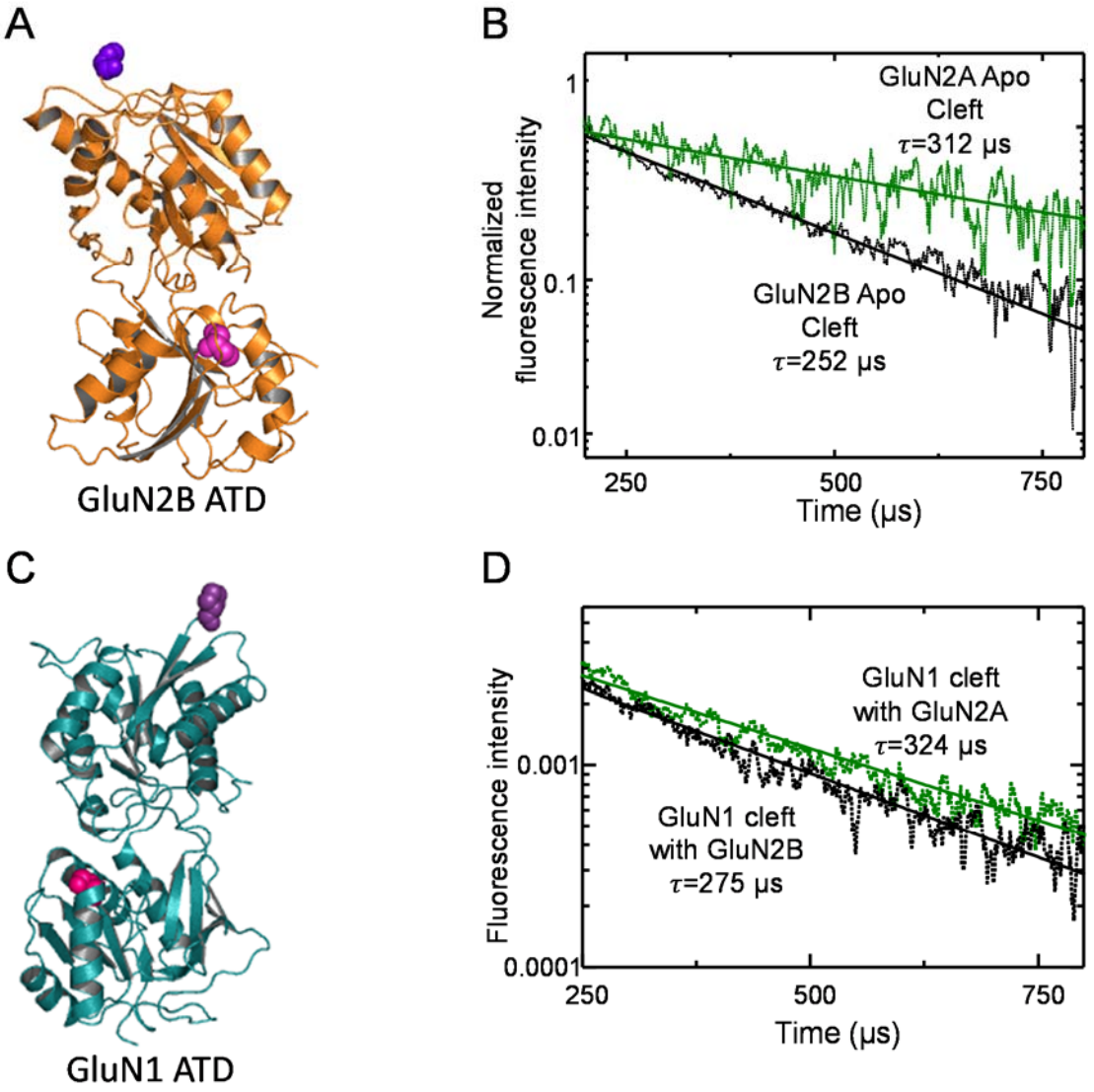

Figure 7.4: The different conformations adopted by apo ATDs. (A) Shown is the crystal structure of the GluN2B ATD (PDB ID 3JPW) in the zinc free state. Highlighted in purple and magenta are the inherent cysteine in the lower lobe of the ATD (conserved in GluN2A – Cys231) and the location of the insertion of the hexa-his tag at the N-terminus, which is again the same site used in GluN2A cleft measurements. (B) The LRET lifetimes of the apo GluN2B cleft (black) and the tricine-buffered GluN2A cleft (green) are shown. (C) The crystal structure of the GluN1 ATD (PDB ID 3Q41) is shown highlighting residues that were mutated to cysteines to accept fluorophores. (D) The LRET lifetimes from the GluN1 ATD vary when GluN1 is co-expressed with GluN2A or GluN2B.

Ligated State (n)	Donor Only Lifetime (μs)	Donor-Acceptor Lifetime (μs)	Distance (Å)
GluN2B Cleft – GluN1 + GluN2B*^{cleft} (Ni(NTA)$_2$Cy3)*			
Apo (3)	1649 ± 1	204 ± 1.3	48.8 ± 0.4
GluN2A Cleft – GluN1 + GluN2A* ^{cleft} (Ni(NTA)$_2$Cy3)			
Apo (2)	1590 ± 1.3	312 ± 5.4	51.2 ± 0.1
GluN1 Cleft – GluN1^{cleft} + GluN2B*(Alexa555)*			
Apo (2)	1740 ± 1	275 ± 4	49.2 ± 0.1
GluN1 Cleft – GluN1^{cleft} + GluN2A*(Alexa555)*			
Apo (2)	1685 ± 1	324 ± 13	51.2 ± 0.3

Table 7.1: LRET lifetimes and distances for Apo ATDs. The error in the lifetimes is the SEM.

Chapter 8:
Zinc Induces a Cleft-Closure Conformational Change

This research was originally published in the Journal of Biological Chemistry. Sirrieh, R.E., MacLean, D.M., Jayaraman, V. Amino-terminal Domain Tetramer Organization and Structural Effects of Zinc Binding in the N-Methyl-d-aspartate (NMDA) Receptor. *Journal of Biological Chemistry*. 2013; 288: 22555-64.

8.1 Zinc Induced Conformational Changes

To study the conformational changes within the ATD of GluN2A subunits upon binding zinc, LRET lifetimes were obtained using the GluN2A^{cleft} construct, which retains Cys231,

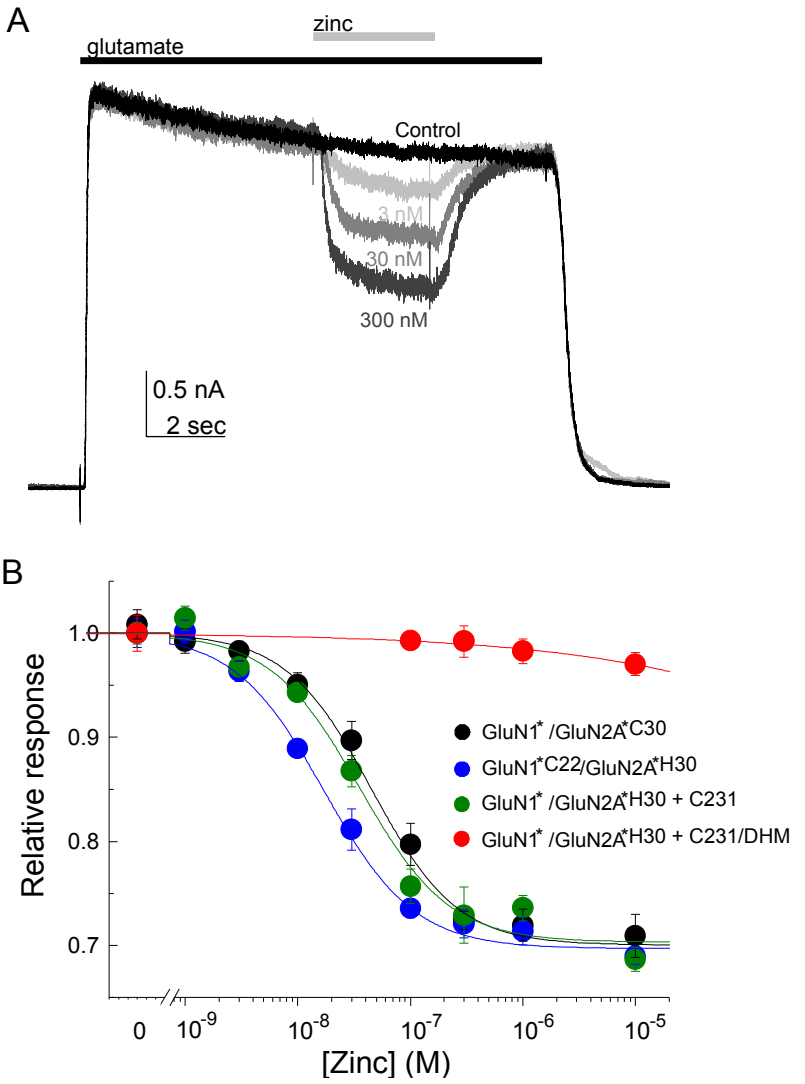

Figure 8.1: Zinc sensitivity of constructs used for LRET. (A) Representative whole cell recording from CHO cell expressing GluN1*/GluN2A*$^{H30+C231}$ receptors in response to 100 μM glutamate alone or with 3, 30 or 300 nM free zinc. (B) Summary zinc inhibition curves for each construct recorded at +50 mV with 4-8 cells for each point. Note that each construct shows high affinity zinc block with an IC_{50} between 17 and 45 nM zinc, except for the zinc-insensitive GluN2A*$^{H30+C231/DHM}$ mutant (red circles). Electrophysiology performed by Dr. David MacLean.

located in the lower lobe of the ATD. The receptor composed of GluN1*/GluN2A^{cleft} retains high affinity zinc inhibition with an IC_{50} of 35 ± 2 nM (Figure 8.1), which is consistent with previously reported wild-type affinities (Fayyazuddin, Villarroel et al. 2000, Zheng, Erreger et al. 2001, Erreger and Traynelis 2005). GluN2A^{cleft} was co-expressed with GluN1* in CHO cells, and receptors were labeled with a maleimide derivative of terbium chelate, which binds to Cys231 and a Ni-NTA conjugate of Cy3, which binds the hexa-His tag. This labeling strategy eliminated energy transfer between the N-termini of GluN2A subunits within the tetramer, allowing us to directly measure the GluN2A ATD cleft. The sensitized acceptor and donor only lifetime measurements (Figure 8.2) yield a distance of 51.6 ± 0.2 Å and 51.2 ± 0.1 Å in CHO cells using standard solutions or tricine buffered solutions, respectively (Table 2). Zinc binding induced a 3.5-4 Å decrease in distance between the donor and acceptor sites relative to the unligated states, with the distance being 47.7 ± 0.1 Å (Figure 8.2 and Table 8.1). This result suggests a cleft-closure conformational change takes place in the ATD upon zinc binding. Subsequent binding of the agonists glutamate and glycine does not alter the intra-subunit distance of the GluN2A ATD cleft (Figure 8.2). These measurements were completed to determine if binding of the agonists to the LBD altered the conformation of the ATD because, as discussed in Chapter 2, zinc and glutamate binding is cooperative. The cooperativity suggests that the conformation may be altered at the ATD by agonist binding. In our ensemble measurements, however, no differences were detected when the agonists were bound.

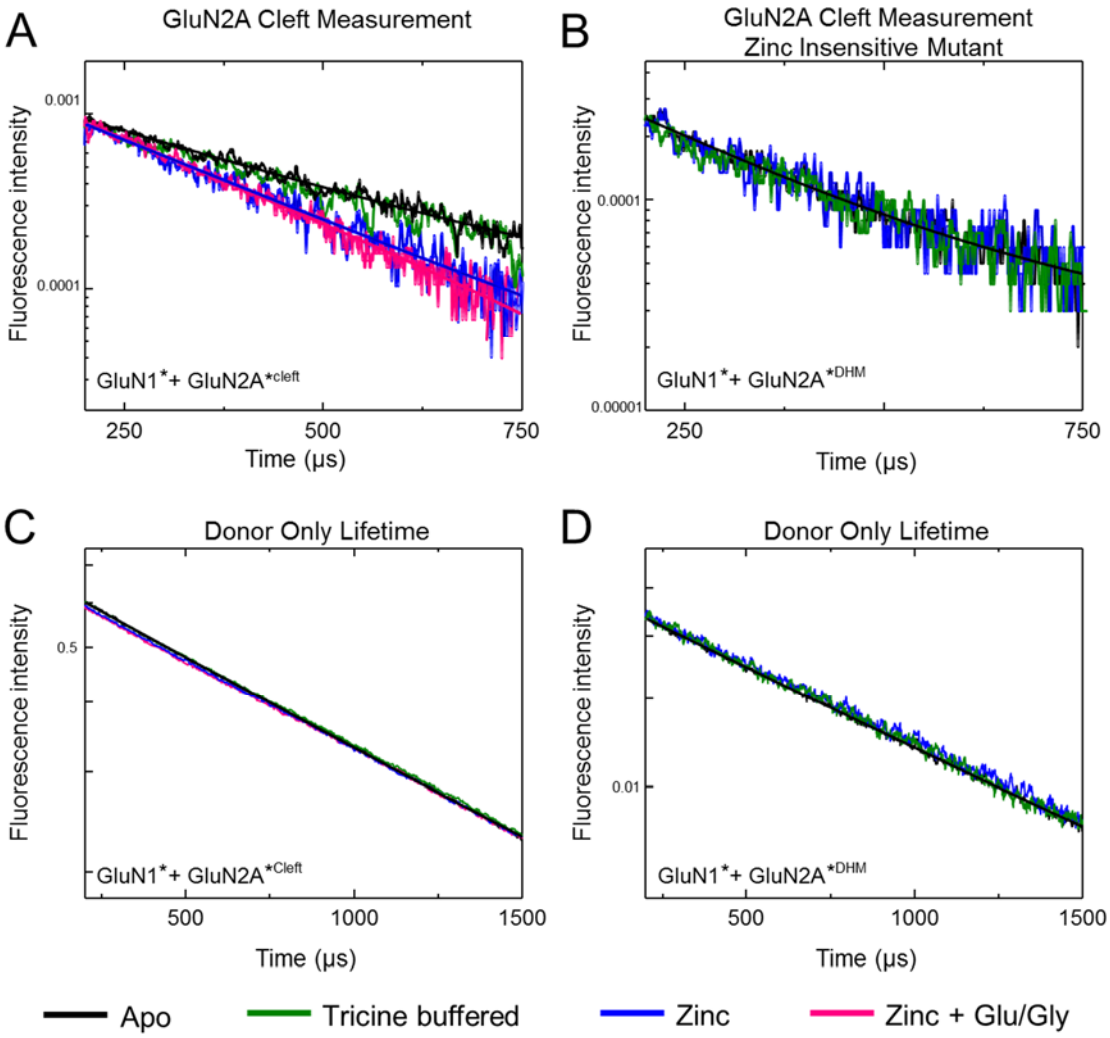

Figure 8.2: LRET lifetime measurements of the GluN2A ATD cleft. A) The LRET lifetimes measured across the intra-subunit ATD cleft of GluN2A, obtained by co-expressing GluN1* and GluN2A^{*clft} and labeling with terbium chelate and Ni(NTA)$_2$Cy3. B) The same lifetime measurement as in A) performed on a zinc-insensitive GluN2A with mutations H44A and H128S. This measurement was obtained by co-expressing GluN1* and GluN2A^{*DHM} and labeling with terbium chelate and Ni(NTA)$_2$Cy3. C) and D) Donor only lifetimes for the cleft measurements from constructs in panels A) and B), respectively. In all panels, the black line represents lifetimes from receptors in extracellular buffer, green shows tricine-buffered solutions, blue illustrates solutions with saturating zinc, and pink represents solutions with both saturating zinc and glutamate/glycine.

Wild Type Zinc Binding Constructs: GluN1* + GluN2A*cleft			
Ligated State (n)	**Donor Only Lifetime (μs)**	**Donor-Acceptor Lifetime (μs)**	**Distance (Å)**
Apo (4-6)	1546 ± 1.4	316 ± 8.1	51.6 ± 0.2
Tricine buffered (2)	1590 ± 1.3	312 ± 5.4	51.2 ± 0.1
Zinc (4)	1592 ± 1.3	219 ± 3.4	47.7 ± 0.1
Zinc, Glu/Gly (1)	1610 ± 1.4	211 ± 1.6	47.4 ± 0.1
Zinc Insensitive Mutant Constructs: GluN1* + GluN2A*DHM			
Apo (4-6)	1539 ± 2.0	302 ± 2.8	51.4 ± 0.1
Tricine buffered (2)	1547 ± 2.7	304 ± 3.2	51.4 ± 0.1
Zinc (4)	1591 ± 3.1	313 ± 5.5	51.4 ± 0.2

Table 8.1: Lifetimes and distances from LRET measurements. In parentheses after the ligated state for each construct is the n value. The error in the LRET lifetime is the SEM, and the error in the distances was calculated by propagating the errors in the lifetimes.

In order to confirm that the cleft-closure was caused by zinc binding to the ATD, we combined two mutations in the ATD (H44A and H128S) which individually reduce zinc inhibition (Choi and Lipton 1999, Fayyazuddin, Villarroel et al. 2000) onto the background of our GluN2A^{cleft} construct used for cleft-closure measurements, called GluN2A^{DHM}. Electrophysiology experiments confirm that this construct shows no substantial voltage-independent inhibition by zinc at concentrations as high as 10 μM (Figure 8.1). These experiments reveal that the cleft-closure is zinc dependent because acceptor and donor only lifetimes of receptors in the apo state, receptors in tricine-buffered solutions, and receptors in zinc-added solutions all yielded distances that were identical, 51.4 ± 0.1 Å (Figure 8.2 and Table 8.1). The distance matches the cleft distance in the apo receptor with wild type zinc

binding (Table 8.1). These experiments demonstrate that zinc induces a cleft-closure conformational change in the bi-lobed ATD structure of GluN2A.

GluN1-GluN2 interactions may also play a role in zinc modulation. Recent work by Zhu and colleagues argue that the GluN1 ATD undergoes both twisting and cleft-closure conformational changes as well as interacting with the GluN2B ATD to influence glutamate binding at the LBD (Zhu, Stroebel et al. 2013). However, any such interactions would arise without causing large scale motions between the upper lobes in intact functional receptors (Figures 6.1 and 6.2). These findings and recent computational studies suggest that the NTDs of both GluN1 (Zhu, Stroebel et al. 2013) and GluN2B undergo lateral twisting motions (Burger, Yuan et al. 2012, Dutta, Shrivastava et al. 2012) as well as cleft-closure movements (Dutta, Shrivastava et al. 2012, Zhu, Stroebel et al. 2013).

To map potential twisting motions in the lower lobe of the GluN2A ATD, the inherent Cys231 in GluN2A was maintained in a cys-free background (GluN2A*^{C231}) and co-expressed with GluN1*^{C22} to measure between the lower lobe of GluN2A and the upper lobe of GluN1. The receptor was labeled with terbium chelate and Alexa555. The lifetime from the apo receptor was 187 ± 5.6 μs (Figure 8.3), a distance of 45.9 ± 0.2 Å (Table 8.2), and the lifetime decreased to 156 ± 8.7 μs (Figure 8.3), a distance of 44.4 ± 0.4 Å when zinc was bound (Table 8.2). On average, the distance between these two sites decreased by ~2 Å. A second measurement was made between GluN2A Glu211Cys (GluN2A*^{211}), which is on the adjacent helix to Cys231, and the upper lobe of GluN1 (co-express with GluN1*^{C22}). Receptors were labeled with terbium chelate and Fluorescein. The LRET lifetimes again decreased when zinc was bound (Figure 8.3 and Table 8.2), corresponding to ~2 Å decrease in the distance between these two sites. Given that both of these distances decreased, and the GluN2A ATD closed around the zinc, the best explanation we can propose is that the lower lobe of the GluN2A ATD does indeed rotate towards the upper lobe of the GluN1 ATD.

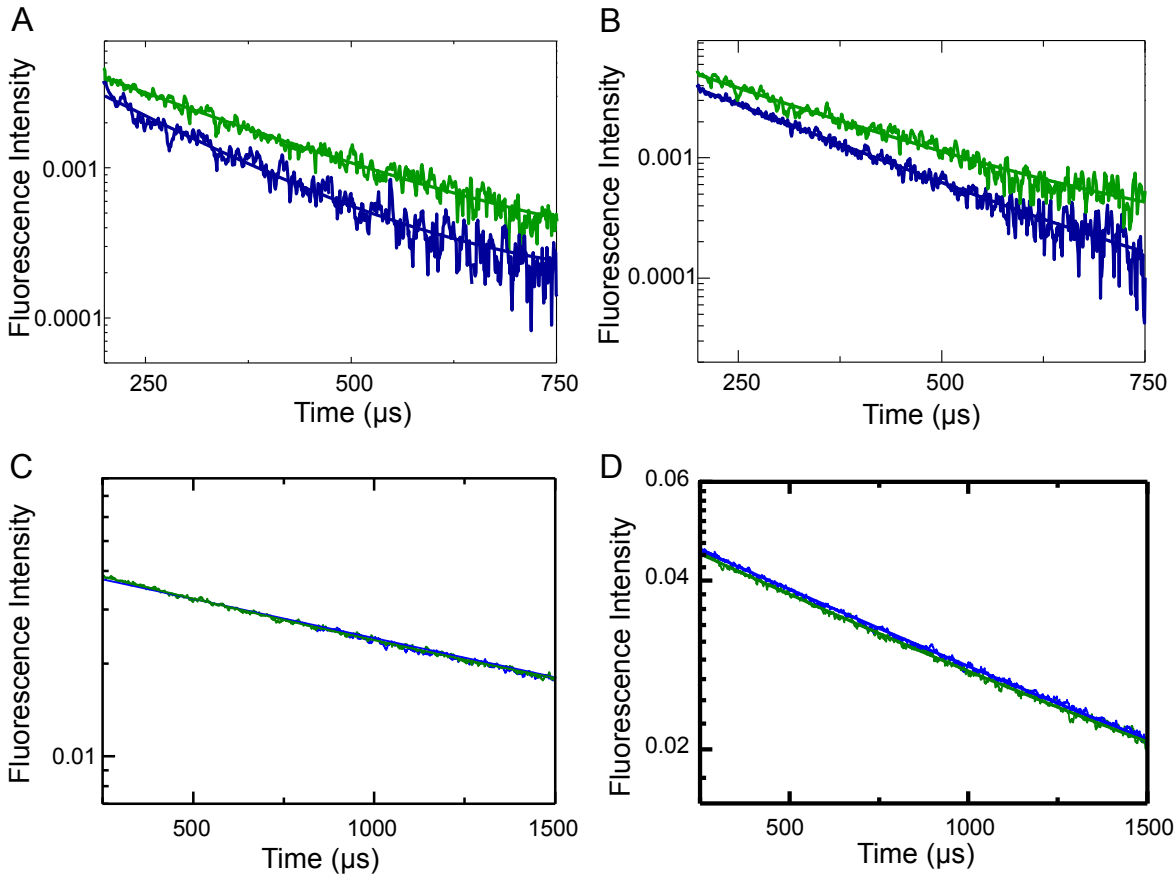

Figure 8.3: Zinc induces a rotational movement in the GluN2A ATD. (A) LRET measurements from the upper lobe of GluN1 to the lower lobe of GluN2A (Glu211Cys) are shown. The apo curve is in green and the zinc-bound receptor is in blue. (B) The LRET lifetimes from the measurement between the upper lobe of GluN1 to the lower lobe of GluN2A (Cys231) are shown with the apo receptor in green and the zinc-bound receptor in blue.

Ligated State (n)	Donor Only Lifetime (μs)	Donor-Acceptor Lifetime (μs)	Distance (Å)
GluN1^{C22} + GluN2A*^{C231} (Alexa555)*			
Apo (3)	1692 ± 0.9	187 ± 5.6	45.9 ± 0.2
Zinc (2)	1683 ± 0.8	156 ± 8.7	44.4 ± 0.4
GluN1^{C22} + GluN2A*^{211} (Fluorescein)*			
Apo (2)	1710 ± 0.9	239 ± 1.3	33.2 ± 0.1
Zinc (2)	1702 ± 0.9	176 ± 1.4	31.4 ± 0.1

Table 8.2 LRET Lifetimes and Distances of GluN2A twisting. The lifetimes and distances measuring between the lower lobe of GluN2A and the upper lobe of GluN1.

8.2 Discussion

NMDA receptors differ from the AMPA and kainate receptor subtypes in their ability to bind small molecule allosteric inhibitors at their ATD. Crosslinking and cleft-locking experiments provide indirect evidence for a cleft-closure conformational change induced by these small molecules (Gielen, Le Goff et al. 2008, Gielen, Retchless et al. 2009). However, the crystal structures of the isolated GluN2B ATD in the apo and zinc-bound forms (PDB IDs 3JPW and 3JPY) are both in the closed cleft conformation, with only a 0.3 Å difference between the α-carbons of residues labeled in our experiments (Figure 2.1) (Karakas, Simorowski et al. 2009). The LRET data presented here shows that on average the GluN2A ATD cleft is more closed in the zinc bound state relative to the cleft in the absence of zinc. This is further confirmed by the absence of this change in the zinc-insensitive mutant (Figure 8.2).

In both the absence and presence of zinc, crystal structures capture a closed-cleft state of the ATD, suggesting that this domain samples a range of conformations from an open

to a closed cleft state (Figure 2.1) (Karakas, Simorowski et al. 2009). A similar situation occurs with the LBD of AMPA receptors where single molecule FRET (smFRET) studies show that the LBD samples a spectrum of open and closed cleft conformations in both apo and agonist-bound states (Landes, Rambhadran et al. 2011, Ramaswamy, Cooper et al. 2012), with the agonist bound forms on average being more closed. Similar NMR and smFRET studies such as those performed on the AMPA receptor LBD may be able to provide insight into the role of such dynamics in zinc modulation of the receptor function (Maltsev, Ahmed et al. 2008, Maltsev and Oswald 2010, Landes, Rambhadran et al. 2011, Ramaswamy, Cooper et al. 2012).

Chapter 9:
Cleft Closure is a Common Mechanism of Inhibition: Cue Ifenprodil

This research has been submitted for consideration for publication to the Journal of General Physiology. Sirrieh, R.E., MacLean, D.M., Jayaraman, V. “A conserved structural mechanism of NMDA receptor inhibition: a comparison of ifenprodil and zinc.”

9.1 Mechanism of Ifenprodil Inhibition

Zinc inhibits the NMDA receptor by stabilizing a closed GluN2 ATD cleft (Gielen, Le Goff et al. 2008, Sirrieh, MacLean et al. 2013). To determine if the GluN2B specific inhibitor ifenprodil, which binds at the interface between the GluN1 and GluN2B ATDs (Figure 1.4), induces a cleft closure in the GluN2B ATD similarly to zinc, we used LRET to monitor the conformational state of the GluN2B ATD. The same inherent cysteine in the lower lobe of the GluN2 ATD as used for the zinc measurements and a hexa-histidine tag at the N-terminus of the ATD (Sirrieh, MacLean et al. 2013) were labeled with terbium chelate and $Ni(NTA)_2Cy3$, as the donor and acceptor fluorophores, respectively. The lifetime from the apo receptor was 252 ± 12 μs, which is a distance of 48.8 ± 0.4 Å between the two fluorophores. Upon ifenprodil binding, the lifetime decreases to 227 ± 26 μs, a distance of 47.0 ± 0.9 Å, about 2 Å of cleft closure. Importantly, the receptors encoded by these mutants were inhibited by 10 μM ifenprodil to the same degree, 81.6 ± 2.7 % inhibition in wild type receptors and 81.7 ± 2.9 % inhibition for the $GluN2B^{cleft}$-GluN1* receptor (Figure 9.2).

Since the GluN1 ATD adopts different conformations when co-assembled with different GluN2 subunits, we knew that it was able to undergo conformational changes. We wanted to determine if ifenprodil, which binds at the interface between GluN1 and GluN2B affects the conformation of the GluN1 ATD. We used LRET to measure the distances between the upper and lower lobes of the GluN1 ATD in the presence of ifenprodil. The distance of the GluN1 cleft for the apo receptor 49.2 Å (Figure 9.1, Table 9.1, Chapter 7). The lifetime for the ifenprodil-bound receptor was 263 ± 1.5 μs (Figure 9.1), corresponding to an almost identical distance of 48.7 ± 0.1 Å. Ifenprodil does not affect the overall conformation of the GluN1 ATD. The receptor was 79.6 ± 2.7% inhibited by ifenprodil, similar to the wild type receptor (Figure 9.2).

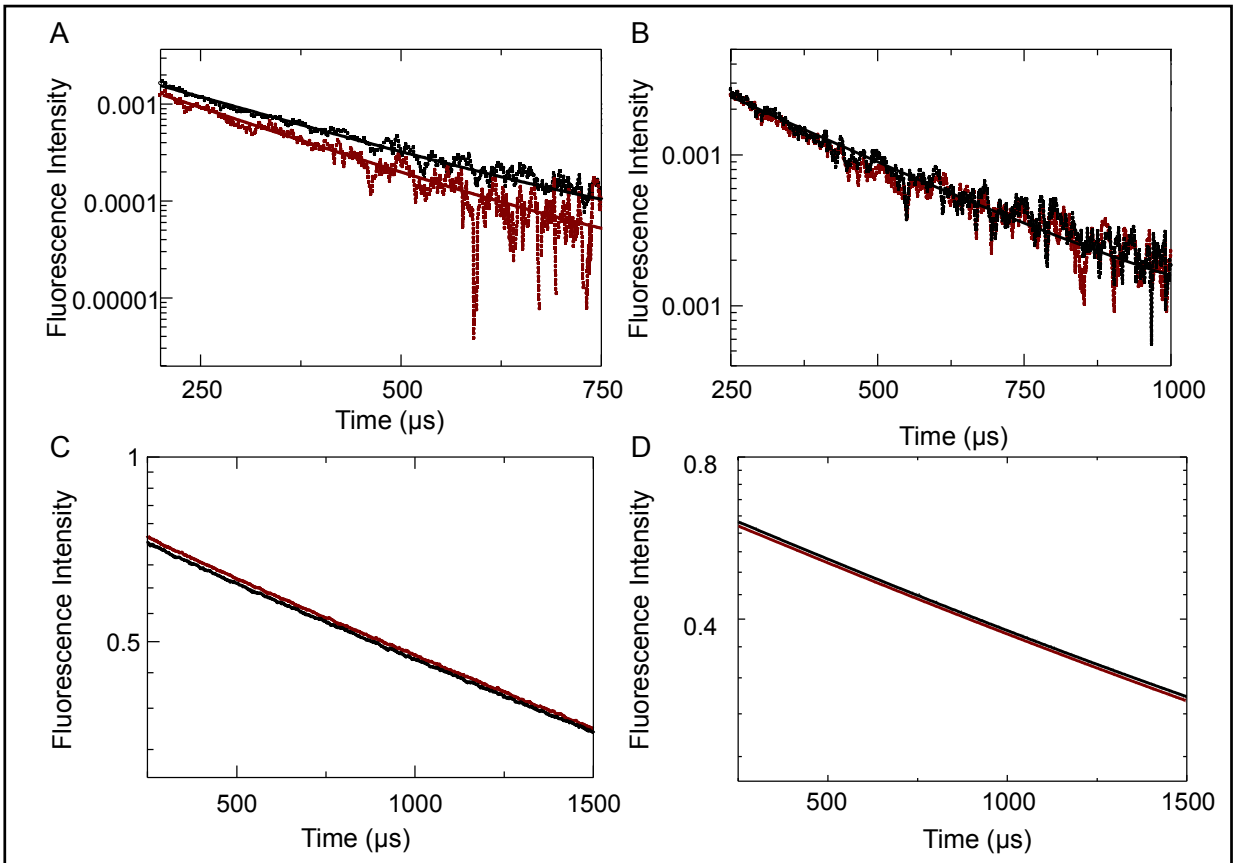

Figure 9.1: Ifenprodil's effects on ATD cleft Conformations. (A) LRET measurements in the GluN2B cleft reveal that ifenprodil induces a cleft-closure. (B) LRET measurements of the GluN1 cleft. Shown in panels (C) and (D) are the donor only lifeteims for the GLuN2B and GluN1 clefts, respectively. In all panels, the black curve is from the apo receptor and the maroon curve is from the ifenprodil bound receptor.

Although zinc induced no change in the GluN1-GluN2A distance, we wanted to confirm that this stability at the upper lobes extended to modulators which bind at the ATD interface. To measure the distance between the upper lobes of the GluN1 and GluN2B ATDs, we co-expressed the GluN1*^{C22} construct with GluN2B*^{H30} and labeled the receptor with terbium chelate and $Ni(NTA)_2Cy3$. The LRET lifetime for the apo receptor was 362 ± 26 μs (Figure 9.3), a distance of 52.1 ± 0.6 Å. The lifetime when the receptor was bound by ifenprodil was 347 ± 26 μs (Figure 9.3), corresponding to a similar distance of 52.0 ± 0.6 Å (Table 9.1).

Although the distances between the upper lobes of the ATDs does not change at the sites we measured, this data does not preclude the possibility that the GluN1 and GluN2B

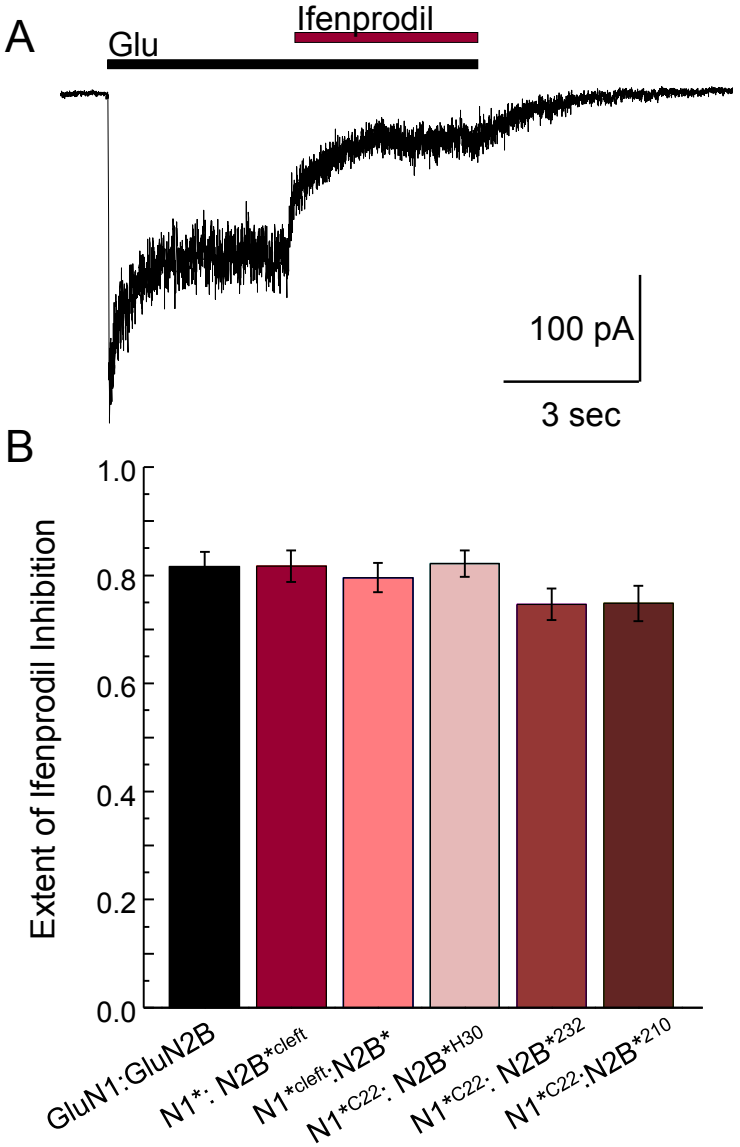

Figure 9.2: Ifenprodil Inhibition Electrophysiology. (A) A sample whole-cell recording showing ifenprodil inhibition of NMDA receptors. (B) The extent of ifenprodil inhibition is plotted in comparison to the wild type receptor. Electrophysiology was performed by Dr. David MacLean.

ATDs are forming new contacts during modulation. In fact, crosslinking studies between the two ATDs suggest that mobility is required and that the two subunits may indeed be interacting (Karakas, Simorowski et al. 2011). If the upper lobes of the ATDs are not moving with respect to each other, but there are conformational changes taking place within an ATD, the data

suggests the lower lobes of the ATDs are moving. Zinc was found to induce a rotational movement in the lower lobe of the GluN2A ATD, so that it moves closer to the upper lobe of the GluN1 ATD. To map the movement of the lower lobe of the GluN2B ATD, which seems to close when ifenprodil binds, we measured the LRET between the lower lobe of the GluN2B ATD and the upper lobe of the GluN1 ATD. First, we co-expressed the GluN1*^{C22} with GluN2B*^{232} and labeled the receptor with terbium chelate and Alexa555. The sensitized acceptor lifetime of the apo receptor was 229 ± 9 µs (Figure 9.4), giving a distance of 47.8 ± 0.4 Å (Table 9.1). The lifetime decreased to 194 ± 8 µs when the receptor was bound by ifenprodil, corresponding to 46.2 ± 0.3 Å. Ifenprodil inhibition is normally maintained with 74.6 ± 2.9 % inhibition at saturating concentrations of ifenprodil (Figure 9.2). Additionally, zinc induces a decrease in this distance between the upper and lower lobes of the GluN2B ATD (Figure 9.3 and Table 9.1). Second, we will measure between a second set of sites by co-expressing the GluN1*^{CT} with GluN2B*^{210} constructs and labeling the receptor with terbium chelate and fluorescein. This construct has already been functionally characterized and is normally inhibited by ifenprodil, 74.8 ± 3.3 % inhibition. When ifenprodil binds, the cleft closes, but the lower lobe also twists towards the upper lobe of the GluN1 ATD as demonstrated by

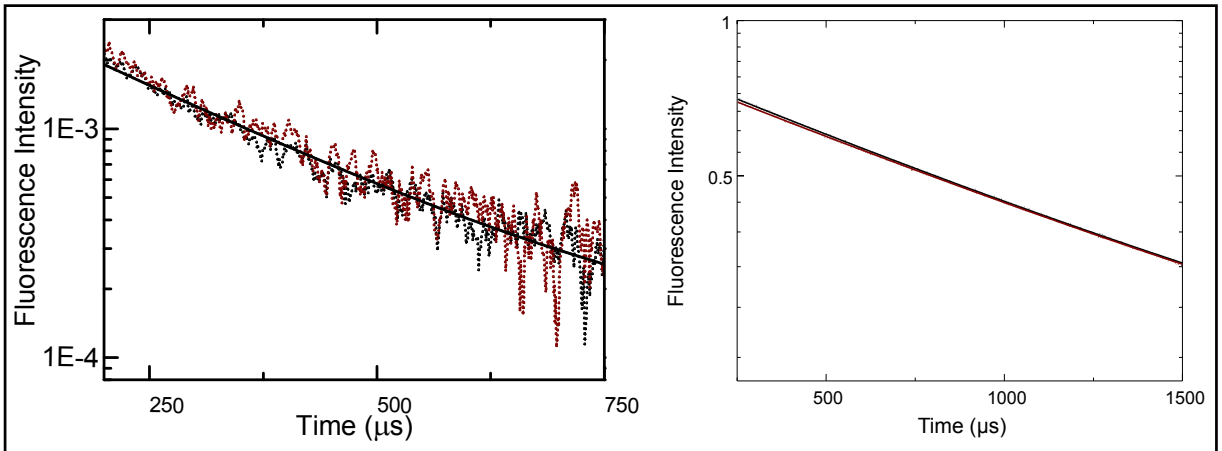

Figure 9.3: Inter-subunit measurements with Ifenprodil. Shown in panel (A) is the LRET measurement between the upper lobes of the GluN1 and GluN2B ATDs. In black is the apo receptor and in maroon is the ifenprodil-bound receptor. (B) Donor only lifetimes for the GluN1-GluN2B upper lobes measurements.

the decrease in both of the measurements made between the lower lobe of the GluN2B ATD and the upper lobe of the GluN1 ATD.

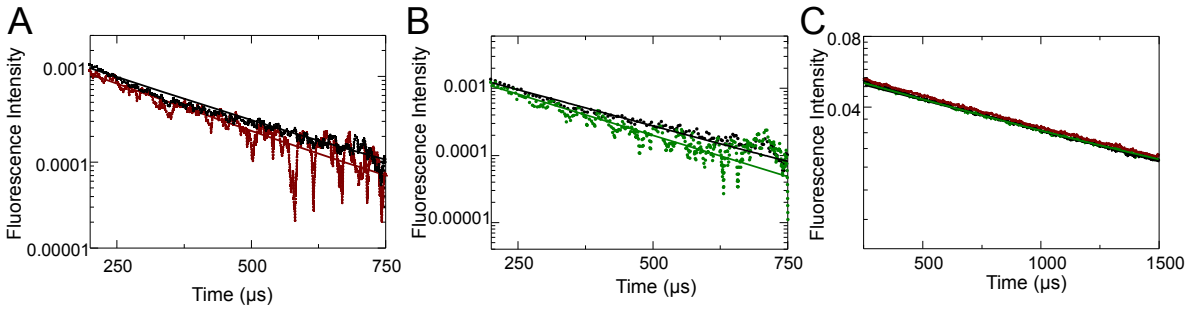

Figure 9.4: LRET measurements showing twist of GluN2B ATD. (A) Changes in the LRET lifetime induced by ifenprodil. In black is the LRET lifetime from the apo receptor and in maroon is the lifetime with ifenprodil. (B) Zinc similarly induces a reduction in the LRET lifetime. In black is the LRET lifetime from the apo receptor, and the zinc-bound receptor is in green. (C) The donor only lifetimes from the apo (black), ifenprodil-bound (maroon), and zinc-bound (green) receptors.

Ligated State (n)	Donor Only Lifetime (μs)	Donor-Acceptor Lifetime (μs)	Distance (Å)
GluN2B Cleft – GluN1 + GluN2B*^{cleft} (Ni(NTA)$_2$Cy3)*			
Apo (3)	1847 ± 1	252 ± 12	48.8 ± 0.4
Ifenprodil (4)	1826 ± 1	227 ± 26	47.0 ± 0.9
GluN1 Cleft – GluN1^{cleft} + GluN2B*(Alexa555)*			
Apo (2)	1740 ± 1	275 ± 4	49.2 ± 0.1
Ifenprodil (2)	1747 ± 1	263 ± 1.5	48.7 ± 0.1
GluN1-GluN2B Upper Lobes – GluN1^{CT} + GluN2B*^{HT}(Ni(NTA)$_2$Cy3)*			
Apo (5)	1738 ± 1	362 ± 26	52.1 ± 0.6
Ifenprodil (2)	1807 ± 1	374 ± 26	52.0 ± 0.6
GluN1 Upper Lobe-GluN2B Lower Lobe – GluN1^{CT} + GluN2B*^{232} (Alexa555)*			
Apo (3)	1674 ± 16	228 ± 9	47.8 ± 0.3
Ifenprodil (3)	1694 ± 3.5	194 ± 8	46.2 ± 0.3
Zinc (3)	1727 ± 1	184 ± 4	45.6 ± 0.2

Table 9.1: Ifenprodil LRET lifetimes and Distances. Shown are the lifetimes and distances from measurements in GluN1/GluN2B receptors in the apo, ifenprodil bound, and zinc bound states.

9.2 Discussion

Ifenprodil induces similar conformational changes upon binding to GluN1-GluN2B receptors as zinc does upon binding to GluN1-GluN2A receptors. The GluN2 domain closes upon binding of the inhibitor, and the lower lobe of the GluN2 ATD moves towards the upper lobe of the GluN1 ATD in a rotational movement. The GluN1 ATD conformation is unaffected by the binding of either zinc or ifenprodil. Interestingly, ifenprodil induces a much smaller conformational change than does zinc. We suggest that the lesser degree of conformational change stems from the inherently more closed ATD of the GluN2B subtype relative to the

GluN2A subtype. Ifenprodil pushes the GluN2B ATD towards the limit of domain closure as a mechanism to achieve inhibition, and it has less to close the domain than an inhibitor of the GluN2A subtype. Interestingly, the distance between the upper lobes of the GluN1 and GluN2B subunits, within an ATD dimer, are almost identical (~51 Å) to the distance between the upper lobes of GluN1 and GluN2A subunits. This similarity suggests that the lower lobes of the ATDs are oriented differently in GluN2A and GluN2B subunits.

Ideally, we would have liked to complete measurements of the GluN2B cleft and the GluN1-2B distance at the upper lobes of the ATDs with zinc, to be able to draw a complete comparison between zinc and ifenprodil inhibition. However, the higher concentration of zinc required to saturate GluN2B containing receptors caused a displacement of the terbium from the chelate or the $Ni(NTA)_2Cy3$ from the hexa-his tag, making it impossible to subtract background and accurately measure the lifetime.

Chapter 10:
Spermine potentiates via a reverse inhibition structural mechanism

This research was originally published in the Journal of Biological Chemistry. Sirrieh, R.E., MacLean, D.M., Jayaraman, V. Subtype dependent NMDA receptor amino-terminal domain conformations and modulation by spermine. *Journal of Biological Chemistry*. 2015; 290: 12812-20. © The American Society for Biochemistry and Molecular Biology.

10.1 Spermine Induced Conformational Changes

To determine the effect of spermine binding, the LRET lifetime was again measured across the GluN2B cleft (using the GluN2B^{cleft} construct co-expressed with GluN1*) in the presence of the GluN2B specific potentiator spermine. The LRET lifetime increases to 369 ± 34 μs (Figure 10.1), corresponding to a distance of 52.8 ± 0.8 Å (Table 10.1). The increase in the distance upon addition of spermine is consistent with an opening of the cleft of the GluN2B ATD. Importantly, this construct was potentiated by spermine to the same extent as the wild-type receptor (K., Zappia et al. 1994, Mony, Zhu et al. 2011), with equilibrium responses increasing by 1.66 ± 0.10 (n=3) fold and 1.41 ± 0.05 (n=5) fold, respectively, in the presence of spermine (Figure 10.2). Spermine binding stabilizes an open conformation of the GluN2B ATD, and, since spermine likely binds at the interface between the GluN1 and GluN2B ATDs, the conformation of the GluN1 ATD can be influenced by spermine binding.

It has been shown that the GluN1 ATD is necessary to the mechanism of allosteric modulation as its deletion or cleavage affects allosteric inhibition and potentiation (Madry, Mesic et al. 2007, Mony, Zhu et al. 2011). The structural role of the GluN1 ATD in spermine modulation, however, is unclear, aside from potentially contributing amino acids to the spermine binding site (Mony, Zhu et al. 2011, Tomitori, Suganami et al. 2012). The GluN1 ATD can be passive, simply acting as a wedge that supports the GluN2 ATD so that conformational changes in the GluN2 ATD can be efficiently propagated to the LBDs and the pore. Alternatively, the GluN1 ATD can be directly influenced and undergo conformational changes upon binding of the modulator, particularly a modulator like spermine which likely binds at the interface between the GluN1 and GluN2B ATDs. To determine the role of the GluN1 ATD in spermine potentiation, we measured conformational changes in the GluN1 cleft by introducing two cysteines, one each in the upper and lower lobes of the ATD. These cysteines, the inherent one at position 22 and the second introduced by the Ser224Cys

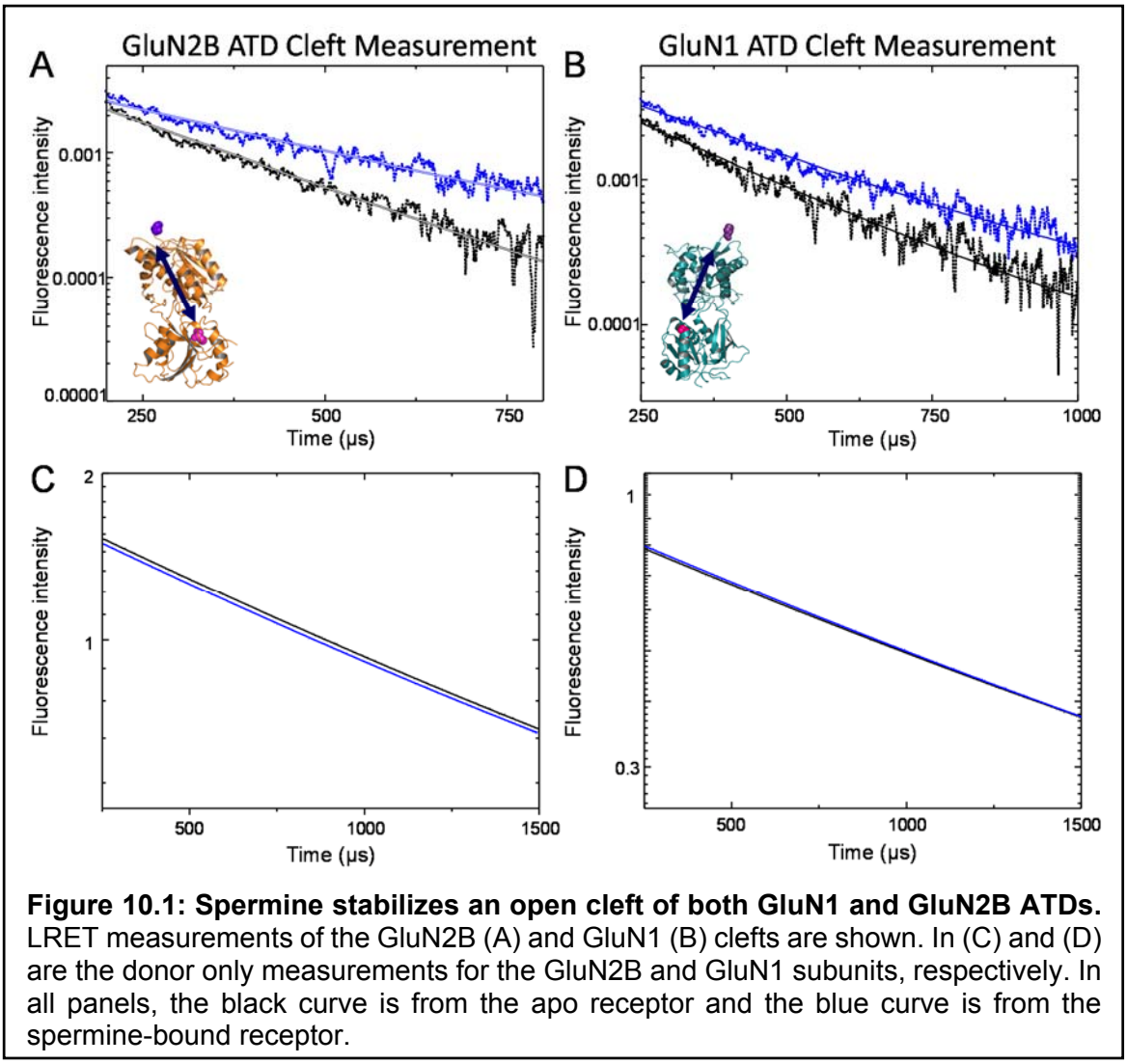

Figure 10.1: Spermine stabilizes an open cleft of both GluN1 and GluN2B ATDs. LRET measurements of the GluN2B (A) and GluN1 (B) clefts are shown. In (C) and (D) are the donor only measurements for the GluN2B and GluN1 subunits, respectively. In all panels, the black curve is from the apo receptor and the blue curve is from the spermine-bound receptor.

mutation in the GluN1 ATD, would allow for direct monitoring across the cleft of the bi-lobed ATD. This GluN1^{cleft} construct was co-expressed with a cys-free GluN2B (GluN2B*). The LRET lifetime of the GluN1 cleft for the apo receptor could be well represented with a single exponential decay corresponding to 275 ± 4 μs (Figure 10.1), giving a distance of 49.2 ± 0.1 Å (Table 10.1). Again, based on the crystal structure this distance is consistent with the measurement being within a single ATD and not across the subunits. Additionally, this construct was normally potentiated with equilibrium responses increasing by 1.79 ± 0.07 (n=9) fold in the presence of spermine (Figure 10.2). Addition of spermine led to an increase in the

LRET lifetime to 340 ± 29 μs (Figure 10.1), corresponding to a distance of 51.5 ± 0.7 Å (Table 10.1). These data suggest that spermine binding stabilizes the GluN1 ATD in an open conformation, meaning that the GluN1 ATD plays a direct role in modulating NMDA receptor function and is not a passive player.

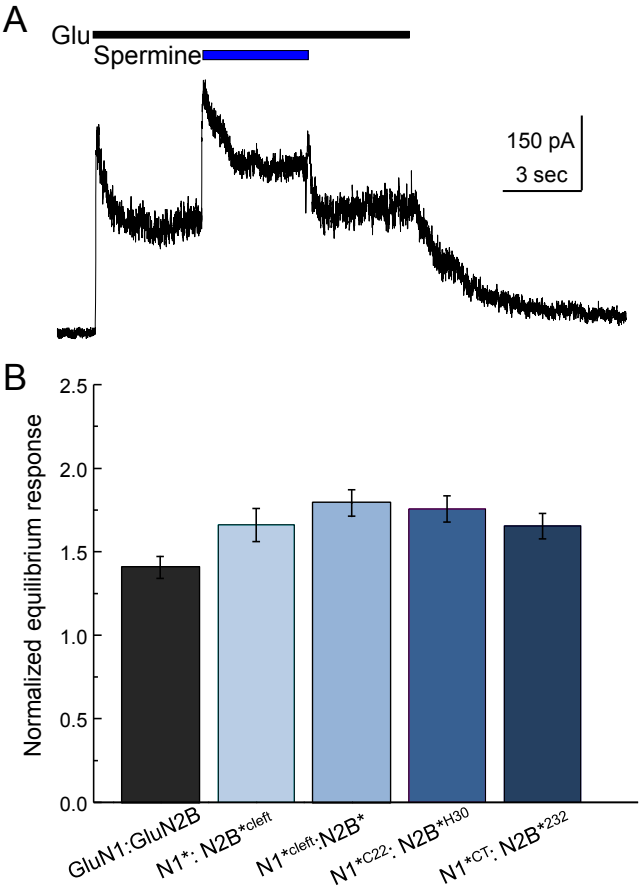

Figure 10.2: Electrophysiological characterization of the mutants used for the LRET experiments. (A) A sample trace is shown of spermine potentiating the whole-cell currents obtained from CHO cells. (B) Group data showing the extent of spermine potentiation for the various mutants as compared to the wild-type receptor. Error bars represent the SEM. Electrophysiology was performed by Dr. David MacLean.

The fact that the GluN1 ATD undergoes a conformational change does not preclude its possible role as a wedge supporting the GluN2B ATD. In fact, we would expect that interactions between the subunits are critical to the mechanism of allosteric modulation; if the ATDs underwent conformational changes and were free to move independent of each other, how could those conformational changes be responsible for modulating the function of the receptor? The ATDs require an anchor point so that conformational changes can be propagated towards the LBDs and pore of the receptor. In the case of zinc inhibition, we have previously shown that the upper lobes of the ATDs do not undergo any conformational changes during zinc inhibition or upon binding of the agonists glutamate and glycine (Sirrieh, MacLean et al. 2013). To probe the upper lobes of the ATDs during spermine

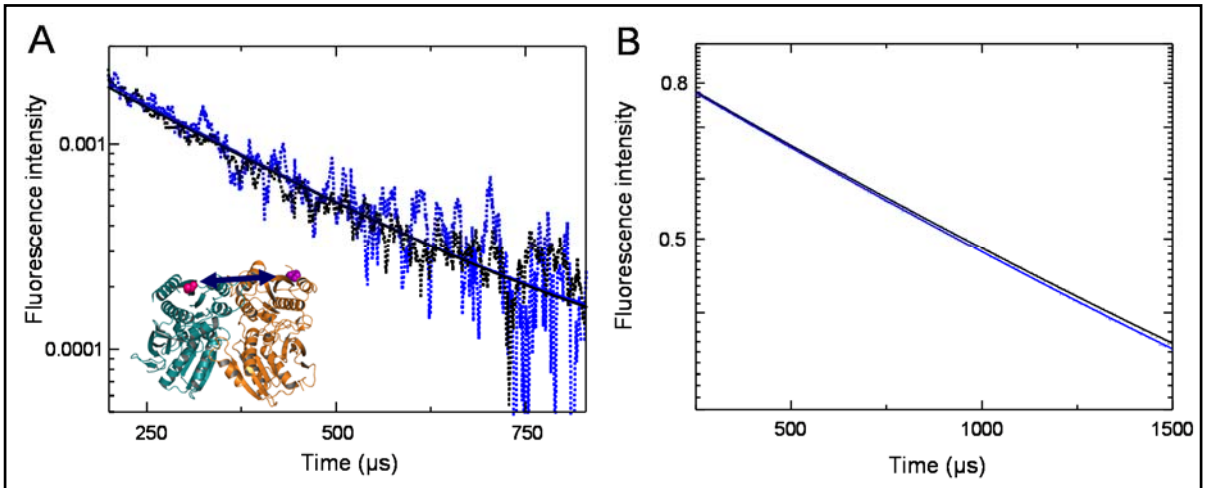

Figure 10.3: Spermine binding does not affect the upper lobes of the ATDs. (A) These curves are the sensitized acceptor emission for receptors labeled at the upper lobes of the ATDs. The lifetime does not change when spermine is bound. (B) The donor only lifetimes for the measurements between the upper lobes of the ATDs are shown. In all panels, the black curve is from the apo receptor and the blue curve is from the spermine-bound receptor.

potentiation, measurements were next made by co-expressing the GluN1*^{C22} construct with GluN2B*^{H30} and labeling the receptor with terbium chelate and Ni(NTA)$_2$Cy3. These constructs allowed for the specific introduction of the donor fluorophore at the upper lobe (N-terminus) of the GluN1 ATD and the acceptor fluorophore at the upper lobe (N-terminus) of the GluN2B ATD. As with previous constructs, the potentiation by spermine was near wild-type levels, with the equilibrium response increased by 1.76 ± 0.08 (n=7) fold (Figure 10.2). The LRET lifetime for the apo receptor was well represented by a single lifetime of 362 ± 26 μs (Figure 10.3), corresponding to a distance of 52.1 ± 0.6 Å (Table 10.1). The binding of spermine to the receptor resulted in no change in the distance, as the lifetime was 311 ± 43 μs (Figure 10.3), giving a distance of 50.7 ± 1.2 Å (Table 10.1). The upper lobes of the ATDs are not moving with respect to each other when spermine binds, but spermine opens up both the GluN1 and GluN2B ATDs. Collectively, these data suggest that spermine binding causes the movement of the lower lobes of the ATDs.

To map the movement of the lower lobe of the GluN2B ATD, which is stabilized in an open conformation when spermine binds, we measured the LRET between the lower lobe of the GluN2B ATD and the upper lobe of the GluN1 ATD. The GluN1*^{C22} construct was co-expressed with GluN2B*^{232} and labeled with terbium chelate and Alexa555. Spermine potentiation was preserved in this construct, with a 1.65 ± 0.08 (n=9) fold increase in equilibrium response (Figure 10.4). The sensitized acceptor lifetime of the apo receptor was 228 ± 16 μs (Figure 10.4), a distance of 47.6 ± 0.6 Å (Table 10.1). The lifetime decreased to 161 ± 14 μs (Figure 10.4) when the receptor was bound by spermine, corresponding to a distance of 44.6 ± 0.6 Å (Table 10.1).

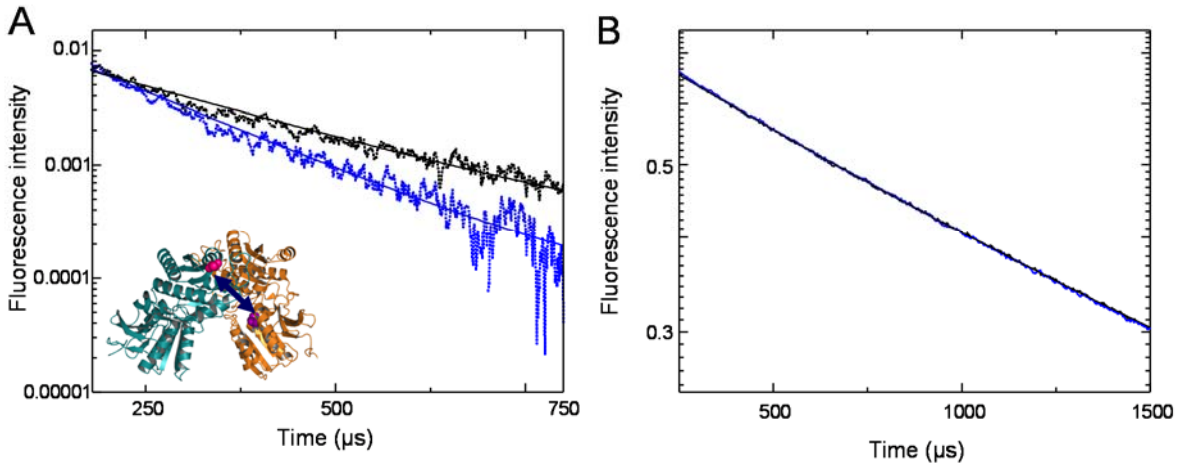

Figure 10.4: The lower lobe of the GluN2B ATD rotates towards the upper lobe of the GluN1 ATD. (A) LRET measurements between the lower lobe of the GluN2B ATD (Cys232) and the upper lobe of the GluN1 ATD show that the lifetime decreases when spermine is bound. (B) Donor only lifetimes for these constructs are shown. In all panels, the black curve is from the apo receptor and the blue curve is from the spermine-bound receptor.

Ligated State (n)	Donor Only Lifetime (μs)	Donor-Acceptor Lifetime (μs)	Distance (Å)
GluN2B Cleft – GluN1 + GluN2B*^{cleft} (Ni(NTA)$_2$Cy3)*			
Apo (3)	1649 ± 1	252 ± 12	48.8 ± 0.4
Spermine (4)	1659 ± 1	369 ± 34	52.8 ± 0.8
GluN1 Cleft – GluN1^{cleft} + GluN2B*(Alexa555)*			
Apo (2)	1740 ± 1	275 ± 4	49.2 ± 0.1
Spermine (2)	1714 ± 1	340 ± 29	51.5 ± 0.7
GluN1-GluN2B Upper Lobes – GluN1^{CT} + GluN2B*^{HT}(Ni(NTA)$_2$Cy3)*			
Apo (5)	1724 ± 1	362 ± 26	52.1 ± 0.6
Spermine (2)	1693 ± 1	311 ± 43	50.7 ± 1.2
GluN1 Upper Lobe-GluN2B Lower Lobe – GluN1^{CT} + GluN2B*^{232} (Alexa555)*			
Apo (3)	1706 ± 1	228 ± 16	47.6 ± 0.6
Spermine (3)	1682 ± 1	161 ± 14	44.6 ± 0.6

Table 10.1: Lifetimes and distances from LRET measurements with Spermine. In parentheses after the ligated state for each construct is the n value. Also, listed next to the constructs is the acceptor fluorophore used. The donor fluorophore for all measurements was terbium chelate. The error in the LRET lifetime is the SEM, and the error in the distances was calculated by propagating the errors in the lifetimes.

10.2 Discussion

Spermine causes the GluN2B cleft to open but the lower lobe of GluN2B seems to be rotated towards the upper lobe of the GluN1 ATD. These data suggest that although spermine binding stabilizes an open GluN2B ATD, the lower lobe of the ATD additionally rotates bringing Cys232 closer to the upper lobe of the GluN1 ATD. Studies attempting to identify the binding site of spermine identified several acidic residues at the lower lobes of both the GluN1 and GluN2B ATDs that have an effect on spermine affinity. Residues including Asp170, Glu181, Glu185, and Glu186 in GluN1 and Glu191, Glu198, Glu200, and Glu201 in GluN2B were

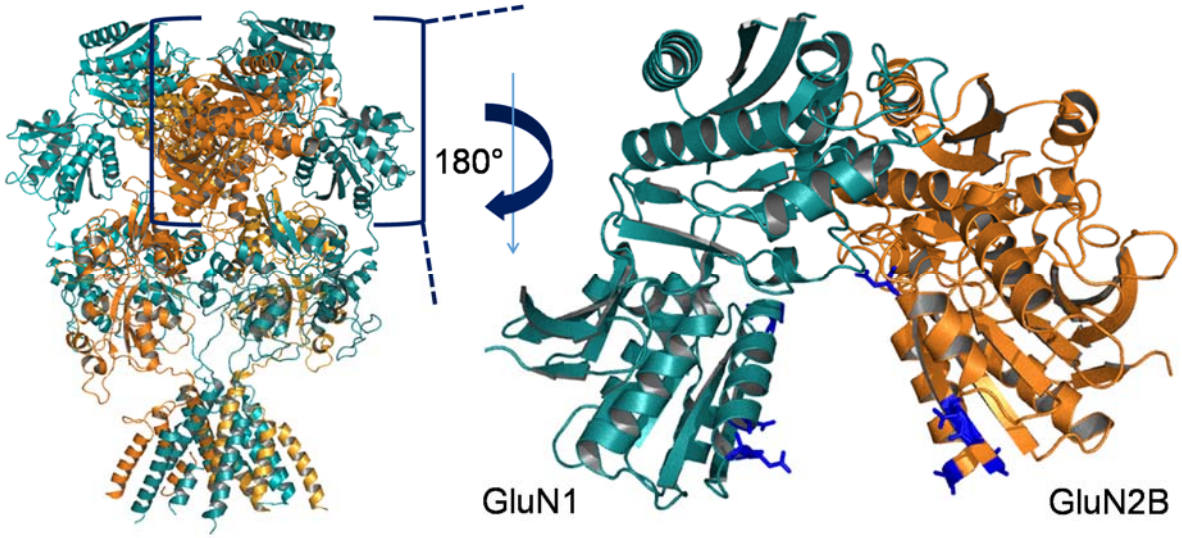

Figure 10.5: Spermine binding residues. GluN1 subunits are in teal and GluN2B subunits are in orange. Highlighted in blue on the GluN1/GluN2B ATD dimer are the proposed spermine binding residues including Asp170, Glu181, Glu185, and Glu186 in GluN1 and Glu191, Glu198, Glu200, and Glu201 in GluN2B (Mony, Zhu et al. 2011, Tomitori, Suganami et al. 2012).

identified (residues highlighted in blue in Figure 10.5) (Mony, Zhu et al. 2011, Tomitori, Suganami et al. 2012). Based on the crystal structure of the full length NMDA receptor (Karakas and Furukawa 2014, Lee, Lü et al. 2014), it is clear that these residues are too far apart in the structure to be able to bind spermine. Distances measured between spermine binding residues highlighted in Figure 10.5 range from 18-23 Å in the crystal structure, but thiol reactive reagents less than 8 Å in length are able to cross-link the lower lobes of the GluN1-GluN2B ATDs (Mony, Zhu et al. 2011). In further support of the closer proximity of these domains at the lower lobes is that cross-linkers less than 8 Å in length can be used to crosslink the lower lobes of the GluN1-GluN2B ATDs (Mony, Zhu et al. 2011). The crystal structures were obtained in the presence of the allosteric inhibitors ifenprodil in one case and Ro25-6981 in the other (Karakas and Furukawa 2014, Lee, Lü et al. 2014). These structures thus would correspond to an inhibited state of the receptor. Consequently, spermine binding to these residues should be expected to move the lower lobes of the ATDs closer.

This work provides insight into the conformational changes occurring upon potentiator binding to the ATDs of the NMDA receptor. We can conclude that the upper lobes of the ATDs are stable and do not undergo any large conformational changes on average when spermine binds (Figure 10.3). However, spermine binding does cause an opening of the ATDs of both the GluN1 and GluN2B ATDs (Figure 10.1). The measured distances of the GluN1 and GluN2B ATDs match the distances in the ATDs in the full-length structure (Karakas and Furukawa 2014, Lee, Lü et al. 2014). The lack of movement of the upper lobes of the ATDs suggests that the movements taking place are due to movement of the lower lobes of the ATDs. When looking at the crystal structures of the full length NMDA receptor (Karakas and Furukawa 2014, Lee, Lü et al. 2014), the residues are too far apart in that, presumably inhibited, state to bind spermine. For binding to occur, these residues must be brought closer, requiring a rotation of the lower lobes of the ATDs in order to bridge the distance. We infer this rotation from the combined opening of the GluN1 and GluN2B ATDs and the movement of the lower lobe of the GluN2B ATD towards the upper lobe of the GluN1 ATD. Moreover, these findings are consistent with cross-linking studies that suggested that mobility of the lower lobes of the ATDs are critical to allosteric modulation (Karakas, Simorowski et al. 2011). Overall, the data suggest that spermine potentiates the NMDA receptor by stabilizing open conformations of both the GluN1 and GluN2B ATDs.

Chapter 11:
Conclusions, Impact, and Future Directions

11.1 Conclusions

Our data show that the ATDs of NMDA receptors are indeed organized as a dimers of heterodimers. Further, the data show that the ATDs of NMDA receptors adopt a significantly more compact arrangement than the ATDs of AMPA and kainate receptors. The upper lobes of the ATDs do not undergo any large-scale conformational changes upon binding any ligand (Sirrieh, MacLean et al. 2013). The binding of the agonists and subsequent desensitization was thought to cause a rupture in the ATDs so that they separated, something that has now been demonstrated in AMPA receptors (Meyerson, Kumar et al. 2014). However, in our steady state measurements of ATD organization, the binding of glutamate and glycine and subsequent desensitization of the receptor yielded no changes in the distances between subunits, suggesting that NMDA receptors have a unique mechanism of desensitization that does not result in separation of the ATDs. Further, it can be conjectured that the compact nature of the ATD layer results in close contacts between the subunits which would be energetically unfavorable to break. The lack of change in the ATD inter-subunit distances upon binding of an allosteric modulator corresponds well with a mechanism that involves the propagation of conformational changes within an ATD to the LBD layer and ultimately the pore of the receptor to influence the function. In order for this mechanism to work, the receptor requires an anchor point, which our data suggest is provided by the upper lobes of the ATDs. The binding of zinc, ifenprodil, or spermine induces conformational changes in the ATDs, but the upper lobes remain stable.

The GluN2A and GluN2B ATDs have unique inherent conformations, with the more open GluN2A ATD correlating with a higher Po of the receptor and the more closed GluN2B ATD corresponding to a lower Po of the receptor. Additionally, we show that the GluN1 ATD adopts a different conformation depending on the GluN2 subunit with which it is co-assembled. Based on these data, we propose that the differences in both GluN1 and GluN2

ATDs contribute to unique interfaces between the GluN1/GluN2 ATDs that underlie subtype specific modulators. Furthermore, both the GluN1 and GluN2 ATDs together dictate Po of the receptor.

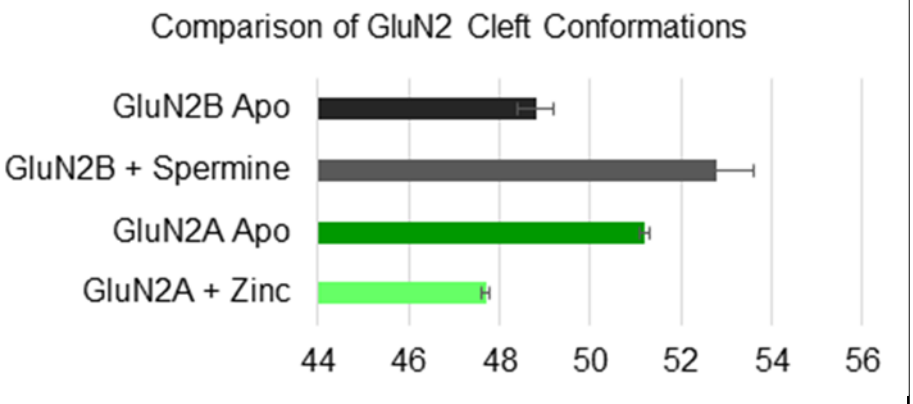

Figure 11.1: Comparison of GluN2 Cleft Conformations. Plotted are the distances measured using the GluN2cleft constructs. GluN2B is inherently more closed than GluN2A, and the modulators shift the distances to be more like the other GluN2 subtype.

We found that zinc inhibition of GluN2A receptors occurs by stabilizing a closed conformation of the GluN2A ATD, inducing a ~4 Å decrease between sites in the upper and lower lobes (Sirrieh, MacLean et al. 2013). This cleft-closure in the ATD seems to be a common mechanism of allosteric inhibition, as ifenprodil induces a cleft-closure in the GluN2B ATD. Conversely, spermine, which potentiates, causes an opening of the GluN2B ATD. Additionally, the lower lobe of the GluN2 ATD undergoes a rotational movement, independent of the opening or closing of the domain. The conformation of the ATD can be correlated to the Po of the receptor. This correlation is not unexpected as correlations have been demonstrated between the extent of LBD closure and activation of the receptor (Rambhadran, Gonzalez et al. 2011, Dolino, Cooper et al. 2014). The correlation is similar for receptors composed of GluN2A or GluN2B receptors, as the slope of the lines is similar (Figure 11.2).

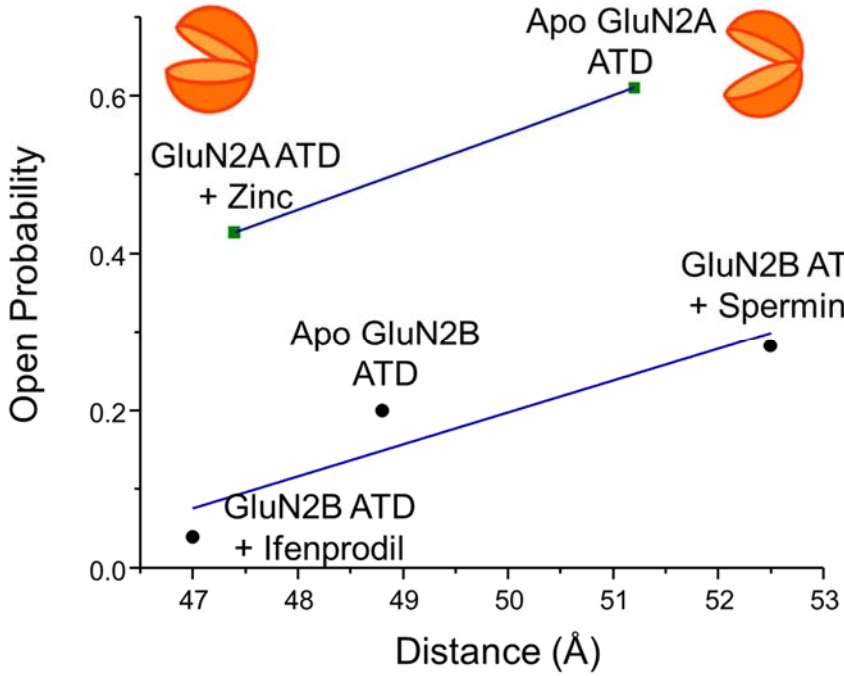

Figure 11.2: Correlation between ATD conformation and Po. The points represent a given conformation of the ATD which corresponds to a certain Po of the receptor. The best fit lines connecting the points have similar slopes for receptors composed of GluN2A or GluN2B receptors, suggesting a correlation.

The GluN1 ATD conformation is only affected by the potentiator spermine. Zinc binding does not influence the overall conformation of the GluN1 ATD. Interestingly, the conformation of the zinc-bound GluN2A ATD (i.e. low P_{open}) is similar to the apo GluN2B ATD (48.8 Å and low P_{open}) (Figures 11.1 and 11.2). Further, the state of the spermine-bound GluN2B ATD (52.4 Å and high P_{open}) is comparable to that of the apo GluN2A ATD (51.4 Å and high P_{open}) (Figures 11.1 and 11.2). Taken together, such correlations explain how zinc and spermine inhibit and potentiate the receptor, respectively, by influencing the average conformation of the ATD. An inhibitor closes the ATD cleft, while a potentiator opens the GluN2 ATD cleft. If zinc binding causes a cleft-closure in the GluN2B ATD as expected, then the inherent difference in the cleft conformation of GluN2A and GluN2B explains why zinc completely inhibits GluN1-GluN2B receptors but only partially inhibits GluN1-GluN2A receptors (Erreger

and Traynelis 2005, Rachline, Perin-Dureau et al. 2005). Our results also suggest why spermine is unable to potentiate GluN2A containing receptors as the resting GluN2A ATD is already an open conformation. Further, these data suggest that ifenprodil induces smaller conformational changes because the GluN2B ATD is inherently in a more closed conformation. To inhibit GluN2B requires less of a conformational change; both GluN1 and GluN2B are more closed.

11.2 Impact

The studies discussed here provide insight into the structural mechanism of allosteric modulation. Our data support the mechanism whereby an open ATD conformation results in a potentiated receptor and a closed ATD results in an inhibited receptor. These studies identify how a receptor would be manipulated by a drug that seeks to modulate the receptor in a subtype dependent fashion. The hope is that a subtype specific modulator would allow for normal, basal synaptic transmission, but still inhibit or potentiate the receptor as needed in a disease state. Our data have identified the GluN1-GluN2 ATD interface as a unique site on the receptor that could be used to develop subtype specific modulators. Additionally, the LRET technique combined with the constructs developed for these studies are great tools to potentially help characterize new drugs.

11.3 Future directions

The mechanism of propagation of conformational changes at the ATDs to the gating machinery remains very poorly understood. Stabilizing the LBD interface yields receptors that are not as greatly inhibited by zinc, suggesting that zinc inhibition proceeds by destabilizing the dimer interface at the LBD. However, is the conformational change propagated through the ATD-LBD linker or are new contacts formed between the bottom of the ATD and the top of the LBD? This question is especially pertinent as there is cooperativity between the LBD

and ATD. These two domains are linked on a deeper level than that related simply to channel activation.

To attempt to address this question, we inserted a glycine residue into the linker between the ATD and LBD. This technique was used in the S2-M3 linker and the insertion was able to decouple conformational changes at the LBD from the pore of the receptor and demonstrated that tension in the S2-M3 linker was required for gating of the receptor (Kazi, Dai et al. 2014). If the conformational changes at the ATD were similarly propagated to the LBD through tension in the linkers, we would similarly expect a decreased extent of inhibition.

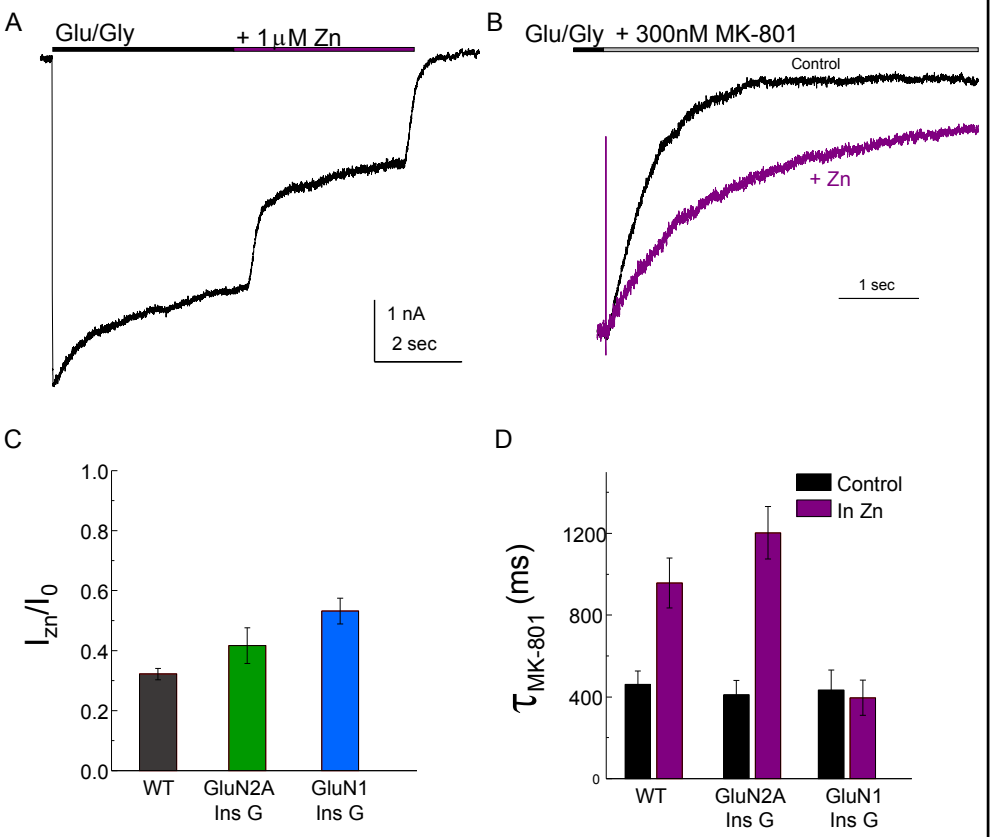

Figure 11.3: Effect of Glycine Insertions in the ATD-LBD Linker. (A) A representative trace of zinc inhibition of a GluN1-GluN2A receptor. (B) A representative trace showing the rate of MK-801 binding in the presence and absences of zinc. (C) Summary data from recordings from mutants with a single glycine inserted in the GluN1 (blue) or GluN2A (green) ATD-LBD linker. (D) The rates of MK-801 binding in the presence and absence of zinc for wild type receptors and the mutants with glycines inserted in the ATD-LBD linkers. Electrophysiology performed by Dr. David MacLean.

A single glycine inserted in the ATD-LBD linker of either the GluN1 or the GluN2A subunit resulted in modest reductions in the extent of zinc inhibition (Figure 11.3). However, to determine that only zinc inhibition and not the inherent function of the receptor was altered by this mutation, the Po of the mutant channel needed to be determined. As a way of estimating the Po of these mutants, the rate of binding of the open channel blocker MK-801 was used as a marker of activation. In the wild type receptor, MK-801 binding was markedly slower in the presence of zinc, as expected because zinc inhibition proceeds by reducing Po. The GluN2A mutant followed this trend, and had similar rates of MK-801 binding to the wild type receptor. However, the GluN1 mutant was quite strange because, despite normal MK-801 binding in the absence of zinc, it had identical MK-801 binding in the presence of zinc (Figure 11.3), suggesting that some compensatory effect of the mutation had taken place. The reduction in zinc inhibition was insufficient to explain the increased rate of MK-801 binding in the presence of zinc. These results suggest that it is not simply tension in the linker that connects conformational changes in the ATD to the LBD. However, they do suggest that the GluN1 linker has an interesting role in channel gating that remains uncharacterized. The recent full-length structures revealed that there are extensive contacts between the ATD and LBD layers in the NMDA receptor (Karakas and Furukawa 2014, Lee, Lü et al. 2014) (Figure 11.4). Probing the interfaces between these domains for changes accompanying modulation may also provide insight into how allosteric modulators affect the LBDs and ultimately the pore of the receptor. The linkers are one of the more underrated sections of the receptor. Due to their modification and the deletion of residues to generate a stable structure for crystallography, we do not have a clear picture of the structure adopted by the linkers. How the linkers, despite their relatively short length, manage the crossover between subunits is an interesting structural question that may be difficult to answer with crystallography due to their dynamic nature.

The question of proton inhibition in light of the conformational changes characterized here is a very interesting question. The binding of zinc, ifenprodil, and spermine do induce conformational changes. How do those conformational changes relate to proton inhibition? Attempts to answer these questions were not possible to address with LRET because repeating the measurements at different pHs did not induce significant changes in the LRET

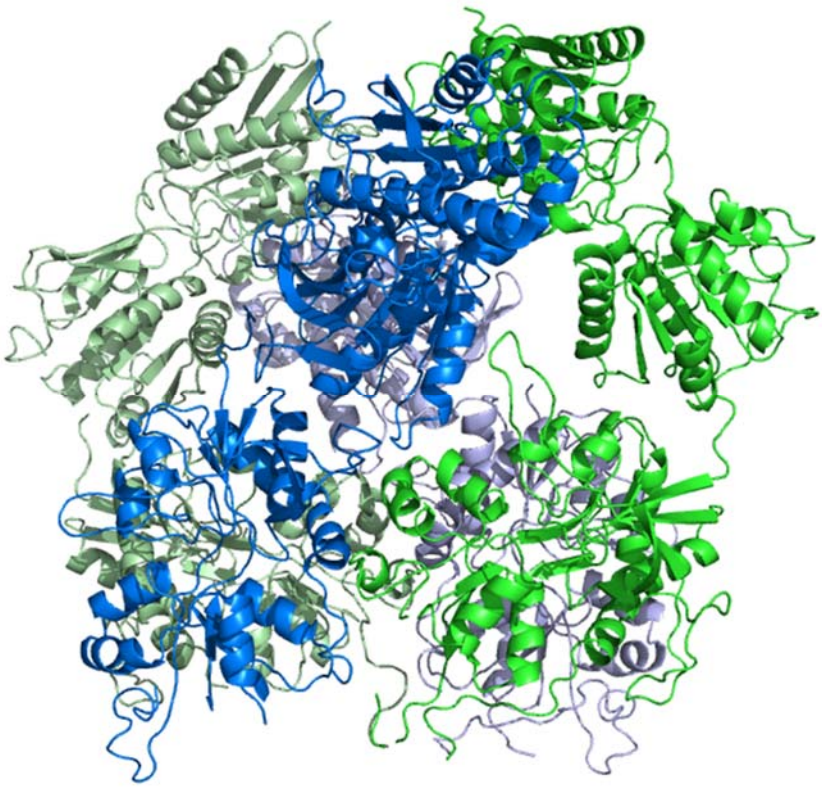

Figure 11.4: ATD-LBD contacts. The crystal structure highlighting the contacts between the ATD and LBD layers is shown. The GluN2B subunit is in blue and the GluN1 subunit is in green. The GluN2B ATD is positioned such that it can make direct contacts with both the GluN1 and GluN2B LBDs.

lifetime, suggesting that either the conformation is not affected by pH or that the LRET technique is not sensitive enough to detect small changes in distributions.

Finally, more work is needed on triheteromeric receptors to characterize the kinetics of their activation and to better understand how they are modulated. In the central nervous system, NMDA receptors are believed to assemble as triheteromeric receptors; in

hippocampal neurons that express both GluN2A and GluN2B receptors, close to two-thirds of receptors are composed of two GluN1 subunits, one GluN2A subunit, and one GluN2B subunit (Tovar, McGinley et al. 2013). In studying the kinetics of these receptors in neurons, triheteromeric receptors were found to have intermediate decay kinetics between GluN1/2A and GluN1/2B diheteromeric receptors (Tovar, McGinley et al. 2013). To address the question of allosteric modulation in triheteromeric receptors, a set of mutations that modify an individual subunit's response to magnesium, zinc, or glutamate were introduced (Hatton and Paoletti 2005). The results of this study show that triheteromeric receptors have intermediate inhibition by ifenprodil and zinc compared to their diheteromeric counterparts, although they retain roughly the same affinity as the diheteromeric receptor (Hatton and Paoletti 2005). Receptors with only one zinc binding site retain nanomolar zinc affinity, but are inhibited to a much lesser degree (Hatton and Paoletti 2005). Another recent effort to study triheteromeric receptors employed ER retention signals in the CTD that would be suppressed by the assembly of a triheteromeric receptor (Hansen, Ogden et al. 2014). This study similarly found that triheteromeric GluN1/GluN2A/GluN2B receptors retain high affinity zinc binding, but are inhibited only to the same extent as GluN1/GluN2A wild type receptors, which are incompletely inhibited by saturating zinc (Hansen, Ogden et al. 2014). These receptors are also inhibited by ifenprodil, but to a lesser degree than GluN1/GluN2B receptors, and they had a lower affinity to ifenprodil (Hansen, Ogden et al. 2014). The Paoletti group also took advantage of this technique to express triheteromeric receptors and found that these GluN1/GluN2A/GluN2B receptors had intermediate deactivation kinetics, agonist EC_{50}s, and zinc, ifenprodil, and proton IC_{50}s compared to the diheteromeric species but were only mildly potentiated by spermine (Stroebel, Carvalho et al. 2014). The extent of inhibition was also intermediate (Stroebel, Carvalho et al. 2014).

The techniques that allow for the isolation of triheteromeric receptors is still a challenge even with the development of the C-terminal retention signals. Diheteromeric receptors expressed using the retention signals have an abnormally low Po (Hansen, Ogden et al. 2014), so, though they reflect great progress, they are still not an accurate in vitro representation of these receptors. As the technologies develop, studying triheteromeric receptors, including receptors that have GluN3 subunits, will provide the greatest insight into the way NMDA receptors are involved in neural network formation physiologically and really help us understand how synaptic transmissions are fine-tuned, because triheteromeric receptors are very prevalent in the central nervous system. Advances in our ability to recombinantly express triheteromeric receptors will definitely help the field to do the necessary experiments.

NMDA receptors are well-balanced structures; binding of an agonist or modulator adds energy to the system and tips the balance in a direction that alters the function of the receptor. Multiple ligands binding simultaneously modulate each other's binding to the receptor (cooperativity between binding sites) in addition to their functional effect. Simple features such as electrostatics also contribute to this balance, and the links between all the binding sites and functions of this intricate machine are still works in progress. Our work contributes to the understanding of how modulators which bind to the ATDs affect the structure and cause a functional effect.

Appendix: *Definitions of Terms Describing Ion Channel Properties*

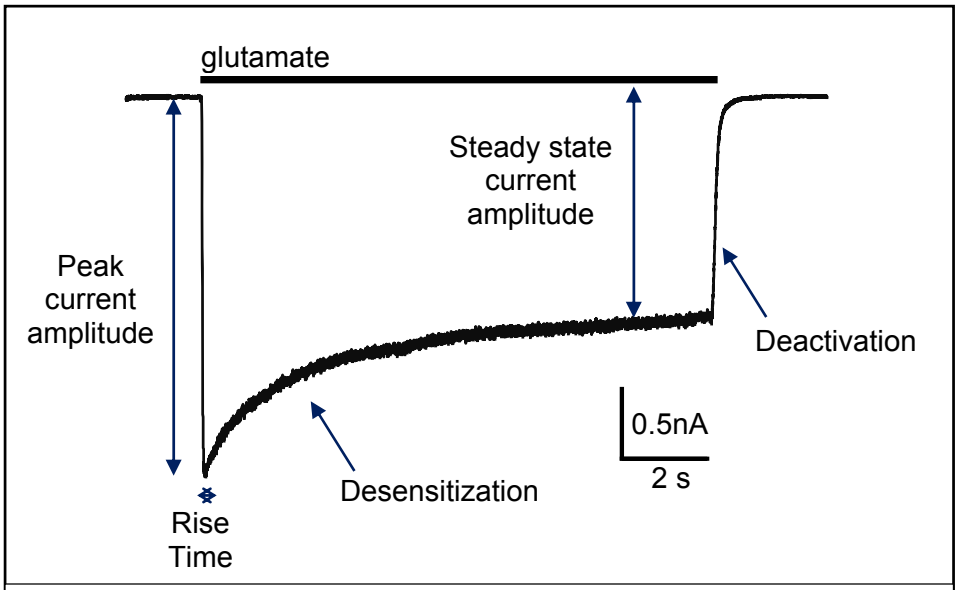

Appendix Figure 1: Anatomy of an electrophysiological recording from an NMDA receptor. One can see the rapid rise time, little desensitization, and rapid deactivation. By convention, only glutamate is listed because the cell is kept in the continual presence of glycine, as the receptors are thought to be at synapses.

- **allosteric modulation:** binding of modulator to a site on the receptor other than the agonist-binding site (non-competitive) results in a modification of the function of the receptor.
- **burst:** period of activity in single-channel recordings during continuous application of the agonist
- **conductance:** charge per unit time passed through the pore of an ion channel. There can be one conductance state or several conductance states, where the smaller conductance states are typically called subconductance states. The conductance is an inherent property of the receptor/channel in question.
- **cooperativity:** The binding of a ligand to one site on a protein changes the affinity for another ligand which binds at a different site on the receptor. Cooperativity is one mechanism by which allosteric modulation may proceed.
- **deactivation:** the closing of the channel due to removal of the agonist.

- **desensitization:** the state in which a channel is in the closed conformation despite being bound by agonist, during the continual application of agonist. The desensitized state has a higher affinity for the agonist than the apo state.
- **extent of desensitization:** can be defined as the ratio of steady state current to peak current.
- **holding potential:** the membrane potential at which a patch or cell is maintained during electrophysiological recording.
- **mean closed time:** The length of time within a burst during single-channel recordings when the channel is closed.
- **mean open time:** the length of time within a burst during single-channel recordings when the channel is open
- **open probability (Po):** The chance that the channel will be open at any given time. The Po increases significantly upon application of the agonist. The open probability is typically expressed on a scale from 0 to 1, with 1 being 100% chance of activation.
- **peak current amplitude:** the amplitude of current passed through the ion channels in a patch or whole-cell configuration immediately upon activating the receptor with agonist. This current is expressed in nAmps or pAmps.
- **rise time:** the time it takes for a channel to go from 10-90% current upon application of the agonist. The range of 10-90% is somewhat arbitrary, and is sometimes replaced with time from 20-80%.
- **steady state current amplitude:** The current that passes through the channels in a patch or whole-cell configuration during continuous application of the agonist after the channel has equilibrated between open, closed, and desensitized states.

References

Amico-Ruvio, S. A., S. E. Murthy, T. P. Smith and G. K. Popescu (2011). "Zinc Effects on NMDA Receptor Gating Kinetics." Biophysical Journal **100**(8): 1910-1918.

Amico-Ruvio, S. A., M. A. Paganelli, J. M. Myers and G. K. Popescu (2012). "Ifenprodil Effects on GluN2B-Containing Glutamate Receptors." Molecular Pharmacology **82**(6): 1074-1081.

Aniksztejn, L., G. Chraton and Y. Ben-Ari (1987). "Selective release of endogenous zinc from the hippocampal mossy fibers in situ." Brain Research **404**(1-2): 58-64.

AR, K. (2003). "Evidence for chelatable zinc in the extracellular space of the hippocampus, but little evidence for synaptic release of Zn." The Journal of Neuroscience **23**(17): 6847-6855.

Armstrong, N. and E. Gouaux (2000). "Mechansims for activation and antagonism of an AMPA-sensitive glutamate receptor: crystal structures of the GluR2 ligand binding core." Neuron **28**(1): 165-181.

Assaf, S. Y. and S.-H. Chung (1984). "Release of endogenous Zn2+ from brain tissue during activity." Nature **308**: 734-736.

Ataman, Z. A., L. Gakhar, B. R. Sorensen, J. W. Hell and M. A. Shea (2007). "The NMDA Receptor NR1 C1 Region Bound to Calmodulin: Structural Insights into Functional Differences between Homologous Domains." Structure **15**(12): 1603-1617.

Baker, N. A., D. Sept, S. Joseph, M. J. Holst and J. A. McCammon (2001). "Electrostatics of nanosystems: Application to microtubules and the ribosome." Proceedings of the National Academy of Sciences of the USA **98**(18): 10037-10041.

Besser, L., E. Chorin, I. Sekler, W. F. Silverman, S. Atkin, J. T. Russell and M. Hershfinkel (2009). "Synaptically released zinc triggers metabotropic signaling via a zinc-sensing receptor in the hippocampus." J Neurosci **29**(9): 2890-2901.

Bettler, B., J. Boulter, I. Hermans-Borgmeyer, A. O'Shea-Greenfield, E. S. Deneris, C. Moll, U. Borgmeyer, M. Hollmann and S. Heinemann (1990). "Cloning of a novel glutamate receptor subunit, GluR5: Expression in the nervous system during development." Neuron **5**(5): 583-595.

Borschel, W. F., S. E. Murthy, E. M. Kasperek and G. K. Popescu (2011). "NMDA receptor activation requires remodelling of intersubunit contacts within ligand-binding heterodimers." Nature Communications **2**: 498.

Boulter, J., M. Hollmann, A. O'Shea-Greenfield, M. Hartley, E. Deneris, C. Maron and S. Heinemann (1990). "Molecular Cloning and Functional Expression of Glutamate Receptor Subunit Genes." Science **249**(4972): 1033-1037.

Burger, P. B., H. Yuan, E. Karakas, M. Geballe, H. Furukawa, D. C. Liotta, J. P. Snyder and S. F. Traynelis (2012). "Mapping the Binding of GluN2B-Selective N-Methyl-d-aspartate Receptor Negative Allosteric Modulators." Molecular Pharmacology **82**(2): 344-359.

C., C., J. Benavies, P. Legendre, J. D. Vincent, F. Noel, F. Thuret, K. G. Lloyd, S. Arbilla, B. Zivkovic and E. T. MacKenzie (1988). "Ifenprodil and SL 82.0715 as cerebral anti-ischemic agents. II. Evidence for N-methyl-D-aspartate receptor antagonist properties." The Journal of Pharmacology and Experimental Therapeutics **247**(3): 1222-1232.

Chen, J. and P. R. Selvin (1999). "Thiol-Reactive Luminescent Chelates of Terbium and Europium." Bioconjugate Chemistry **10**: 311-315.

Chen, N., T. Luo and L. A. Raymond (1999). "Subtype-Dependence of NMDA Receptor Channel Open Probability." The Journal of Neuroscience **19**(16): 6844-6854.

Chizh, B. A., P. M. Headley and T. M. Tzschentke (2001). "NMDA receptor antagonists as analgesics: focus on the NR2B subtype." Trends in Pharmacological Sciences **22**(12): 636-642.

Choi, U. B., R. Kazi, N. Stenzoski, L. P. Wollmuth, V. N. Uversky and M. E. Bowen (2013). "Modulating the intrinsic disorder in the cytoplasmic domain alters the biological activity of the N-methyl-D-aspartate-sensitive glutamate receptor." J Biol Chem **288**(31): 22506-22515.

Choi, Y.-B. and S. A. Lipton (1999). "Identification and Mechanism of Action of Two Histidine Residues Underlying High-Affinity Zn2+ Inhibition of the NMDA Receptor." Neuron **23**(1): 171-180.

CM, Y. K. a. T. (1993). "Benzothiadiazides inhibit rapid glutamate receptor desensitization and enhance glutamatergic synaptic currents." Journal of Neuroscience **13**(9): 3904-3915.

.

Dolino, D. M., D. Cooper, S. Ramaswamy, H. Jaurich, C. F. Landes and J. Vasanthi (2014). "Structural Dynamics of the Glycine-binding Domain of the N-Methyl-D-Aspartate Receptor." The Journal of Biological Chemistry **290**(2): 797-804.

Dolinsky, T. J., P. Czodrowski, H. Li, J. E. Nielsen, J. H. Jensen, G. Klebe and N. A. Baker (2007). "PDB2PQR: expanding and upgrading automated preparation of biomolecular structures for molecular simulations." Nucleic Acids Res **35**(Web Server issue): W522-525.

Dolinsky, T. J., J. E. Nielsen, J. A. McCammon and N. A. Baker (2004). "PDB2PQR: an automated pipeline for the setup of Poisson-Boltzmann electrostatics calculations." Nucleic Acids Res **32**(Web Server issue): W665-667.

dos Remedios, C. G. and P. D. Moens (1995). "Fluorescence resonance energy transfer spectroscopy is a reliable "ruler" for measuring structural changes in proteins. Dispelling the problem of the unknown orientation factor." J Struct Biol **115**(2): 175-185.

Durand, G. M., M. V. Bennett and R. S. Zukin (1993). "Splice variants of the N-methyl-D-aspartate receptor NR1 identify domains involved in regulation by polyamines and protein kinase C." Proceedings of the National Academy of Sciences of the United States of America **90**(14): 6731-6735.

Dutta, A., I. H. Shrivastava, M. Sukumaran, I. H. Greger and I. Bahar (2012). "Comparative Dynamics of NMDA- and AMPA-Glutamate Receptor N-Terminal Domains." Structure **20**(11): 1838-1849.

Egebjerg, J., B. Bettler, I. Hermans-Borgmeyer and S. Heinemann (1991). "Cloning of a cDNA for a glutamate receptor subunit activated by kainate but not AMPA." Nature **351**(6329): 745-748.

Ehlers, M. D., S. Zhang, J. P. Bernhadt and R. L. Huganir (1996). "Inactivation of NMDA receptors by direct interaction of calmodulin with the NR1 subunit." Cell **84**(5): 745-755.

Erreger, K., S. M. Dravid, T. G. Banke, D. J. Wyllie and S. F. Traynelis (2005). "Subunit-specific gating controls rat NR1/NR2A and NR1/NR2B NMDA channel kinetics and synaptic signalling profiles." The Journal of Physiology **563**(2): 345-358.

Erreger, K. and S. F. Traynelis (2005). "Allosteric interaction between zinc and glutamate binding domains on NR2A causes desensitization of NMDA receptors." The Journal of Physiology **569**: 381-393.

Erreger, K. and S. F. Traynelis (2008). "Zinc inhibition of rat NR1/NR2A N-methyl-d-aspartate receptors." The Journal of Physiology **586**(3): 763-778.

Fayyazuddin, A., A. Villarroel, A. Le Goff, J. Lerma and J. Neyton (2000). "Four Residues of the Extracellular N-Terminal Domain of the NR2A Subunit Control High-Affinity Zn2+ Binding to NMDA Receptors." Neuron **25**(3): 683-694.

Forster, T. (1946). "Intermolecular energy migration and fluorescence." Annals of Physics **2**: 55-75.

Furukawa, H. (2012). "Structure and function of glutamate receptor amino terminal domains." The Journal of Physiology **590**: 63-72.

Furukawa, H. and E. Gouaux (2003). "Mechanisms of activation, inhibition and specifcity: crystal structures of the NMDA receptor NR1 ligand-binding core." The EMBO Journal **22**(12): 2873-2885.

Furukawa, H., S. K. Singh, R. Mancusso and E. Gouaux (2005). "Subunit arrangement and function in NMDA receptors." Nature **438**(7065): 185-192.

Furukawa, H., S. K. Singh, R. Mancusso and E. Gouaux (2005). "Subunit arrangement and function in NMDA receptors." Nature **438**(7065): 185-192.

Gallagher, M. J., H. Huang, D. B. Pritchett and D. R. Lynch (1996). "Interactions between Ifenprodil and the NR2B Subunit of the N-Methyl-D-aspartate Receptor." The Journal of Biological Chemistry **271**(16): 9603-9611.

Geall, A. J., R. J. Taylor, M. E. Earll, M. A. W. Eaton and I. S. Blagbrough (2000). "Synthesis of Cholesteryl Polyamine Carbamates: pKa Studies and Condensation of Calf Thymus DNA." Biocunjugate Chemistry **11**(3): 314-326.

Gielen, M., A. Le Goff, D. Stroebel, J. W. Johnson, J. Neyton and P. Paoletti (2008). "Structural Rearrangements of NR1/NR2A NMDA Receptors during Allosteric Inhibition." Neuron **57**(1): 80-93.

Gielen, M., B. S. Retchless, L. Mony, J. W. Johnson and P. Paoletti (2009). "Mechanism of differential control of NMDA receptor activity by NR2 subunits." Nature **459**(7247): 703-707.

Giffard, R. G., H. Monyer, C. W. Christine and D. W. Choi (1990). "Acidosis reduces NMDA receptor activation, glutamate neurotoxicity, and oxygen-glucose deprivation neuronal injury in cortical cultures." Brain Res **506**(2): 339-342.

Gonzalez, J., M. Du, K. Parameshwaran, V. Suppiramaniam and V. Jayaraman (2010). "Role of dimer interface in activation and desensitization in AMPA receptors." Proceedings of the National Academy of Sciences of the United States of America **107**(21): 9891-9896.

Gonzalez, J., A. Rambhadran, M. Du and V. Jayaraman (2008). "LRET Investigations of Conformational Changes in the Ligand Binding Domain of a Functional AMPA Receptor." Biochemistry **47**(38): 10027-10032.

Hansen, K. B., K. K. Ogden, H. Yuan and S. F. Traynelis (2014). "Distinct Functional and Pharmacological Properties of Triheteromeric GluN1/GluN2A/GluN2B NMDA Receptors." Neuron **81**(5): 1084-1096.

Hatton, C. J. and P. Paoletti (2005). "Modulation of triheteromeric NMDA receptors by N-terminal domain ligands." Neuron **46**(2): 261-274.

Hollmann, M., A. O'Shea-Greenfield, S. W. Rogers and S. Heinemann (1989). "Cloning by functional expression of a member of the glutamate receptor family." Nature **342**(6250): 643-648.

Howell, G. A., M. G. Welch and C. J. Frederickson (1984). "Stimulation-induced uptake and release of zinc in hippocampal slices." Nature **308**: 736-738.

Indira, R. M. and L. O. Trussell (1992). "The kinetics of the response to glutamate and kainate in neurons of the avian cochlear nucleus." Neuron **9**(1): 173-186.

JL, Q. J. a. N. (2006). "Exocytosis of vesicular zinc reveals persistent depression of neurotransmitter release during metabotropic glutamate receptor long-term depression at the hippocampal Ca3-CA1 synapse." The Journal of Neuroscience **26**(22): 6089-6095.

K., W., A. M. Zappia, D. B. Pritchett, Y. M. Shen and P. B. Molinoff (1994). "Sensitivity of the N-methyl-D-aspartate receptor to polyamines is controlled by NR2 subunits." Molecular Pharmacology **45**(5): 803-809.

Karakas, E. and H. Furukawa (2014). "Crystal structure of a heterotetrameric NMDA receptor ion channel." Science **344**(6187): 992-997.

Karakas, E. and H. Furukawa (2014). "Crystal structure of a heterotetrameric NMDA receptor ion channel." Science **344**(6187): 992-997.

Karakas, E., N. Simorowski and H. Furukawa (2009). "Structure of the zinc-bound amino-terminal domain of the NMDA receptor NR2B subunit." The EMBO Journal **28**(24): 3910-3920.

Karakas, E., N. Simorowski and H. Furukawa (2011). "Subunit arrangement and phenylethanolamine binding in GluN1/GluN2B NMDA receptors." Nature **475**: 249-253.

Kay, A. R. and K. Tóth (2008). "Is zinc a neuromodulator?" Sci Signal **1**(19): re3.

Kazi, R., J. Dai, C. Sweeney, H.-X. Zhou and L. P. Wollmuth (2014). "Mechanical coupling maintains the fidelity of NMDA receptor-mediated currents." Nature Neuroscience **17**: 914-922.

Keiko, K., J.-I. Fukuchi, J. Chao, K. Igarashi and K. Williams (1996). "An aspartate residue in the extracellular loop of the N-methyl-D-aspartate recepetor controls sensitivity to spermine and protons." Molecular Pharmacology **49**(1131-1141).

Kew, J. N., G. Trube and J. A. Kemp (1996). "A novel mechanism of activity-dependent NMDA receptor antagonism describes the effect of ifenprodil in rat cultured cortical neurones." J Physiol **497 (Pt 3)**: 761-772.

Khatri, A., P. B. Burger, S. A. Swanger, K. B. Hansen, S. Zimmerman, E. Karakas, D. C. Liotta, H. Furukawa, J. P. Snyder and S. F. Traynelis (2014). "Structural Determinants and Mechanism of Action of a GluN2C-selective NMDA Receptor Positive Allosteric Modulator." Molecular Pharmacology **86**: 548-560.

Kobayashi, T., K. Washiyama and K. Ikeda (2006). "Inhibition of G protein-activated inwardly rectifying K+ channels by ifenprodil." Neuropsychopharmacology **31**(3): 516-524.

Landes, C. F., A. Rambhadran, J. N. Taylor, F. Salatan and V. Jayaraman (2011). "Structural landscape of isolated agonist-binding domains from single AMPA receptors." Nature Chemical Biology **7**: 168-173.

Le Bail, M., M. Martineau, S. Sacchi, N. Yatsenko, I. Radzishevsky, S. Conrod, K. Ait Ouares, H. wolosker, L. Pollegioni, J.-M. Billard and J.-P. Mothet (2014). "Identity of the NMDA receptor coagonist is synapse specific and developmentally regulated in the hippocampus." Proceedings of the National Academy of Sciences of the United States of America **112**(2).

Lee, C.-H., W. Lü, J. C. Michel, A. Goehring, J. Du, X. Song and E. Gouaux (2014). "NMDA receptor structures reveal subunit arrangement and pore architecture." Nature **511**: 191-197.

Li, Y., C. J. Hough, S. W. Suh, J. M. Sarvey and C. J. Frederickson (2001). "Rapid Translocation of Zn2 From Presynaptic Terminals Into Postsynaptic Hippocampal Neurons After Physiological Stimulation." Journal of Neurophysiology **86**(5): 2597-2604.

Low, C.-M., P. Lyuboslavsky, A. French, P. Le, K. Wyatte, W. H. Thiel, E. M. Marchan, K. Igarashi, K. Kashiwagi, K. Gernert, K. Williams, S. F. Traynelis and F. Zheng (2003). "Molecular Determinants of Proton-Sensitive N-Methyl-d-aspartate Receptor Gating." Molecular Pharmacology **63**(6): 1212-1222.

Low, C.-M., F. Zheng, P. Lyuboslavsky and S. F. Traynelis (2000). "Molecular determinants of coordinated proton and zinc inhibition of N-methyl-d-aspartate NR1/NR2A receptors." Proceedings of the National Academy of Sciences **97**(20): 11062-11067.

Madry, C., I. Mesic, H. Betz and B. Laube (2007). "The N-terminal domains of both NR1 and NR2 subunits determine allosteric Zn2+ inhibition and glycine affinity of N-methyl-D-aspartate receptors." Mol Pharmacol **72**(6): 1535-1544.

Maki, B. A., T. K. Aman, S. A. Amico-Ruvio, C. L. Kussius and G. K. Popescu (2012). "C-terminal Domains of N-Methyl-d-aspartic Acid Receptor Modulate Unitary Channel Conductance and Gating." The Journal of Biological Chemistry **287**: 36071-36080.

Maki, B. A., N. Program, S. o. M. a. B. Sciences, U. a. Buffalo, N. U. Buffalo, R. Cole, D. o. Biochemistry, S. o. M. a. B. Sciences, U. a. Buffalo, N. U. Buffalo, G. K. Popescu, N.

Program, S. o. M. a. B. Sciences, U. a. Buffalo, N. U. Buffalo, D. o. Biochemistry, S. o. M. a. B. Sciences, U. a. Buffalo, N. U. Buffalo and popescu@buffalo.edu (2013). "Two serine residues on GluN2A C-terminal tails control NMDA receptor current decay times." Channels **7**(2): 126-132.

Maltsev, A. S., A. H. Ahmed, M. K. Fenwick, D. E. Jane and R. E. Oswald (2008). "Mechanism of Partial Agonism at the GluR2 AMPA Receptor: Measurements of Lobe Orientation in Solution." Biochemistry **47**(40): 10600-10610.

Maltsev, A. S. and R. E. Oswald (2010). "Hydrophobic Side Chain Dynamics of a Glutamate Receptor Ligand Binding Domain." The Journal of Biological Chemistry **285**: 10154-10162.

Marchand, P., J. Becerril-Ortega, L. Mony, C. Bouteiller, P. Paoletti, O. Nicole, L. Barré, A. Buisson and C. Perrio (2012). "Confocal microscopy imaging of NR2B-containing NMDA receptors based on fluorescent ifenprodil-like conjugates." Bioconjug Chem **23**(1): 21-26.

Masuko, T., K. Kashiwagi, T. Kuno, N. D. Nguyen, A. J. Pahk, J.-i. Fukuchi, K. Igarashi and K. Williams (1999). "A Regulatory Domain (R1–R2) in the Amino Terminus of theN-Methyl-d-Aspartate Receptor: Effects of Spermine, Protons, and Ifenprodil, and Structural Similarity to Bacterial Leucine/Isoleucine/Valine Binding Protein." Molecular Pharmacology **55**(6): 957-969.

Masuko, T., K. Kusama-Eguchi, K. Sakata, T. Kusama, S. Chaki, S. Okuyama, K. Williams, K. Kashiwagi and K. Igarashi (2003). "Polyamine transport, accumulation, and release in brain." J Neurochem **84**(3): 610-617.

Mayer, M. L., G. L. Westbrook and P. B. Guthrie (1984). "Voltage-dependent block by Mg2+ of NMDA responses in spinal cord neurones." Nature **309**(5965): 261-263.

Meddows, E., B. L. Bourdellès, S. Grimwood, K. Wafford, S. Sandhu, P. Whiting and R. A. J. McIlhinney (2001). "Identification of Molecular Determinants That Are Important in the

Assembly of N-Methyl-d-aspartate Receptors." The Journal of Biological Chemistry **276**: 18795-18803.

Merrill, M. A., Z. Malik, Z. Akyol, J. A. Bartos, A. S. Leonard, A. Hudmon, M. A. Shea and J. W. Hell (2007). "Displacement of alpha-actinin from the NMDA receptor NR1 C0 domain By Ca2+/calmodulin promotes CaMKII binding." Biochemistry **46**(29): 8485-8497.

Meyerson, J. R., J. Kumar, S. Chittori, P. Rao, J. Pierson, A. Bartesaghi, M. L. Mayer and S. Subramaniam (2014). "Structural mechanism of glutamate receptor activation and desensitization." Nature **514**: 328-334.

Molnar, P. and J. V. Nadler (2001). "Synaptically-released zinc inhibits N-methyl-d-aspartate receptor activation at recurrent mossy fiber synapses." Brain Research **910**(Issues 1–2): 205–207.

Mony, L., L. Krzaczkowski, M. Leonetti, A. L. Goff, K. Alarcon, J. Neyton, H.-O. Bertrand, F. Acher and P. Paoletti (2009). "Structural Basis of NR2B-Selective Antagonist Recognition by N-Methyl-d-aspartate Receptors." Molecular Pharmacology **75**(1): 60-74.

Mony, L., S. Zhu, S. Carvalho and P. Paoletti (2011). "Molecular basis of positive allosteric modulation of GluN2B NMDA receptors by polyamines." EMBO Journal **30**(15): 3134-3146.

Morgan, D. M. L. (1999). "Polyamines." Molecular Biotechnology **11**(3): 229-250.

Moriyoshi, K., M. Masu, T. Ishii, R. Shigemoto, N. Mizuno and S. Nakanishi (1991). "Molecular cloning and characterization of the rat NMDA receptor." Nature **354**: 31-37.

Mott, D. D., J. J. Doherty, S. Zhang, M. S. Washburn, M. J. Fendley, P. Lyuboslavsky, S. F. Traynelis and R. Dingledine (1998). "Phenylethanolamines inhibit NMDA receptors by enhancing proton inhibition." Nature Neuroscience **1**(8): 659-667.

Mullasseril, P., K. Hansen, B., K. M. Vance, K. K. Ogden, H. Yuan, N. L. Kurtkaya, R. Santangelo, A. G. Orr, P. Le, K. M. Vellano, D. C. Liotta and S. F. Traynelis (2010). "A

subunit-selective potentiator of NR2C- and NR2D-containing receptors." Nature Communications **1**(90).

Nowak, L., P. Bregestovski, P. Ascher, A. Herbet and A. Prochiantz (1984). "Magnesium gates glutamate-activated channels in mouse central neurones." Nature **307**(5950): 462-465.

Nozaki, C., A. M. Vergnano, D. Filliol, A.-M. Ouagazzal, A. L. Goff, S. Carvalho, D. Reiss, C. Gaveriaux-Ruff, J. Neyton, P. Paoletti and B. L. Kieffer (2011). "Zinc alleviates pain through high-affinity binding to the NMDA receptor NR2A subunit." Nature Neuroscience **14**: 1017-1022.

Nydegger, I., S. M. Rumschik and A. R. Kay (2010). "Zinc is externalized rather than released during synaptic transmission." ACS Chem Neurosci **1**(11): 728-736.

Palmer, B. N. and H. K. J. Powell (1974). "Polyamine complexes with seven-membered chelate rings: complex formation of 3-azaheptane-1,7-diamine, 4-azaoctane-1,8-diamine (spermidine), and 4,9-diazadodecane-1,12-diamine (spermine) with copper(II) and hydrogen ions in aqueous solution." Journal of the Chemical Society, Dalton Transactions(19): 2089-2092.

Palmiter, R. D., T. B. Cole, C. J. Quaife and S. D. Findley (1996). "ZnT-3, a putative transporter of zinc into synaptic vesicles." Proceedings of the National Academy of Sciences in the United States of America **93**(25): 14934-14939.

Paoletti, P. (2011). "Molecular basis of NMDA receptor functional diversity." European Journal of Neuorscience **33**(8): 1351-1365.

Paoletti, P., P. Ascher and J. Neyton (1997). "High-Affinity Zinc Inhibition of NMDA NR1–NR2A Receptors." The Journal of Neuroscience **17**(15): 5711-5725.

Paoletti, P., F. Perin-Dureau, A. Fayyazuddin, A. Le Goff, I. Callebaut and J. Neyton (2000). "Molecular Organization of a Zinc Binding N-Terminal Modulatory Domain in a NMDA Receptor Subunit." Neuron **28**(3): 911-925.

Partin, K. M., D. K. Patneau and M. L. Mayer (1994). "Cyclothiazide differentially modulates desensitization of alpha-Amino-3-hydroxy-5-methyl-4-isoxazolepropionic Acid Receptor Splice Variants." Molecular Pharmacology **46**(1): 129-138.

Perin-Dureau, F., J. Rachline, J. Neyton and P. Paoletti (2002). "Mapping the Binding Site of the Neuroprotectant Ifenprodil on NMDA Receptors." The Journal of Neuroscience **22**(14): 5955-5965.

Peters, S., J. Koh and D. W. Choi (1987). "Zinc Selectively Blocks the Action of N-Methyl-d-Aspartate on Cortical Neurons." Science **236**(4801): 589-593.

Popescu, G. and A. Auerbach (2003). "Modal gating of NMDA receptors and the shape of their synaptic response." Nature Neuroscience **6**(5): 476-483.

Prithwish Pal, a. Brian E. Holmberg and P. A. Knauf (2005). "Conformational Changes in the Cytoplasmic Domain of Human Anion Exchanger 1 Revealed by Luminescence Resonance Energy Transfer." Biochemistry **44**(42): 13638-13649.

Rachline, J., F. Perin-Dureau, A. L. Goff, J. Neyton and P. Paoletti (2005). "The Micromolar Zinc-Binding Domain on the NMDA Receptor Subunit NR2B." The Journal of Neuroscience **12**: 308-317.

Raman, I. M. and L. O. Trussell (1995). "The mechanism of alpha-amino-3-hydroxy-5-methyl-4-isoxazolepropionate receptor desensitization after removal of glutamate." Biophysical Journal **68**(1): 137-146.

Ramaswamy, S., D. Cooper, N. Poddar, D. M. MacLean, A. Rambhadran, J. N. Taylor, H. Uhm, C. F. Landes and V. Jayaraman (2012). "Role of Conformational Dynamics in α-

Amino-3-hydroxy-5-methylisoxazole-4-propionic Acid (AMPA) Receptor Partial Agonism." The Journal of Biological Chemistry **287**: 43557-43564.

Rambhadran, A., J. Gonzalez and V. Jayaraman (2010). "Subunit Arrangement in N-Methyl-d-aspartate (NMDA) Receptors." Journal of Biological Chemistry **285**: 15296-15301.

Rambhadran, A., J. Gonzalez and V. Jayaraman (2011). "Conformational Changes at the Agonist Binding Domain of the N-Methyl-d-Aspartic Acid Receptor." Journal of Biological Chemistry **286**: 16953-16957.

Retchless, B. S., W. Gao and J. W. Johnson (2012). "A single GluN2 subunit residue controls NMDA receptor channel properties via intersubunit interaction." Nature Neuroscience **15**: 406-413.

Riou, M., D. Stroebel, J. M. Edwardson and P. Paoletti (2012). "An Alternating GluN1-2-1-2 Subunit Arrangement in Mature NMDA Receptors." PLOS ONE **7**(4).

Robert, A. and J. R. Howe (2003). "How AMPA Receptor Desensitization Depends on Receptor Occupancy." The Journal of Neuroscience **23**(3): 847-858.

Robert, A., S. N. Irizarry, T. E. Hughes and J. R. Howe (2001). "Subunit Interactions and AMPA Receptor Desensitization." The Journal of Neuroscience **21**(15): 5574-5586.

Rock, D. M. and R. L. MacDonald (1992). "The polyamine spermine has multiple actions on N-methyl-D-aspartate receptor singel-channel currents in cultured cortical neurons." Molecular Pharmacology **41**(1): 83-88.

Rosenmund, C., Y. Stern-Bach and C. F. Stevens (1998). "The tetrameric structure of a glutamate receptor channel." Science **280**(5369): 1596-1599.

Ruiz, A., M. C. Walker, R. Fabian-Fine and D. M. Kullmann (2004). "Endogenous Zinc Inhibits GABAA Receptors in a Hippocampal Pathway." Journal of Neurophysioogy **91**(2): 1091-1096.

Rumbaugh, G., K. Prybylowski, J. F. Wang and S. Vicini (2000). "Exon 5 and spermine regulate deactivation of NMDA receptor subtypes." J Neurophysiol **83**(3): 1300-1306.

Salussolia, C. L., M. L. Prodromou, P. Borker and L. P. Wollmuth (2011). "Arrangement of Subunits in Functional NMDA Receptors." The Journal of Neuroscience **31**(31): 11295-11304.

Selvin, P. R. (2002). "Principles and biophysical applications of lanthanide-based probes." Annu Rev Biophys Biomol Struct **31**: 275-302.

Sindreu, C. B., H. Varoqui, J. D. Erickson and J. Pérez-Clausell (2003). "Boutons Containing Vesicular Zinc Define a Subpopulation of Synapses with Low AMPAR Content in Rat Hippocampus." Cerebral Cortex **13**(8): 823-829.

Sirrieh, R. E., D. M. MacLean and V. Jayaraman (2013). "Amino-terminal domain Tetramer Organization and Structural Effects of Zinc Binding in the N-Methyl-D-aspartate (NMDA) Receptor." Journal of Biological Chemistry **288**: 22555-22564.

Sobolevsky, A. I., M. P. Rosconi and E. Gouaux (2009). "X-ray structure, symmetry and mechanism of an AMPA-subtype glutamate receptor." Nature **462**(7274): 745-756.

Stern-Bach, Y., S. Russo, M. Neuman and C. Rosenmund (1998). "A Point Mutation in the Glutamate Binding Site Blocks Desensitization of AMPA Receptors." Neuron **21**(4): 907-918.

Stroebel, D., S. Carvalho, T. Grand, S. Zhu and P. Paoletti (2014). "Controlling NMDA Receptor Subunit Composition Using Ectopic Retention Signals." The Journal of Neuroscience **34**(50): 16630-16636.

Stroebel, D., S. Carvalho and P. Paoletti (2011). "Functional evidence for a twisted conformation of the NMDA receptor GluN2A subunit N-terminal domain." Neuropharmacology **60**(1): 151–158.

Stryer, L. and R. P. Haugland (1967). "Energy transfer: a spectroscopic ruler." Proceedings of the National Academy of Science **58**(2): 719-726.

Sugihara, H., K. Moriyoshi, T. Ishii, M. Masu and S. Nakanishi (1992). "Structures and properties of seven isoforms of the NMDA receptor generated by alternative splicing." Biochemical and Biophysical Research Communications **185**(3): 826-832.

Suzuki, Y., T. A. Goetze, D. Stroebel, D. Balasuriya, S. H. Yoshimura, R. M. Henderson, P. Paoletti, K. Takeyasu and J. M. Edwardson (2013). "Visualization of Structural Changes Accompanying Activation of N-Methyl-D-aspartate (NMDA) Receptors Using Fast-scan Atomic Force Microscopy Imaging." The Journal of Biological Chemistry **288**(2): 778-784.

Talukder, I., P. Borker and L. P. Wollmuth (2010). "Specific sites within the ligand-binding domain and ion channel linkers modulate NMDA receptor gating." J Neurosci **30**(35): 11792-11804.

Talukder, I. and L. P. Wollmuth (2011). "Local constraints in either the GluN1 or GluN2 subunit equally impair NMDA receptor pore opening." Journal of General Physiology **138**(2): 179-194.

Tang, C. M. (2001). "Rapid solution application methods." Curr Protoc Neurosci **Chapter 6**: Unit 6 9.

Tang, C. M., M. Dichter and M. Morad (1990). "Modulation of the N-methyl-D-aspartate channel by extracellular H+." Proc Natl Acad Sci U S A **87**(16): 6445-6449.

Tomitori, H., A. Suganami, R. Saiki, S. Mizuno, Y. Yoshizawa, T. Masuko, Y. Tamura, K. Nishimura, T. Toida, K. Williams, K. Kashiwagi and K. Igarashi (2012). "Structural changes of regulatory domain heterodimer of N-methyl-D-aspartate receptor subunits GluN1 and GluN2B through the binding of spermine and ifenprodil." The Journal of Pharmacology and Experimental Therapeutics **343**(1): 82-90.

Tovar, K. R., M. J. McGinley and G. L. Westbrook (2013). "Triheteromeric NMDA receptors at hippocampal synapses." J Neurosci **33**(21): 9150-9160.

Traynelis, S. F., M. F. Burgess, F. Zheng, P. Lyuboslavsky and J. L. Powers (1998). "Control of Voltage-Independent Zinc Inhibition of NMDA Receptors by the NR1 Subunit." The Journal of Neuroscience **18**(16): 6163-6175.

Traynelis, S. F. and S. G. Cull-Candy (1990). "Proton inhibition of N-methyl-D-aspartate receptors in cerebellar neurons." Nature **345**(6273): 347-350.

Traynelis, S. F. and S. G. Cull-Candy (1991). "Pharmacological properties and H+ sensitivity of excitatory amino acid receptor channels in rat cerebellar granule neurones." J Physiol **433**: 727-763.

Traynelis, S. F., M. Hartley and S. F. Heinemann (1995). "Control of proton sensitivity of the NMDA receptor by RNA splicing and polyamines." Science **268**(5212): 873-876.

Traynelis, S. F., L. P. Wollmuth, C. J. McBain, F. S. Menniti, K. M. Vance, K. K. Ogden, K. B. Hansen, H. Yuan, S. J. Myers and R. Dingledine (2010). "Glutamate Receptor Ion Channels: Structure, Regulation, and Function." Pharmacological Reviews **62**(3): 405-496.

Trombley, P. Q., L. J. Blakemore and B. J. Hill (2011). "Zinc Modulation of Glycine Receptors." Neuroscience **186**: 32-38.

Trussell, L. O., S. Zhang and I. M. Ramant (1993). "Desensitization of AMPA receptors upon multiquantal neurotransmitter release." Neuron **10**(6): 1185-1196.

Ueno, S., M. Tsukamoto, T. Hirano, K. Kikuchi, M. K. Yamada, N. Nishiyama, T. Nagano, N. Matsuki and Y. Ikegaya (2002). "Mossy fiber Zn2+ spillover modulates heterosynaptic N-methyl-d-aspartate receptor activity in hippocampal CA3 circuits." Journal of Cellular Biology **158**(2): 215-220.

Vance, K. M., K. B. Hansen and S. F. Traynelis (2013). "Modal gating of GluN1/GluN2D NMDA receptors." Neuropharamacology **71**: 184-190.

Veran, J., J. Kumar, P. S. Pinheiro, A. Athané, M. L. Mayer, D. Perrais and C. Mulle (2012). "Zinc Potentiates GluK3 Glutamate Receptor Function by Stabilizing the Ligand Binding Domain Dimer Interface." Neuron **76**(3): 565-578.

Vogt, K., J. Mellor, G. Tong and R. Nicoll (2000). "The Actions of Synaptically Released Zinc at Hippocampal Mossy Fiber Synapses." Neuron **26**(1): 187-196.

Wang, J. Q., M.-L. Guo, D.-Z. Jin, B. Xue, E. E. Fibuch and L.-M. Mao (2014). "Roles of subunit phosphorylation in regulating glutamate receptor function." European Journal of Pharmacology **728**: 183–187.

Werner, P., M. Voigt, K. Keinänen, W. Wisden and P. H. Seeburg (1991). "Cloning of a putative high-affinity kainate receptor expressed predominantly in hippocampal CA3 cells." Nature **351**(6329): 742-744.

Westbrook, G. L. and M. L. Mayer (1987). "Micromolar concentrations of Zn2+ antagonize NMDA and GABA responses of hippocampal neurons." Nature **328**: 640-643.

Williams, K. (1993). "Ifenprodil discriminates subtypes of the N-methyl-D-aspartate receptor: selectivity and mechanisms at recombinant heteromeric receptors." Molecular Pharmacology **44**(4): 851-859.

Woster, P. M. and W. S. University (2006). Polyamine Structure and Synthetic Analogs. Polyamine Structure and Synthetic Analogs: Physiology, Pharmacology, and Cancer Research. J.-Y. Want and R. A. Casero Jr., Humana Press**:** 3-24.

Yuan, H., K. B. Hansen, K. M. Vance, K. K. Ogden and S. F. Traynelis (2009). "Control of NMDA Receptor Function by the NR2 Subunit Amino-Terminal Domain." The Journal of Neuroscience **29**(39): 12045-12058.

Zhang, S., M. D. Ehlers, J. P. Bernhardt, C. T. Su and R. L. Huganir (1998). "Calmodulin mediates calcium-dependent inactivation of N-methyl-D-aspartate receptors." Neuron **21**(2): 443-453.

Zhang, W., J. R. Howe and G. K. Popescu (2008). "Distinct gating modes determine the biphasic relaxation of NMDA receptor currents." Nature Neuroscience **11**(12): 1373-1375.

Zheng, F., K. Erreger, C.-M. Low, T. Banke, C. J. Lee, P. J. Conn and S. F. Traynelis (2001). "Allosteric interaction between the amino terminal domain and the ligand binding domain of NR2A." Nature Neuroscience **4**(9): 894-901.

Zheng, F., M. B. Gingrich, S. F. Traynelis and P. J. Conn (1998). "Tyrosine kinase potentiates NMDA receptor currents by reducing toniczinc inhibition." Nature Neuroscience **1**(3): 185-191.

Zhu, S., D. Stroebel, C. A. Yao, A. Taly and P. Paoletti (2013). "Allosteric signaling and dynamics of the clamshell-like NMDA receptor GluN1 N-terminal domain." Nature Structural & Molecular Biology **20**: 477-485.

VITA

Rita Evelyn Sirrieh was born on September 9, 1988 at Memorial Hospital in Houston, Texas to Peter and Flavia Sirrieh. After completing school at Hastings High School in Houston, Texas in May 2006, she entered The Honors College at the University of Houston in Houston, Texas. She received the degree Bachelor of Science in Biochemical and Biophysical Sciences, *magna cum laude* with University Honors and Honors in Major in May 2010. In August 2010, she entered The University of Texas Graduate School of Biomedical Sciences in Houston, Texas. She completed her doctoral work in the laboratory of Dr. Vasanthi Jayaraman.

Permanent Address:

10911 Coldwater Bridge Ct.

Sugar Land, TX 77498